Flavor identification in ORCA

Masterarbeit aus der Physik

vorgelegt von
Thomas Heid
Tag der Abgabe: 24. 10. 2013

Erlangen Centre for Astroparticle Physics
Physikalisches Institut 4
Friedrich-Alexander-Universität
Erlangen-Nürnberg

1. Gutachter: Prof. Dr. Gisela Anton
2. Gutachter: Dr. Thomas Eberl

Contents

Chapter 1

Introduction

Neutrinos are among the most mysterious particles we know. One strange property is flavor oscillation first proposed in the late 1950s by Pontecorvo [1]. However, the neutrino community only became aware of it when the solar neutrino problem arose. The first experiment that observed neutrino oscillations was the Homestake experiment [2]. Later on, experiments investigated the properties of oscillating neutrinos. Finally the SNO experiment delivers a direct evidence for the neutrino oscillations in the year 2002 [3]. The experiments were used to measure parameters such as the squared mass splitting between the different mass eigenstates of neutrinos. The experiments were not able to determine the sign of the mass splitting, and therefore it is not clear how the states are ordered.
Recently a measurement of the mixing angle Θ_{13} yielded a surprisingly big value [4]. This leads to a measurable difference in the oscillating properties of neutrinos in matter for different mass hierarchies. In the different cases different numbers of neutrinos can be detected. Counting the neutrinos one can decide which hierarchy is the correct one. [5]
A feasibility study for an experiment aiming at the determination of the mass hierarchy has been initiated. It is called "Oscillation Research with Cosmics in the Abyss" (ORCA). The ORCA-detector is to be built with the same technology as KM3NeT, the future cubic kilometer sized neutrino telescope in the Mediterranean Sea [6].
On the one hand, one can use atmospheric neutrinos for the experiment. On the other hand, there are considerations about a so-called beam option. In this case the electrons are created in a man-made accelerator pointing its neutrino beam to the detector. All options have the same detection principle. They use the products of the interaction between neutrinos and particles in the detector, which partly emit Cherenkov light or decay to photons. The Cherenkov light is used to reconstruct the parameters of the trajectory of the incoming neutrinos.
The main challenges are the low statistics in the regarded energy regime due to the low cross section of neutrinos. Furthermore the detector has to reach a good angular and energy resolution, because the effects of different mass hierarchies are visible with respect to the zenith angle and the energy of the incoming neutrinos.
The challenge in this thesis is to deal with the appearance of different kinds of neutrino events in the detector, as the experimental design is aimed measure muon neutrinos in the charged current interaction channel. Other events diminish the discrimination power for the mass hierarchy [7]. The algorithms developed in this thesis try to distinguish between track-like and shower-like events. Track-like events are the charged current events caused by muon neutrinos and shower-like events are caused by electron neutrinos in charged current or all neutrino flavors in neutral current interactions.
The thesis is structured in the following way. In Chapter 2 properties of neutrinos, like oscillation and the detection principle are introduced. Chapter 3 introduces the detector principle.Chapter 4 is about the different possibilities of neutrino mass hierarchies. Additionally, the chapter shows how it is possible to decide which hierarchy is the correct one. The main part of this thesis is Chapter 5 describing the methods to distinguish track-like and shower-like events.

Chapter 2

Neutrino Physics

2.1 Current Knowledge

In quantum field theory the description of particles and their interaction is achieved with a Lagrangian. The Lagrangian of one single neutrino is written as follows [8]:

$$\mathcal{L} \subset \underbrace{\overline{\nu_{\alpha L}} \imath \partial \!\!\!/ \nu_{\alpha L}}_{\text{kinetic term}} + \underbrace{\underbrace{\frac{g}{\sqrt{2}}(W^{\mu\dagger}\overline{\nu_{\alpha L}}\gamma_\mu l_{\alpha L} + h.c.)}_{\text{charged current}} + \underbrace{\frac{g}{1\sin\Theta_W}(Z^\mu\overline{\nu_{\alpha L}}\gamma_\mu \nu_{\alpha L} + h.c)}_{\text{neutral current}}}_{\text{interaction term}} + \underbrace{\frac{1}{2}m_{\alpha\beta}\overline{\nu_{\alpha L}{}^C}\nu_{\beta L} + h.c.}_{\text{mass term}} \quad (2.1)$$

The most interesting parts are the kinetic part, interaction part and the mass term. The kinetic part shows the free propagation of neutrinos. Interaction with other particles is described in the interaction term. The mass is introduced in the mass term. In the shown equation there is the Dirac mass term stated. An other possibility or an additional term could be the Majorana mass term. This term would lead to the identity of the neutrino to its antineutrino. Further, an additional mass term leads with the seasaw mechanism to an explanation of the tiny mass of neutrinos.[8]
For calculations concerning the oscillations the mixing matrix is needed. It is the transformation matrix to diagonalize the mass matrix $m_{\alpha\beta}$. The Matrix is commonly defined as:

$$U_{PNMS} = \begin{pmatrix} 1 & 0 & 0 \\ 0 & c_{23} & s_{23} \\ 0 & -s_{23} & c_{23} \end{pmatrix} \cdot \begin{pmatrix} c_{13} & 0 & s_{13}e^{-\imath\delta} \\ 0 & 1 & 0 \\ -s_{13}e^{-\imath\delta} & 0 & c_{13} \end{pmatrix} \cdot \begin{pmatrix} c_{12} & s_{12} & 0 \\ -s_{12} & c_{12} & 0 \\ 0 & 0 & 1 \end{pmatrix} \quad (2.2)$$

with $s_{ij} = \sin\Theta_{ij}$ and $c_{ij} = \cos\Theta_{ij}$. This matrix is the simplest form of a unitary matrix with a phase factor δ [8]. One sees that there are four oscillation parameters to describe the oscillation. θ_{ij} is called the mixing angle.
Table 2.1 shows the current values for each neutrino parameter. Additionally to the oscillation parameters there is also the mass of neutrinos which is not known till now. The mass differences are known very well except of the sign of the atmospheric mass difference.
Neutrino mixing angles are also known, but the CP violating phase is not.

2.2 Neutrino Mass Hierarchy

The project ORCA is supposed to solve the question, if nature realizes the normal or the inverted mass hierarchy. Figure 2.1 shows the two possibilities. The squared masses are sketched on the y-axis. The value and sign of the smaller squared mass difference is known from solar neutrino experiments like Kamland [10]. The value of Δm^2_{13} is known from these experiments, too. The knowledge about

Table 2.1: *Best fit values of neutrino oscillation parameters with the 1sigma range taken from [9] (where* $\Delta m \equiv m_{23} - (m_{21} + m_{22})/2$*)*

Parameter	Best fit	1σ range
$\delta m^2_{12}/10^5 eV^2$ (NH or IH)	7.54	7.32 7.80
$\sin^2(\theta_{12})/101$(NH or IH)	3.07	2.91 3.25
$\Delta m^2/10^3 eV^2$ (NH)	2.43	2.33 2.49
$\Delta m^2/10^3 eV^2$ (IH)	2.42	2.31 2.49
$\sin^2(\Theta_{13})/10^2$(NH)	2.41	2.16 2.66
$\sin^2\Theta_{13}/10^2$(IH)	2.44	2.19 2.67
$\sin^2\Theta_{23}/10^1$ (NH)	3.86	3.65 4.10
$\sin^2\Theta_{23}/10^1$(IH)	3.92	3.70 4.31
δ/π/(NH)	1.08	0.77 1.36
δ/π(IH)	1.09	0.83 1.47

the bigger squared mass difference comes from experiments using the muon neutrino (μ_ν) survival probability like Super-Kamiokande 1 [11]. They are only sensitive to the absolute value of Δm^2_{13}. Further dependencies are suppressed [12]. As the sign of Δm^2_{12} is the only known one, two possible hierarchies are left.
Which hierarchy is the correct one is not predicted by any theoretical approach. Grand unified theories would favor the normal mass hierarchy as they claim an underlying relationship to the quark sector[13]. On the other hand, there is no excluding reason for the inverted mass hierarchy. The recent

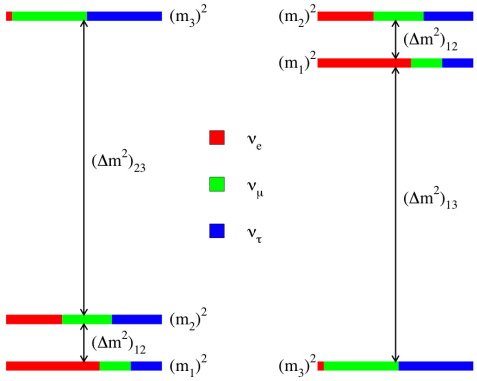

Figure 2.1: *Possible neutrino mass hierarchies [12]*

measurement for the surprisingly large value of Θ_{13} [4] leads to the possibility of using atmospheric neutrinos to determine the mass hierarchy [5]. This alternative is less expensive and time-consuming than other experiments expecting results not earlier than 2025.

2.3 Neutrino Production and Fluxes in the Atmosphere

Most probably the proposed ORCA experiment will use atmospheric neutrinos. In many other experiments in the past these neutrinos were regarded as unwanted background, which has to be suppressed. Atmospheric neutrinos are created by cosmic rays in the atmosphere. Cosmic rays are mainly protons and a few heavier nuclei. For cosmic rays the energy distribution is well-known, which is important for the calculation of neutrino fluxes. The cosmic particles collide with nuclei in the atmosphere. This interaction inevitably creates pions. These pions decay to muons and muon neutrinos as described in the following:

$$\pi^+ \rightarrow \mu^+ + \nu_\mu \tag{2.3}$$

and

$$\pi^- \rightarrow \mu^- + \bar{\nu}_\mu. \tag{2.4}$$

The higher the energies the more kaons contribute to the production of neutrinos and muons, too. The produced muons decay further to electrons and neutrinos:

$$\mu^+ \rightarrow e^+ + \nu_e + \bar{\nu}_\mu \tag{2.5}$$

and

$$\mu^- \rightarrow e^- + \bar{\nu}_e + \nu_\mu. \tag{2.6}$$

As one can see from the multiplicities in the equations 2.3 to 2.6 the flavor ratio results in

$$\frac{\Phi_{\nu_\mu} + \Phi_{\bar{\nu}_\mu}}{\Phi_{\nu_e} + \Phi_{\bar{\nu}_e}} = 2, \tag{2.7}$$

if all muons decay. As the proportion of muons decaying until they reach the detector decreases with increasing energy the flavor ration decreases [8]. In ORCA, commonly the HKKM'11 flux is used. It is not explicitly calculated for any possible ORCA sites, but for the Frejus site [14].

2.4 Neutrino Oscillations

Neutrino oscillations came into mind as there was the solar neutrino problem. Several neutrino experiments counted less neutrinos produced by the sun as expected. One experiment to be mentioned here is the Homestake experiment [2]. However, Pontecorvo predicted the possibility of neutrino oscillations before these experiments [15]. The standard derivation of neutrino oscillations was developed in 1975-76. The derivation uses the plane-wave approximation. The following explanation follows the description of [8]. First the oscillations in vacuum will be derived, afterwards the modified equations for the matter case will be motivated.

2.4.1 Neutrino Oscillations in Vacuum

Neutrinos are produced in charged current events, as can be seen in the corresponding Lagrangian in equation 2.1. That means it is created by a weak-interaction process involving a charged lepton like it was written in Chapter 2.3. The neutrino in a flavor state can be described by the mass eigenstates with

$$\nu_\alpha = \sum_k U^*_{\alpha k} |\nu_k\rangle \tag{2.8}$$

with $\alpha \in \{e, \mu, \tau\}$ and k the index of the massive neutrino. U is the unitary mixing matrix. The other way round, the neutrino in the mass basis is given as

$$\nu_k = \sum_k U_{\alpha k} |\nu_\alpha\rangle. \tag{2.9}$$

We are now considering the time-evolution of the neutrinos. The massive neutrinos are eigenstates of the Hamiltonian with the energy as eigenvalue

$$\mathscr{H}|\nu_k\rangle = E_k|\nu_k\rangle. \tag{2.10}$$

The energy of any massive particle and here of the massive neutrino is given by

$$E_k = \sqrt{p_k^2 + m_k^2}, \tag{2.11}$$

where the units are chosen so that for the speed of light yields $c = 1$.
The solution of the Schrödinger equation

$$\imath \frac{d}{dt}|\nu_k(t)\rangle = \mathscr{H}|\nu_k\rangle \tag{2.12}$$

is given by

$$|\nu\rangle = e^{-\imath E_k t}|\nu_k\rangle. \tag{2.13}$$

Resulting in the equation of motion for a neutrino started with flavor α

$$|\nu_\alpha(t)\rangle = \sum_{(\beta=e,\mu,\tau)} \left(\sum_k U_{\alpha k}^* e^{-\imath E_k t} U_{\beta k}^* \right) |\nu_\beta\rangle. \tag{2.14}$$

The quantum mechanical transition amplitude from one state to another is defined as

$$A_{\nu_\alpha \to \nu_\beta}(t) = \langle \nu_\beta | \nu_\alpha(t) \rangle \tag{2.15}$$

resulting in the probability of the transition from ν_α to ν_β

$$P_{\nu_\alpha \to \nu_\beta}(t) = |A_{\nu_\alpha \to \nu_\beta}(t)|^2 = \sum_{k,j} U_{\alpha k}^* U_{\beta k} U_{\alpha j} U_{\beta j}^* e^{-\imath (E_k - E_j)t} \tag{2.16}$$

For antimatter one has to substitute the matrix entries by their complex conjugated ones.
With ultra relativistic neutrinos this equation and the energy relation 2.11 with its expansion leads to

$$P_{\nu_\alpha \to \nu_\beta}(t) = \sum_{k,j} U_{\alpha k}^* U_{\beta k} U_{\alpha j} U_{\beta j}^* e^{-\imath \frac{\Delta m_{kj}^2}{2E} t} \tag{2.17}$$

As the neutrinos are ultra relativistic the substitution $L = t$ is useful, where L is the distance from the starting point.
Further, one defines the oscillation length

$$L_{kj}^{osc} \coloneqq \frac{2\pi E}{\Delta m_{kj}^2}. \tag{2.18}$$

After propagating for one oscillation length the phase of the probability is accumulated to 2π. So the probability is back to the starting value. At half of the oscillation length the largest effect is expected. Here one would install a detector, if you have the source located on a defined place.
Several assumptions were taken into account for this derivation. First of all it is assumed that neutrinos are produced in flavor eigenstates, e.g. no mixing in flavor states as it will occur during propagation. Further all massive components of the neutrinos have the same momentum. Finally the approximation $L = t$ is used. This assumption is justified as the neutrinos can be assumed as wave packets. But in the consideration of a plane wave this approximation is not justified as a plane wave does not propagate like a light ray, but the plane wave covers the whole space-time. [8]

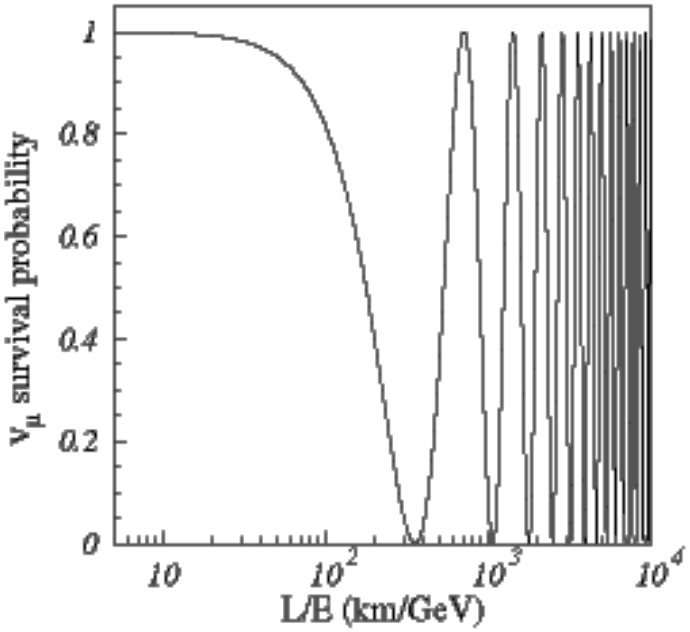

Figure 2.2: *Oscillation diagram [16]*

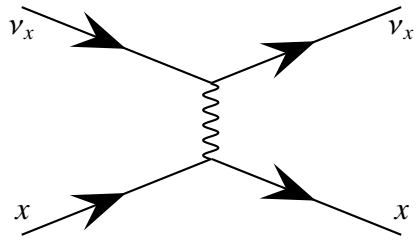

Figure 2.3: *Neutral current for all flavors*

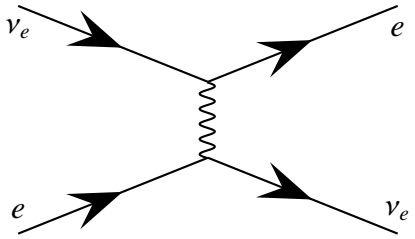

Figure 2.4: *possible "Neutral" charged current for electron neutrinos*

2.4.2 Neutrino Oscillations in Matter

Additionally, to the effects in vacuum, matter causes more oscillations. Coherent forward scattering leads to an additional potential for neutrinos, especially for electron neutrinos. That electron neutrinos are affected more than the others is caused by different possible interactions leading to coherent forward scattering.
For all flavors it is done by neutral current interaction with the exchange of a Z-boson. This reaction is sketched in Figure 2.3. In the case of electron neutrinos additionally the charged current interaction contributes to scattering. The reaction is shown in figure 2.4. The electron neutrino can scatter on other electrons while changing the electron to an electron neutrino and the other way round for the neutrino itself. In the final state the electron and electron neutrino have the same properties as the corresponding particles before the interaction.
This additional potential leads to an effective Hamiltonian shown in the flavor basis as

$$\mathcal{H}_F = (\frac{1}{2E}(UM^2U^* + A) \tag{2.19}$$

with

$$M^2 = \begin{pmatrix} 0 & 0 & 0 \\ 0 & \Delta m^2_{21} & 0 \\ 0 & 0 & \Delta m^2_{31} \end{pmatrix} \tag{2.20}$$

and

$$M^2 = \begin{pmatrix} A_{CC} & 0 & 0 \\ 0 & 0 & 0 \\ 0 & 0 & 0 \end{pmatrix} \tag{2.21}$$

where $A_{CC} = 2\sqrt{2}EG_F N_e$. G_F is the Fermi coupling constant and N_e is the electron density in the matter. The positive sign is used for neutrinos and the negative sign for anti neutrinos.
This Hamiltonian is neither diagonal in the flavor basis nor in massive neutrino basis. However the effective Hamiltonian can be diagonalized resulting in effective masses and effective mixing angles. They are subscripted by a m in the following. To make some effects plausible and for simplification the next equations are shown for the two-neutrino case. The two flavor case leads to almost the same results as the full case. The resulting mixing angle is given by

$$\tan 2\theta_m + \frac{\tan 2\theta}{1 - \frac{A_{CC}}{\Delta m^2 \cos 2\theta}} \tag{2.22}$$

As can be seen easily, there is a resonance at $A^R_{CC} = \Delta m^2 \cos 2\Theta$. So even small mixing angles become big if one can setup the resonance environment. This leads to the resonance condition of

$$N^R_e = \frac{\Delta m^2 \cos 2\theta}{2\sqrt{2}EG_F} \text{ and } E^R = \frac{\Delta m^2 \cos 2\theta}{2\sqrt{2}G_F N_e}. \tag{2.23}$$

In different mass hierarchies the resonance can be full filled for either neutrinos or antineutrinos as otherwise the sign of Δm^2 implies negative electron densities and energies, which is of course not possible.
For the final probability one gets

$$P_{\nu_e \to \nu_\mu}(x) = \sin^2 2\Theta_M \sin^2 \frac{\Delta m^2_M L}{4E}., \tag{2.24}$$

In the mantle and the core of the earth there are electron densities of $2cm^{-3} \cdot N_A$ to $5cm^{-3} \cdot N_A$ causing a resonance energy of 3 to 10 GeV [17]. This region is the most interesting as the best oscillation pattern can be expected.

2.4.3 Set-ups of Oscillation Experiments

According to the different oscillation regimes, e.g. fraction of energy over propagation length and different types of oscillation properties there are several types of experimental set-ups.
First, oscillation leads to two different possibilities of investigations. On the one hand one deals with the disappearance of neutrinos. So neutrinos of one flavor starting started at the production site do not reach the detector due to oscillations. Here one has to measure the difference in the amount of starting neutrinos to detected neutrinos. If the number of vanishing neutrinos is very low with respect to the number of starting ones, low statistics can diminish the effect. So large probabilities are forwarded by this experimental setup. If one is interested in properties causing lower oscillation probabilities the other way round is favored. Experiments dealing with the appearance of neutrinos which were not sent by the initial source are more robust to statistics. The amount of expected neutrinos compared to the number of neutrinos without any oscillation can be determined, even if there is some background.

Experiments are named according their ratio of propagation length to neutrino energy [8] as this places the experiments according to equation 2.17 in certain regions in the oscillation diagram (Figure 2.2). First there are Short Baseline experiments with L/E up to 1km/GeV, which are for example reactor neutrinos detected next to the production site. Experiments with a ratio up to 10^4km/GeV are called Long Baseline experiments. The atmospheric neutrino oscillation experiments like ORCA are Long Baseline experiments with energies up to 30 GeV and distances up to $1.3 \cdot 10^4$km for neutrinos from the nadir.
Experiments with even higher ratios are called Very Long Baseline experiments like set-ups for solar neutrino experiments.
In experiments with artificial neutrino sources the production is quite similar to the production as stated in Chapter 2.3. Heavy particles like protons are accelerated onto a target in which they collide with other matter and produce muons and pions for example. Amongst others these particles decay to neutrinos. As the neutrinos are produced by protons out of a man made accelerator they are called accelerator neutrinos. Additionally, there are reactor neutrinos produced by the beta decay of heavy nuclei.
According, the wished output energy and fraction of neutrino flavors one has to choose the proper setting.

2.5 Neutrino Detection

The neutrinos produced in the earth's atmosphere on the opposite side of the earth travel through the earth to the detector. As the neutrinos are only interacting via the weak interaction and the gravitational force they cannot be detected directly. Previously they have to interact with other particles and produce secondary particles. Detecting these additional particles reconstructing the properties of the incoming neutrino is possible. One distinguishes two channels of interactions. If the neutrino interacts with other particles so that it changes to a charged lepton the event is called a charged current event. The exchange particle is the W boson. On the flip side there are the neutral current events. These are events, in which the neutrino scatters on the other particle. The different interaction channels can be seen in the Feynman graph in figure 2.7 and 2.6.
In both channels the neutrino can transmit energy to the collision partner. Commonly one defines Bjorken-y as the fractional energy loss of the incoming particle. So in this case y is defined as

$$y := \frac{E - E^*}{E} \tag{2.25}$$

where E is the energy of the incoming neutrino and E^* is the energy of the outgoing lepton or neutrino. The Bjorken-y is not fixed so it is different for each event. Only the mean value can be derived. It is different for neutrinos and antineutrinos. The mean value of Bjorken-y for different energies is shown in figure 2.5
The energy transfered to the collision partner leads to reactions. This can lead to a shower of particles. These particles can be charged so that they can detected by ionization or radiation. An other possibility is that they are neutral. These particles only deliver a signal if they interact in a suitable way. If the secondary particles emit some radiation, mostly Cherenkov radiation, one can detect the emitted photons by photomultipliers. To get a lot of information about one event the photomultipliers are arranged in a three dimensional grid with an energy dependent spacing.
As you can see in figure 2.9 and 2.8 the different neutrino flavors lead to different signatures in the detector. On the left side the neutral current events cause an event with a shower as the only visible part. In the charged current interaction cahnnel the produced lepton emits Cherenkov radiation. The differences between the flavors are in the length of the track of the lepton. The lepton has a certain life time and free path length. That means the lepton decays to other particles after a while. Or the other possibility to stop the lepton is to collide with particles in the detector.

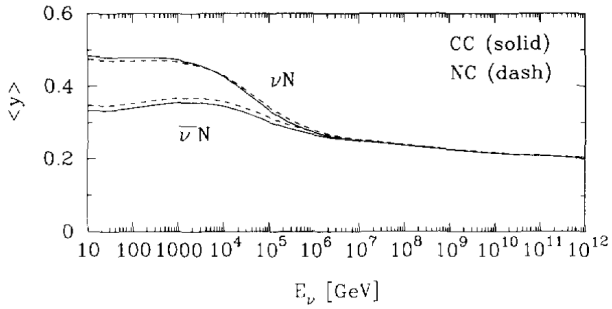

Figure 2.5: *Mean Value of Bjorken-y over the neutrino energy [18]*

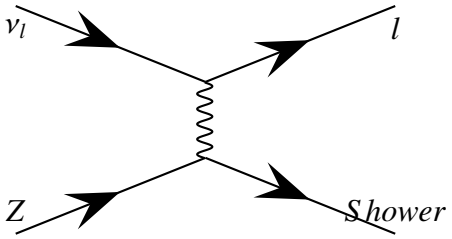

Figure 2.6: *Charged Current($l \in \{e, \mu, \tau\}$)*

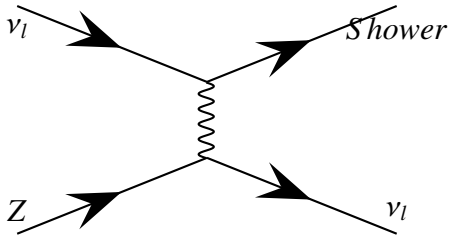

Figure 2.7: *Neutral Current*

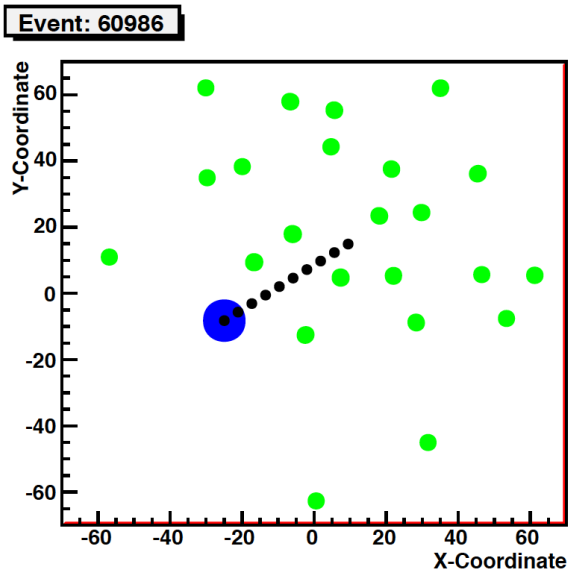

Figure 2.8: *shower-like muon neutrino event in neutral current (green : fired DOMs, blue: interaction Vertex, black: track with distance 5 m)*
$E_\nu = 14.9$ *and* $y = 0.03$

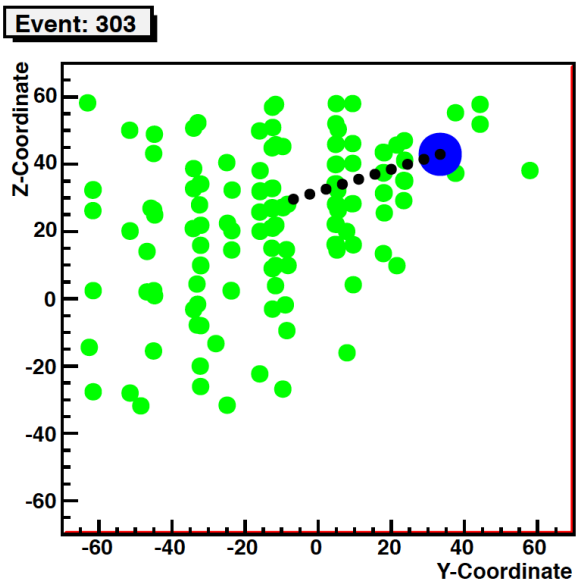

Figure 2.9: *track-like muon neutrino event in charged current*
$E_\nu = 21.0$ *and* $y = 0.33$

One can distinguish mainly two different types of events. The track-like events and the shower-like events. The track-like events are the events with an out going lepton which travels in a longer straight line. These are the charged current events with muon neutrinos. The others are shower like events, as they have shorter tracks of the out going lepton or no lepton at all.
As one can easily assume also the electron and tauon can make a track, which is similar to the muon. Figure 2.9 shows a typical muon neutrino event. The event has a big ratio of muon energy to shower energy. Resulting in a distribution of fired PMTs which is arranged more line shaped. Next to it, the shower event of the neutral current is shown. The distribution of fired PMTs is much more spherical.

That is one of the main problems the classification algorithm deals with in Chapter 5.2. The other part emitting light is the shower. These showers are very diverse. There are many possible compositions of particles building the shower. Also in that part particles can imitate a long track like the muon.

2.6 Neutrino Cross Sections

To calculate the number of neutrinos which can be registered in the detector the cross sections have to be estimated. The Paper [19] gives a summery over all energy regimes. In ORCA the intermediate energy range from 0.1 GeV to 20 GeV is of interest.
In this energy regime three major processes play a role in scattering. In regimes lower than 1GeV, the elastic or quasi-elastic scattering (QE) are the most dominant contribution. Here the neutrino interacts with a nucleon as one entire particle.
Additionally the neutrinos can do resonance production (RES) in which the interacting nucleon is set to a baryonic resonance. This resonance leads in the evolution of the event to the production of more nucleons and mesons.
As the energy becomes higher the neutrino can resolve the constituents of the nucleon. This process is called deep inelastic scattering (DIS). The interaction starts an hadronic shower.
Figure 2.10 shows the dependency of the cross section to the energy for neutrinos.

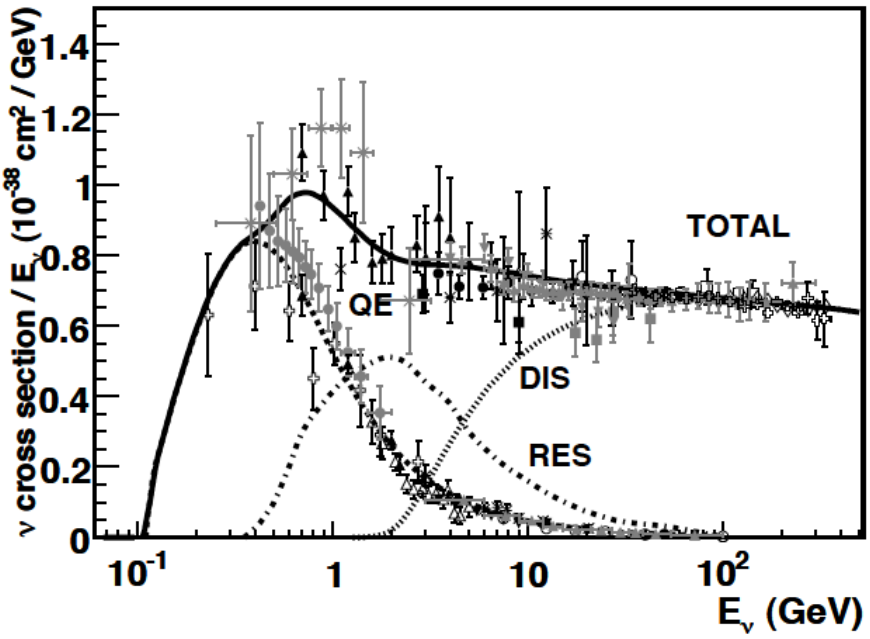

Figure 2.10: *Cross section of neutrinos in the regime of GeV. Data points show the results of various experiments. Figure taken from [19]*

Chapter 3

ORCA Detector

The last chapters explained the properties of neutrinos and the constituents of the neutrino events which a detector has to measure. At first, there are the photons which have to be detected. Further, the time and the place of detection has to be stored. Such detectors are already in use. ANTARES in the Mediterranean Sea is one of these. Mainly, such detectors consist of many photomultipliers arranged as a three dimensional grid. ORCA will be built in a similar way, which is described in this chapter.
The light of the neutrino events has to be collected. The best way to do this is by photomultipliers. They are sensitive to single photons. Additionally, the properties are well known and tested as they are used in many other experiments in particle physics. As there is a neutrino telescope in development, called KM3NeT, ORCA make profit from this expertise and preparatory work. One can use the same technical devices or even use the first phase of KM3NeT to deploy the digital optical modules in an ORCA-like way. So all infrastructure, like data taking, which is built for KM3NeT can also be used in a similar way in ORCA.

Figure 3.1: *KM3NeT Digital Optical Module [20]*

One Digital Optical Module (DOM) as it is used in KM3NeT is shown in figure 3.1. If the reader is interested in more details about the optical module, please refer to [21]. These optical modules consist out of a 17-inch glass sphere. In the inner part there are 31 3" photomultiplier (PMT). To increase the optically sensitive area lenses are placed in front of the PMTs. Further there are so-called Winston cones, which increase the detector sensitivity. The cones surround the PMTs collect photons which other wise would miss the PMT [22]. Additionally, the light transmission is maximized using an optical gel between the PMT and the glass sphere. The DOM itself is fixed on a string. The string is also the connection to the shore to supply the module with energy and send the data to shore. The

whole detector has to be placed in the deep see because as much light as possible has to be blocked before reaching the detector. Additionally, other particles than neutrinos are supposed to be shielded as well as possible. The optical modules are supposed to be placed in a vertical spacing of around six meters. The horizontal distance can be around 20m. This leads to an instrumented mass of 1. 75 Mton with a height of 114 m and a diameter of 140 m. A closer detector is under investigation. The closer the detector the better the reconstruction algorithms can work, because more light can be collected. An even more weighting reason is that events with small energies do not have such long tracks. If one tries to resolve a track it has to be in the size of the distance of two DOMs. As the track length is about 4m/GeV the considerations to make the detector as dense as possible is justified. On the other side there are problems with the deployment if the strings get too close. The modules are not constructed in a way that they can collide with each other. The footprint of the current reference design is shown in figure 3.2. The detector could consist of 50 strings with 20 DOMs on each.[23] The layout has no symmetries in it to avoid any effects in reconstruction which comes from symmetries in the detector layout.

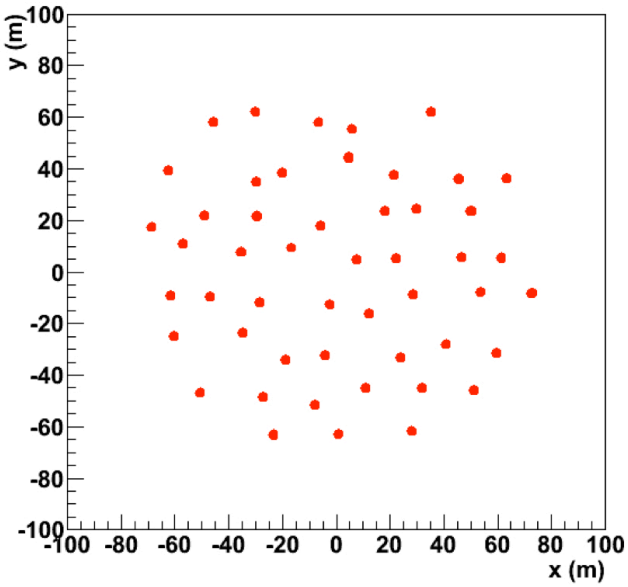

Figure 3.2: *Footprint of ORCA-Detector*

There are currents in the sea and the DOMs will wobble around their mean position. First of all, this explains why it is not possible to place the modules with arbitrary small distances at all. For the reconstruction algorithms the knowledge of the current position of all DOMs is essential (see Chapter 5). Positioning is achieved by acoustical devices, tilt meters and compasses. [21]
As described, daylight from above does not reach the detector. Nevertheless, there is light disturbing the measurement. One of the main background sources is the decay of ^{40}K, which emits photons in the same wavelength as we are interested in from the products of the neutrino interaction. Further, there is bioluminescence from bacteria or bigger organisms. Up to a certain rate algorithms can handle the background, however the whole data taking has to be stopped or the data cannot been used as the data is dominated by these photons. Often high rates caused by bioluminescence are correlated withs effects or currents in the sea. [24]

Chapter 4

Determination of the Neutrino Mass Hierarchy with ORCA

The determination of the mass hierarchy is achieved by using oscillation properties in matter as described in Chapter 2.4. Combined with the knowledge about the flux of atmospheric neutrinos at the detector site (Chapter 2.3) and the cross section of neutrinos with matter in the detector (Chapter 2.6) it is possible to estimate the expected number of detected neutrinos. As there are different numbers for the different mass hierarchies, a log-likelihood ratio test can be used to take the decision about the mass hierarchies.
Figure 4.1 shows the asymmetry between the different hierarchies. Here the asymmetry is defined as the difference of both rates nomralized to the rate of the normal hierarchy.

$$\frac{N_\mu^{IH} - N_\mu^{NH}}{(N_\mu^{NH})^{1/2}} \tag{4.1}$$

The calculation was done by [25] according to [5]. The flux depends on the zenith angle and the energy. The biggest differences in the expected flux are located at the energy regime up to 8 GeV and at the cosine of the zenith angle regime from -1 to 0.7. Most of the information can be gained out of this region.

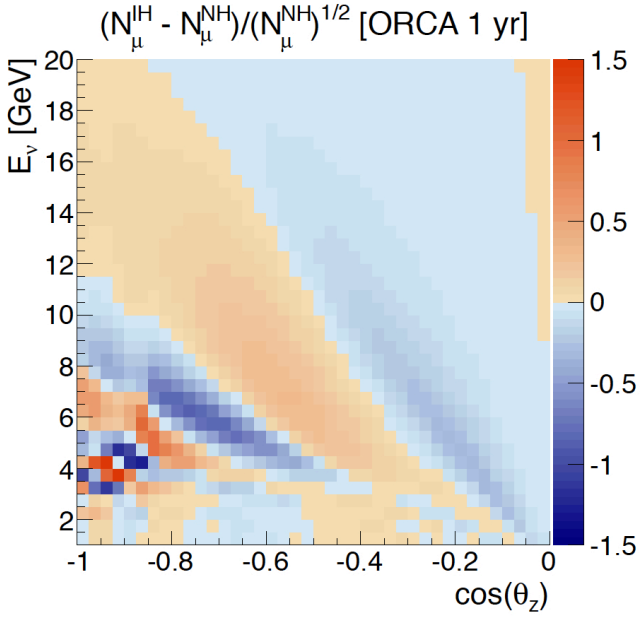

Figure 4.1: *Statistical asymmetry between NH and IH for ORCA after 1 year of exposure [25]*

Once there is data, one can calculate the log-likelihood in each bin:

$$\lambda(data|MH) = \log(L(data|MH)) = \sum_i \log(L_i^{MH}(k_i|\mu_i^{MH})), \tag{4.2}$$

Comparing both hierarchies the log-likelihood ratio is defined as

$$\rho(data) = \frac{\lambda(data|NH)}{\lambda(data|IH)} \tag{4.3}$$

is used.

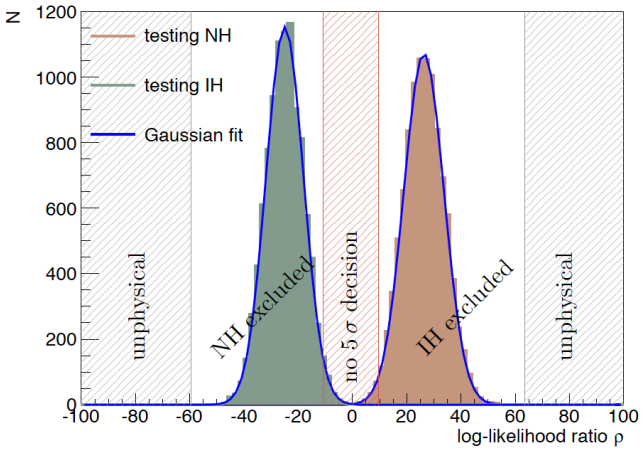

Figure 4.2: *Log-likelihood ratio distribution (10,000 pseudo-experiments) for NH and IH [25]*

The final step to be able to give a quantitative statement of how probable one mass hierarchy is the log-likelihood distribution. The distribution is shown in figure 4.2. It is made out of the result of pseudo experiments. The number of detected neutrinos is drawn from a Poisson distribution. Afterwards the log-likelihood ratio is calculated. One can see that both distributions are overlapping. So it cannot be stated which hierarchy is the underlying one, if one gets a certain log-likelihood ratio. The mid-part stands for the case, in which one cannot make a decision on a 5σ confidence level.[25] That means that one cannot excludeone mass hierarchy with this confidence level.

Chapter 5

Event Reconstruction in the ORCA Detector

In the last years, many reconstruction algorithms were devised to extract information about the topology of a neutrino. In the moment, a very encouraging approach for the reconstruction of muon tracks in ORCA is the so called filtering fit approach, which will be explained later. Beyond the reconstruction of tracks efforts were taken to handle also shower events, even if the reconstruction accuracy did not reach the accuracy of track events, as expected by the intrinsic variations in light output. In events highly dominated by the emission of a muon the direction can be well reconstructed, but events with many different charged and uncharged particles are not so easy to reconstruct.

5.1 Simulations

In this thesis two different samples of simulated events are used. The first sample was employed to see if the classifying algorithms work in the first place. That sample is generated without any simulated noise on the photo multipliers. This setup leads to the best possible reconstruction result that one can obtain. Most results shown in the following are generated from the sample with noise as this is the most interesting and clos to the real case. All samples are produced with the Genie (Generates Events for Neutrino Interaction Experiments) event generator [26]. This generator is currently used by several neutrino experiments like T2K, NOvA and MINERvA.

Premium Events

The sample with which most of the studies were done are the so called premium events. They were proposed by Jannik Hofestädt. The aim is to have as many useful events as possible in one file set. The premium events are defined as such events so that nearly all light is contained in the detector. This is the optimal case one can achieve for one event as all information that the reaction leaves in the detector is detectable and can be used for the identification of the event class. The advantages of these premium events are that all events which are simulated are useful. The next topic is to be free of any edge effects. That means in principle one can study an infinite detector. And thus it is possible to resize the sensitivity calculations to an other detector.
The used events are taken from the June 2013 production of the Catania group. The events are generated with the Genie event generator which is optimized for the low energy regime. They are randomized to events which satisfy the premium event conditions. That means the interaction vertex is uniformly distributed around the center of the detector and the track direction is pointing towards the center. As the weights of the initial events are no longer true they are left out of consideration. The energy range is set to 1 GeV to 30 GeV. The under lying energy distribution is an E^{-1} flux.
The detector response to these events is calculated by the packages km3v4r5 and geasimv4r13seawiet_gtelec. The SHOT value is set to 10 GeV, that means that particles above this threshold are treated with a full simulation. Other particles are simulated by using histograms for the light output. The first

is responsible for the simulation of the muon. The latter simulates the electro magnetic and hadronic showers. There are two types of simulation in this package. On the one side each particle is propagated until it falls under a given energy threshold. On the other side, one can use a parametrization where the light distributions is taken from pre defined distributions. The second method is much faster as the particles are not simulated in such a detailed way.
Finally, the K40 noise is added with the modk40seawiet_gtelec.
It can be seen in figures in the appendix that the electron neutrino events and the muon neutrino events in the neutral current interaction look almost the same. So there are no events used for electron neutrino events of this type of reactions. In contrast, electron neutrinos in the charged current channel have to be taken into account as their topology is somewhere inbetween charged current muon neutrinos and neutral current events.. Table 5.1 shows the number of events for each class. Further, distributions other than the event numbers can be found in the appendix.

Table 5.1: *Number of premium events in each class which can be used for training and testing*

Muon charged current	410000
Muon neutral current	180000
Electron charged current	210000

Physical Events

For algorithm tests under best conditions, where only information from the interaction is to be used, one can also resort to the so called physical events. In these events there is no noise included. The advantages are that the energy and angular distribution is like what it is expected in the experiment. The problem with these events is that one does not know exactly if all light is contained even if one takes an event selector to be sure the Monte Carlo vertex is in the fiducial volume of the detector. This means that the distance of an interaction vertex in the xy-plane to the center and the vertical distance to the center are less than 50 m. So most of the calculations are done with the premium events instead of the physical events. The physical events are used to show that the noise has some influence on the resulting performance of the detector.
Table 5.2 shows the number of events after all selection algorithms which were used for the calculations.

Table 5.2: *Number of physical events in each class which can be used for training and testing*

ν_μ charged current	30000
ν_μ neutral current	15000
ν_e	2500

5.2 Identification of shower-like and track-like event signatures

As the electron neutrinos and muon neutrinos oscillate with different probabilities and a contamination of electron neutrinos contradicts the measurement of the mass hierarchy, the identification of event types is necessary. The following chapter deals with the principles of event separation followed by the application to the current problem. Further algorithms of separation are introduced and compared.

5.2.1 Basic Ideas of Identification

In an experiment there are many events. They can be classified into different classes. In our case there are two groups, the track-like events and the shower like events. As depicted in Chapter 2.5 they differ

in their appearance. The goal of separation is to look for quantities describing properties of events in which they are different. The quantities are called features in the following .

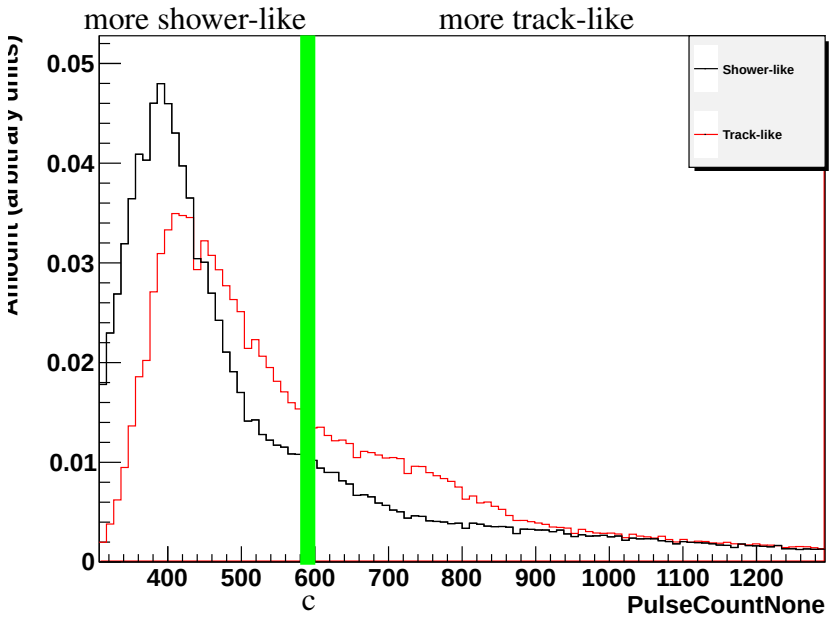

Figure 5.1: *Distribution of the QStrategy-Qualityparameter in Premium-Events*

Figure 5.1 shows the distribution of one feature. For the histogram the feature was calculated for many events. The green line stands for the track-like events and the black one for shower-like events. Here one can see that a decision applied to one event can only be correct up to a certain accuracy as the distributions can overlap. In this easy example a rule of decision could be to take a value c. Consequently, each event with feature greater than c is seen as class 1 and otherwise the event is seen as class 0.
As one can see, the separation due to this single value is not so good and there might be better ways to identify the events, and therefore multi-variate analysis have been developed. All algorithms have in common to optimize many cuts on many features. They can be linear or non linear. This thesis deals with one possibility called the random decision forest. As it was stated in [27] RDFs are quite stable and leads to the best identification results in event classification as it is necessary in neutrino detectors.

5.2.2 Random Decision Forests

In the last chapter the basics of a separation were explained. In the last years one algorithm has become more and more popular: the random decision forest. For example it is used in the event classification of ANTARES [27]. In this thesis the same program package is used.
The forest consists out of many trees leading individually to a separation. However the final step is achieved by making a majority decision of all these trees. Here the majority is not only a single more than 50% question, but the number of trees voting for one case can be a priori chosen arbitrarily as majority. How the trees and forests work in detail is explained in this chapter.
Figure 5.2 shows a tree in the sense of a decision tree. A tree consists of several nodes. In the figure they are symbolized as ellipses. The node at the top side is the root. Each node has some children, the next nodes downwards in the tree. Here there are only two children as there is only a binary decision, track-like or shower-like. But every node is connected to one node before, only. The step from one higher to one lower node represents a decision.

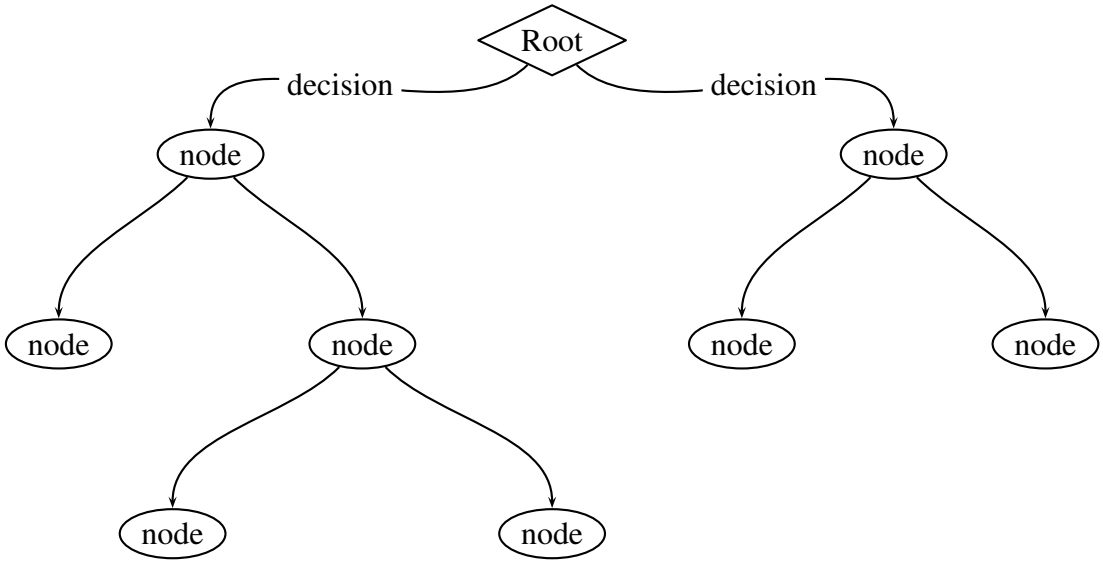

Figure 5.2: *One possible decision tree*

In the classifying phase every event is pushed through the tree. On each node there is a decision and the event is pushed to the one child or the other according to the result of the decision. So the event is classified as more track-like or more shower-like.
The decision process is repeated until the event reaches a leaf, a node without children. The classification is finished at this point. The event is either classified to one class or there is a distinct probability for both classes at each transition from one node to the other there is a decision. How is it possible to find a good decision? First of all, what is done in a decision? In the trees of the random decision forest from [27] a decision makes a cut in one feature. The cut is chosen so that it maximizes the purity or the impurity. The definition

$$i(N) = P(\omega_1) \cdot P(\omega_2) \tag{5.1}$$

is useful. Here $P(\omega_i)$ is the fraction of events of the class i found in the next node. The Gini impurity for multiple class problems defined as

$$i(N) = \sum_{i \neq j} P(\omega_i) \cdot P(\omega_j) \tag{5.2}$$

can be reduced to equation 5.1 for a binary case. The definitions were originally taken from [28].
A major disadvantage of single trees is the low ability to generalize the trained tree. That means to be able to do not only reproduce the features in the training sample. As over-trained trees lead to a reproduction of the training sample. Several methods are proposed to improve the performance. Boosted decision trees are one example. Here one tree is trained more than once. After train one tree the next tree is trained with weighted events. Badly classified events get a higher weight than well classified ones. More iterations are done [29].
In this thesis the approach of random decision forests is used. It works with many trees, too. They are trained simultaneously. Instead of using all features at once for each tree a predefined fraction of features and events is taken. Finally the classification is done by a majority decision of the trees.
A possibility to steer the purity and classification rate is to define other cuts than a 50% majority. (see Chapter 5.4)

5.2.3 Investigation of discriminating Features

The last chapters showed that one should look for features able to distinguish between shower-like and track-like events. In the following chapter the used features are listed and explained how they work. Additionally and more interesting, the chapter tells why they are useful for a separation algorithm.
The features are listed in the order of most impact to the decision. How the impact is measured is described in Chapter 5.3.
There are three different types of plots in the following chapter. One can see them in figure 5.2.3. They have all in common to show the differences of the features according to shower-like and track-like events. At first the energy integrated distributions are the easiest ones. The big drawback for this lies in the inhomogenous distribution of events with respect to the energy, as it is in the real experiment. So the events are weighted according to the appearance in the training files and as one can see in the distributions of event numbers it is an E^{-2}-distribution. Consequently the histogram is dominated by low energy events. We will see these events are the worst ones. As long as there is no adequate weighting of the events this method can be a first hint of any differences. A better way to investigate the distribution is the energy resolved distribution. This distribution bins the events in groups of a small energy range to reduce inhomogeneities within the ranges. So for every energy bin the distribution can be seen in the middle figure. The events are binned with a width of 1 GeV around the integer values. As the human eye cannot resolve such a diagram with much information in it, the third graph is introduced. Here one sees the median of each distribution in the bin. Further the error bar state the 15% and 85% quantiles.

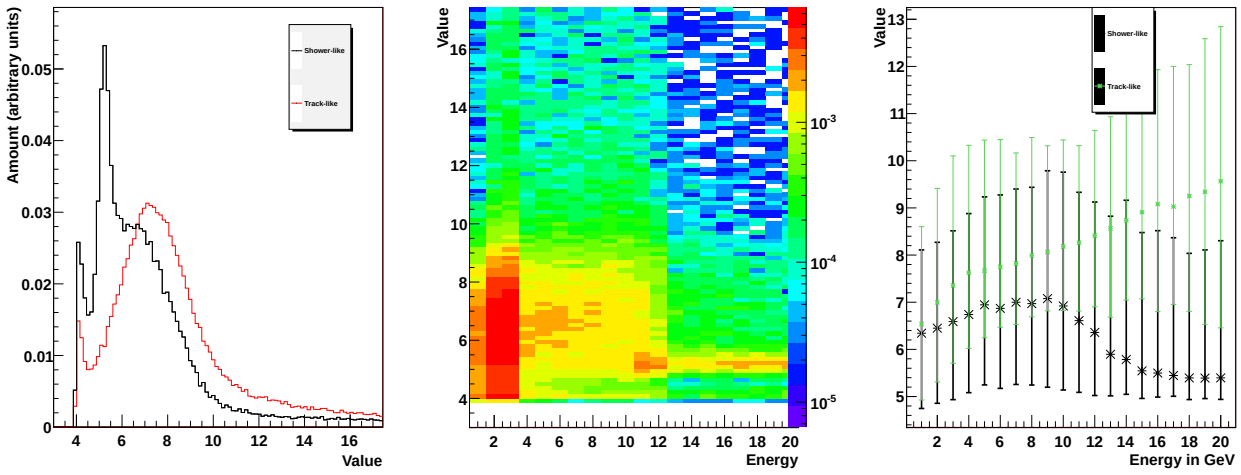

(a) energy integrated (b) energy resolved (c) energy resolved quantiles

Figure 5.3: *different types of plots to investigate the feature distributions*

Quality Parameter of QStrategy

The QStrategy was introduced by Hasankiadeh [30] in ANTARES. It was used to reconstruct shower-like events. The strategy consists of two iterations of reconstruction separated by a hit selection. First, the reconstruction consists of solving an over-constrained set of equations. For a perfect shower the time difference between expected and measured time ΔT, called time-residual, yields

$$\Delta T = \frac{n}{c}|\vec{r}_s - \vec{r}_i| + (t_s - t_i) = 0, \tag{5.3}$$

where the index s indicates the value of the shower vertex, which is to be estimated and i the values of one hit.

Further, the result of the first step is used as seed in the next step, a so-called M-estimator fit. In principle it tries to minimize the sum of all time-residuals. With a suitable function of time residual the effect of outliers can be reduced. [31]
The estimator is defined as follows

$$M = \frac{1}{N} \sum_{i}^{N} 2 * \sqrt{1 + \frac{(\Delta T)^2}{2 * \sigma^2}} + 2. \tag{5.4}$$

Here N is the number of hits used for the calculation. The expected time is calculated assuming the photons coming directly out of the reconstructed vertex and travel with the speed of light to the detection point. So no scattering is taken into account. σ is originally the time resolution of an ANTARES PMT. Here that value is not so important as it only scales the quality parameter. The strategy delivers the final value of M as a quality parameter judging how well the hits fit to a perfect shower.
The minimum is 4 if ΔT equals 0, which equals to a perfect shower-like event. The higher the value the less the event looks like a shower.
The finite range of the feature makes it possible to find a value for non reconstructed events. In these events the observable is set to -1, arbitrarily. Non reconstructed events are caused by non converging algorithms in the QStrategy.

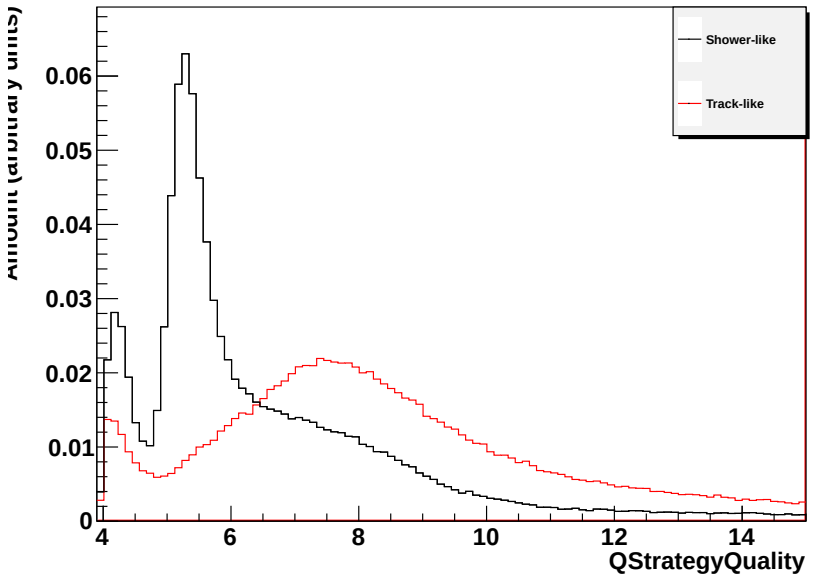

Figure 5.4: *energy integrated distribution of the quality parameter of QStartegy*

Figure 5.4 shows the distribution of the feature. The curve of shower-like events concentrates nearer to the 4 than the curve for track-like events, as expected. Considering the figure a good separation due to this observable is expected. Further in this thesis the QStrategy takes a high rank among the features.
Figure 5.5 shows the distribution in the energy distributed way. As stated above it shows that the discrimination power increases with energy, because more and more energy can be transfered to the outgoing muon. The muon then goes on a longer track which can be identified by the feature.
If the QStrategy is useful also depends on the reconstruction precision, as the reconstructed vertex has an influence on the estimator. A not correctly reconstructed vertex leads to a shift in the values. In the appendix there are figures about the reconstruction accuracy. The algorithm works well. There are no cuts applied, so every reconstructed event is shown in the histograms. The standard deviation in the position is about 20 m without any quality cuts and adaptations to the ORCA detector. This points out that the estimator works quite well for the reconstruction.

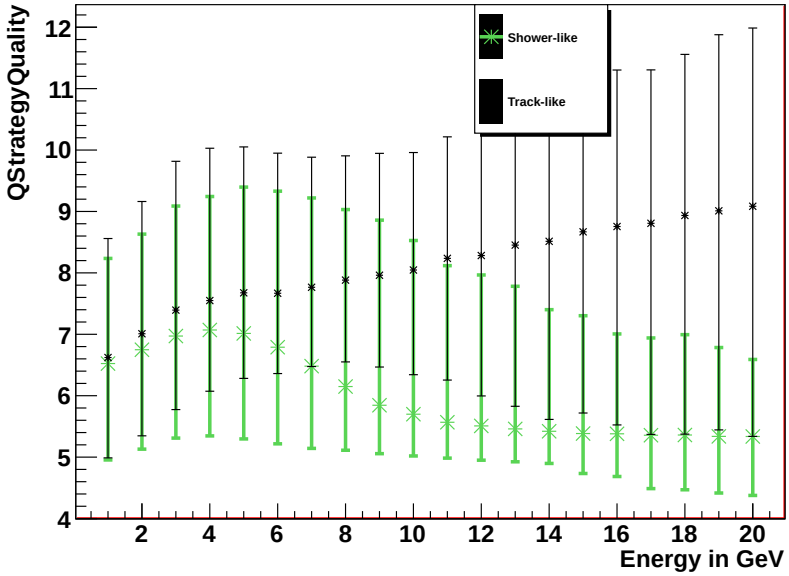

Figure 5.5: *energy resolved profile plot of the quality parameter of QStartegy*

Quality Parameter of FilteringFit

A second reconstruction algorithm optimized for tracks is FilteringFit[32]. It is based on a grid search. At the beginning, a grid of directions is generated. The grid is spread over the search area as uniformly as possible. There is the possibility to search over the whole sky or only on a certain area around a direction. For each direction the following fit is performed.
Further for each direction all hits are rotated in a coordinate system so that the direction points in z-direction. The time is converted to

$$t' = t - zc. \tag{5.5}$$

The goal of the next step is to find the biggest cluster of hits connected to each other. Connected means here that they have their origin on the same muon track. It is claimed

$$c\kappa(|t'_A - t'_B| - t_{\text{extra}} \leq \sqrt{(x_A - x_B)^2 + (y_A - y_B)^2} \tag{5.6}$$

with

$$\kappa = n_{\text{group}} / \sin\theta_C - 1/tan\theta_C. \tag{5.7}$$

t_{extra} is introduced to be aware that not all photons travel directly from the track to the point of detection due to scattering. And the predefined direction is not the actual track direction. Further a cut on the transversal distance of two hits is done.
With the selected hits a linear fit is performed as described in [33]. The fit is based on the time differences between consecutive hits.
The fit writes out a χ^2-value calculated by

$$\chi^2 = \sum_i \frac{(t_i - t_{i;\text{expected}})^2}{\sigma_i^2} \tag{5.8}$$

where σ reflects the uncertainties of the hit's time properties. As reconstructed tracks based on a low number of hits can achieve a very high χ^2 even if the reconstruction cannot be so accurate due to the lack of information. The final track quality classifier Q combines the number of hits with χ^2.

$$Q = N_{\text{hit}} - \omega\chi^2/N_{\text{DOF}} \tag{5.9}$$

This quality parameter favors results with more used hits over results with a low number. ω is a weighting factor, which can be optimized. The standard filteringfit routine takes the best results of this strategy and passes it into a further reconstruction algorithm for a finer reconstruction. The aart-Strategy is used which is a likelihood strategy.
For the same reasons as for QStrategy the reconstruction quality of FilteringFit is important for the benefit of the strategy. In the appendix, you can see the different quality plots of FilteringFit. There you can see that the algorithm reconstructs muon neutrino events quite well up to an RMS of 5 degree in the zenith. The best results can be achieved in looking to the muon neutrino direction in charged current events. The same you can see for electron neutrinos. For more details see the Appendix. Over all the reconstruction without any cuts works well for track-like events. However events with a leaving electron are reconstructed closely with the same accuracy.

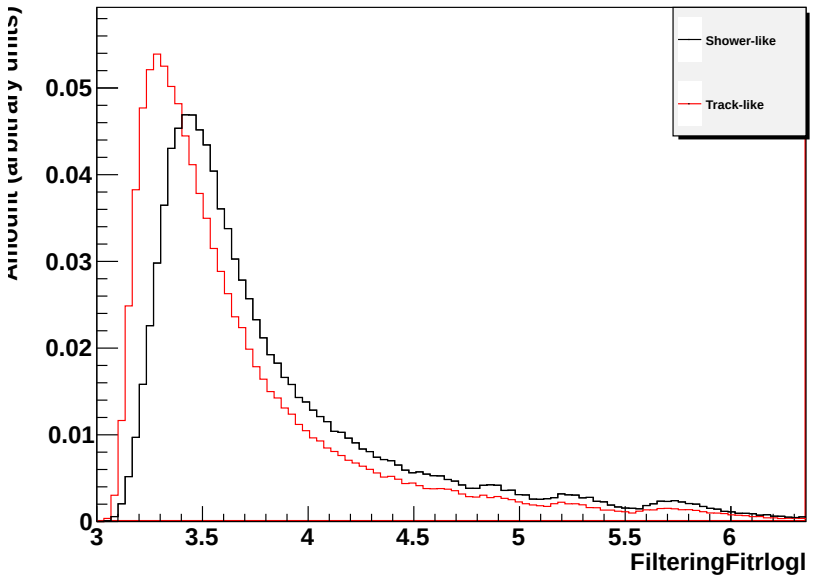

Figure 5.6: *energy integrated distribution of the quality parameter of FilteringFit*

Figure 5.6 shows the distribution of the quality parameter. At the first glance there is no big difference between the two types of events. Also in the energy resolved plot (Figure 5.7) no big difference is recognized except in the high energy regime. In that regime there are less events with high values as in shower-like events. However there is no big difference in the distribution resulting in a bad performance in the separation. Indeed at the final ranking (see Chapter 5.3) of features the FilteringFit feature is at a very high rank.
Nevertheless thinking about FilteringFit is useful as it is mostly used as a reconstruction algorithm resulting in the starting point for more features.

Ratio of Number of Hits in certain Event Regions

In the reconstruction algorithms described above there were several hit selectors. They choose hits out of the whole event with certain properties. For example one can choose all hits which can be assumed as shower hits, that means e.g. they are causally connected to a vertex under a shower hypothesis. On the other side one can take a track hypothesis and look for hits which are causally connected to that assumption. In particular here the selections of hits are chosen according to a shower hypothesis around the reconstructed shower vertex. Further, the endpoint of the track is chosen as shower hypothesis. The endpoint is estimated by the last point of back projected hits on to the reconstructed track. The last sample consists of the hits correlated to the track hypothesis. All hits are selected which are causally connected to the track hypothesis.

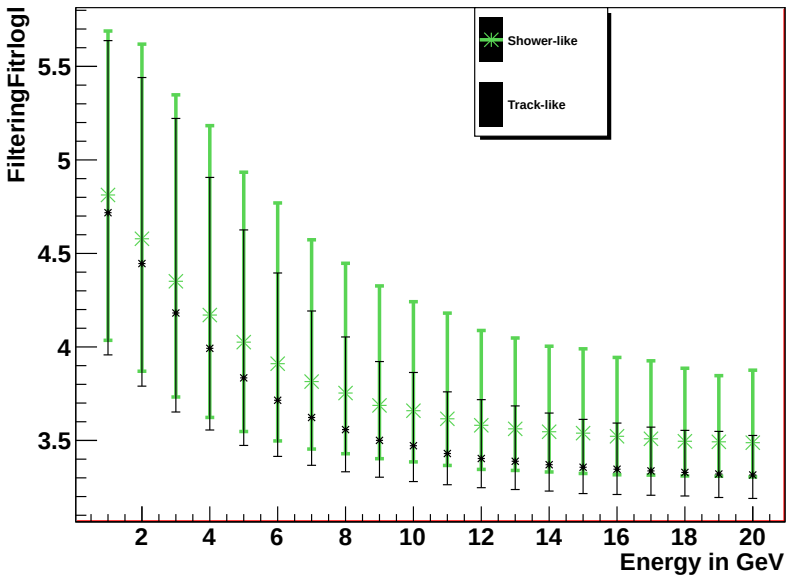

Figure 5.7: *energy resolved distribution of the quality parameter of FilteringFit*

Out of these samples some ratios between the number of hits are calculated. The ratios and their names are defined in table 5.3.

Table 5.3: *Definition of Hit-Selection-Numbers: S:Sample of Hits at the starting point, E: Sample of Hits at the endpoint, T: Sample of Hits at the track, A: All Hits*

Name	Definition
CounterEndAll	$\frac{n(E)}{n(A)}$
CounterEndEndTrack	$\frac{n(E \cap T}{n(E)}$
CounterStartAll	$\frac{n(S)}{n(A)}$
CounterStartStartEnd	$\frac{n(S \cap E)}{n(S)}$
CounterStartStartTrack	$\frac{n(S \cap T)}{n(S)}$
CounterTrackAll	$\frac{n(T)}{n(A)}$

The Figures 5.8 and 5.9 show the two most favored distributions, as they deliver the best discrimination power. The graph of track-like events can be explained by a longer track with higher energy, so the hits do not overlap so much in higher energy regions. On the other side as there should be no good track in shower events the number of hits associated with the endpoint is low. So also complete features lead to a smaller values.
The distribution of $\frac{n(A)}{n(S)}$ shows also a good separation for higher energy regions.

Number of Hits

The next feature deals with the number of hits in one event. The number of events are not so different. The numbers mainly differ in the width of the distribution. That comes from the statistics according

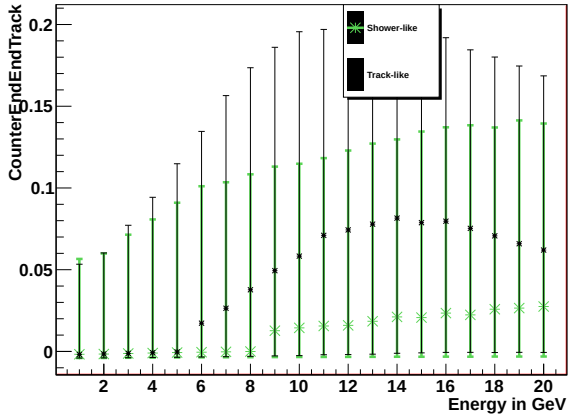

Figure 5.8: *Distribution of* $\frac{n(E \cap T)}{n(E)}$

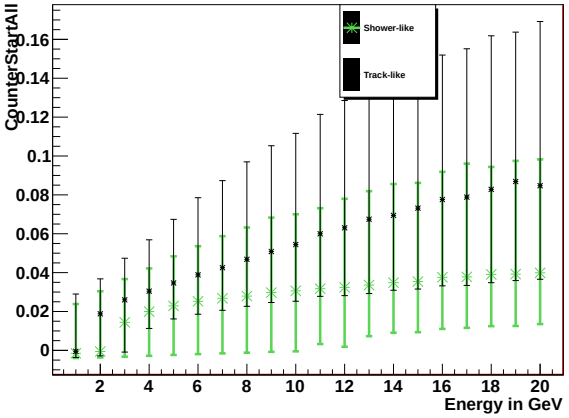

Figure 5.9: *Distribution of* $\frac{n(S)}{n(A)}$

to the hadronic cascades in the events. As the hadronic parts have higher underlying fluctuations the shower-like events have a more widened distribution. The lower median comes out of the fact, that there is the possibility of neutral particles, which transport the energy without delivering photons to the detector.

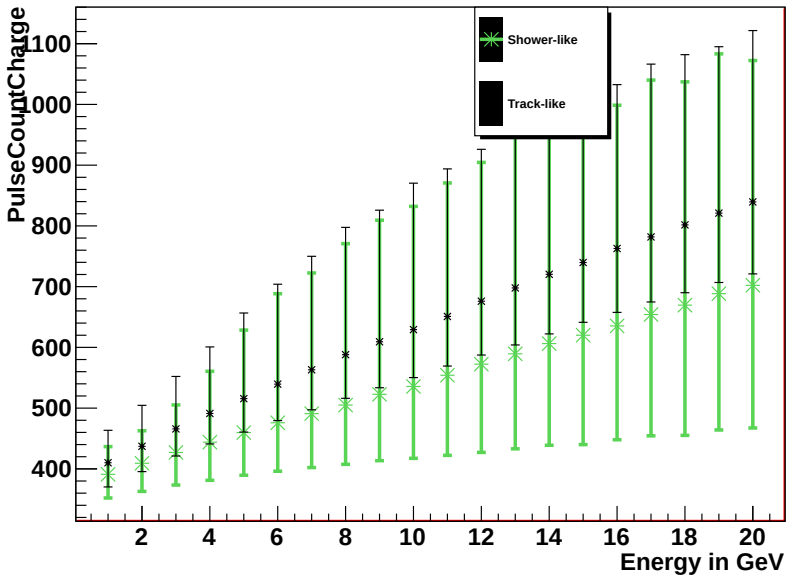

Figure 5.10: *energy resolved distribution of the number of hits weighted with the charge*

In this analysis two kinds of number of hits are studied. First the hits are not weighted and secondly the hits are weighted according to their charge which they cause in the PMTs. Both distributions show the same features.

Time Residuals

Inspired by the thesis of [34] the time residuals are used as a feature. The time residual is defined as the difference between the expected and the actual arrival time of photons under a certain hypothesis at the detector.

$$\text{Time Residual} = \text{expected time} - \text{time of flight} \tag{5.10}$$

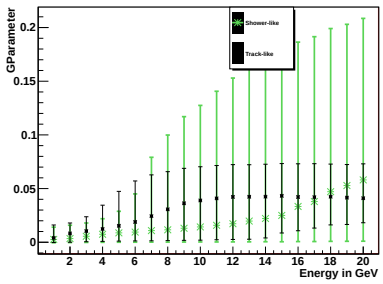

Figure 5.11: *energy resolved distribution of the GParameter*

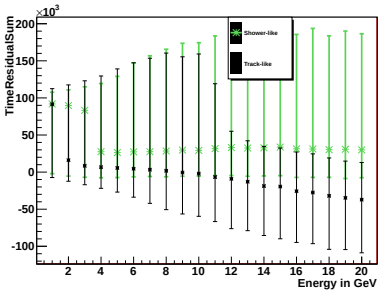

Figure 5.12: *energy resolved distribution of TimeResidualSum*

Both times are different due to scattering on the way to the detector and due to inaccuracies with in the detection unit. Further the hypothesis is an ideal model of photon emission and propagation. For example the shower is not point-like. The particles coming from the shower vertex are producing light on the way outwards. In the thesis mentioned above the time residuals are used to reconstruct the trajectory of the particles in Kamiokande. The goal is to minimize the width of the distribution of time residuals, as in a perfect event the time residuals would be sized to zero.
Enabling the algorithm to get even more information further properties of the distribution are calculated. The values are defined in table 5.4. Additionally, one could introduce higher momenta of the distribution.
For time residuals there has to be a reconstruction result. As in some cases there is no reconstruction for the events. The mean of all hits is taken, resulting in the double peak structure in some distributions of the calculated features related to the time residuals. The time residuals are calculated according to a shower hypothesis.
In the reference introduced above the reconstruction is done with the estimator

$$G = \frac{1}{N}\sum_i \frac{1}{\sigma_i}\exp -\frac{(t_i - t_o)^2}{2(<\sigma> \cdot 1.5)^2}. \tag{5.11}$$

Here σ_i is the inaccuracy of the measurement, which is introduced to take the errors into account. N is the number of hits used for the calculation. The difference is the time residual. Using the exponential function big outliers are suppressed. The distribution for this feature is shown in figure 5.11.
The impressing fact of the feature is that for track-like events the median of the feature remains up to 10 GeV constant and then raises. In the case of shower-like events it is the other way round.
Further features based on time residuals are tested. One of the best is shown in figure 5.12. The median of the feature is negative for track-like events and positive for shower-like events. The hits of shower-like events occur too early with respect to the shower hypothesis where as the other hits are rather too late.
The other features can be found in the table 5.4 and the figures are shown in the appendix.

Time Differences

Similar to the time residuals one can define the time differences Δt.

$$\Delta t = \text{Time of Vertex} - \text{Time of Arrival} \tag{5.13}$$

So hits which are far away from the vertex will lead to a higher absolute difference. One example is shown in figure 5.13. The median of the feature is lower for track-like events than for shower like events. The muon goes out of the interaction vertex and makes it possible that photons can reach optical modules which are further away, than it would be possible in a shower event.
The other features which are already introduced in a similar way with respect to time residuals are shown in table 5.5.

Table 5.4: *Definition of features related to time residuals*

Name	Definition
TimeResidualWidth15_85	difference of 15%-quantile and 85%-quantile
TimeResidualFWHM	full width half maximum
TimeResidualRMS	root mean square
TimeResidualMean	mean time residual
TimeResidualMedian	median time residual
TimeResidualMaximum	maximum of time residuals
TimeResidualMinimum	minimum of time residuals
TimeResidualSum	sum of all time residuals
TimeResidualExp	$G = \frac{1}{N}\sum_i \frac{1}{\sigma_i} \exp - \frac{(t_i - t_o)^2}{2(<\sigma> \cdot 1.5)^2}.$ (5.12)

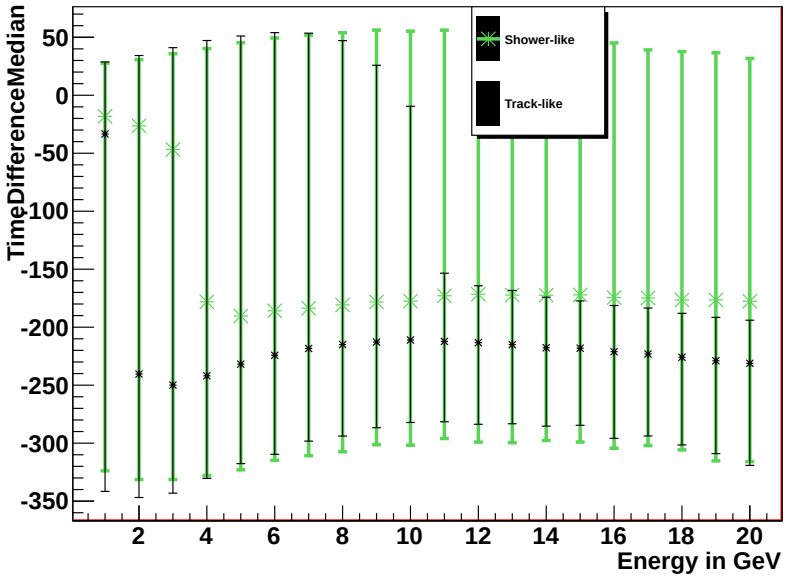

Figure 5.13: *energy resolved distribution of TimeDifferenceMedian*

Table 5.5: *Definition of features related to time differnce*

Name	Definition
TimeDifferenceWidth15_85	difference of 15%-quantile and 85%-quantile of the distribution
TimeDifferenceFWHM	full width half maximum of the distribution
TimeDifferenceRMS	root mean square of the distribution
TimeDifferenceMean	mean time differnce
TimeDifferenceMedian	median time differnce
TimeDifferenceMaximum	maximum of time differnce
TimeDifferenceMinimum	minimum of time differnce

Tensor of Inertia

The shape of a body can be described by the tensor of inertia. From its origin the tensor describes the mass distribution of a body. Here it describes the distribution of hits around a center. As center the

reconstruction result of the QStrategy is taken, if it is available otherwise the mean of all hits is used. The tensor of inertia is defined as following:

$$I = \begin{pmatrix} \int (y^2 + z^2)\mathrm{d}m & -\int xy\mathrm{d}m & -\int xz\mathrm{d}m \\ -\int xy\mathrm{d}m & \int (x^2 + z^2)\mathrm{d}m & -\int zy\mathrm{d}m \\ -\int xz\mathrm{d}m & -\int zy\mathrm{d}m & \int (y^2 + x^2)\mathrm{d}m \end{pmatrix} \tag{5.14}$$

where dm symbols the integration over all hits. dm originates from the definition of the tensor of inertia for a massive body. x, y, z states the coordinates according to the center.

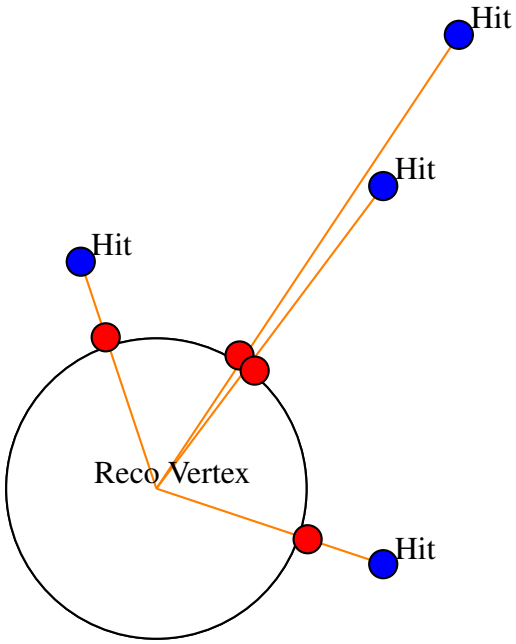

Figure 5.14: *Projection of hits onto a sphere*

At first glance the axis can be chosen arbitrarily. Increasing the compatibility and usage of the resulting values the main centroid axis of each event is chosen. In this representation the matrix is diagonal. The calculation is done by calculating the eigenvalues of the matrix with arbitrary axis. The calculation is done with functions of ROOT [35].
The calculation of the previously defined tensor can be done directly or when one first projects all hits to a unit sphere.
Further all hits get a weight of the inverse number of hits in the event, results in an equal overall mass of the events. So the values of the inertia is comparable between the events.

Table 5.6: *Definition of features connected to the tensor of inertia*

Name	Definition
SmallInertia	Smallest eigenvalue of the tensor
MiddleInertia	middle eigenvalue of the tensor
BigInertia	Biggest eigenvalue of the tensor
RelativeInertia	$\frac{I_S}{I_S+I_M+I_B}$

The values of MiddleInertia and BigInertia are nearly similar for track-like and shower-like events. In the case of the small Inertia there is the biggest difference. The values are shifted to smaller values

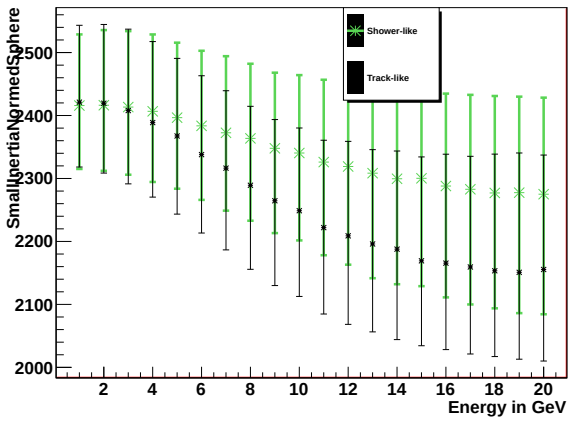

Figure 5.15: *Distribution of the smallest eigenvalue of the projected tensor of inertia*

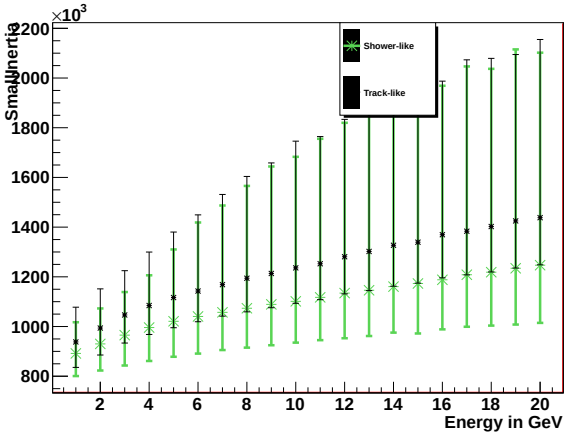

Figure 5.16: *Distribution of the smallest eigenvalue of the tensor of inertia*

for track-like events. Considering the shape of a track-like event the figure should be longer but not so extended to the sides. A fairly good discrimination can be expected for this feature.
Further both figures show that the feature with projected hits could be better than the other one.
In the energy integrated plots there are two peaks as there are two different methods of generating the center of calculation. On the one side there is the reconstructed vertex of QStrategy and on the other side a mean value of all hits in the event. In common the mean leads to the center of the detector, as the whole detector is filled with noise. In these events one does not expect any information out of the tensor of inertia as the position of the event can be far away and so does not have any influence. Indeed the first peak in figure 5.17 is out of unreconstructed events.

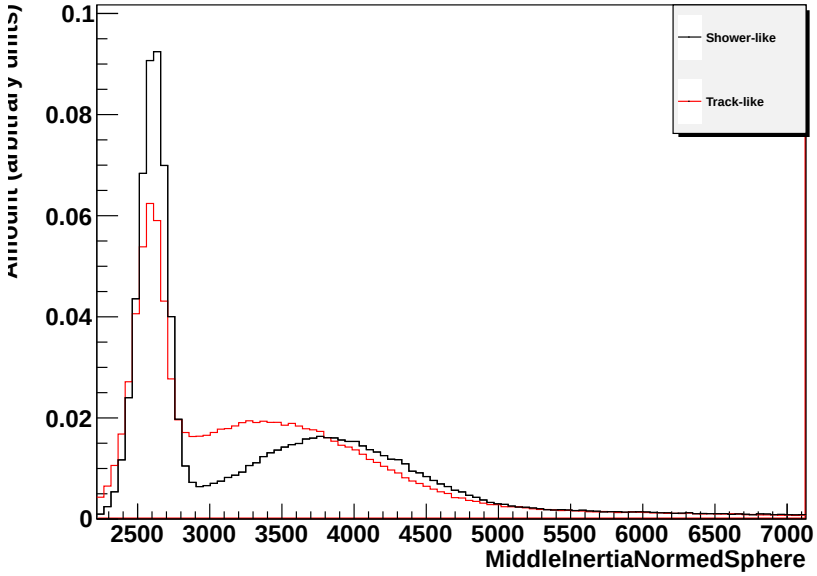

Figure 5.17: *energy resolved distribution of the smallest eigenvalue of the tensor of inertia*

Further a ratio is defined as

$$R = \frac{I_S}{I_S + I_M + I_B} \tag{5.15}$$

but there is no separation power expected.

5.3 Ranking of Features

After training the first time it is interesting to see a ranking of the features. A ranking is useful as features with a low or even no improvement to the classification result can be canceled. This saves computing time. The ranking should tell us which observable performs best, in the sense of leading to a big improvement of the classification. For a ranking there must be a value. Here it is the overall classification rate under a majority decision of 50%.
The ranking is done by, a tool from Stefan Geisselsöder [36] called ̈featureOptimization.
The principles are as follows . A training is started with each feature on its own. Further for each result the performance is calculated and the best feature are taken to the next step. In the next step the algorithm adds one more observable and does the training once more. This is done for every possible configuration. Now the best configurations are chosen to do more iterations in the same way. This process iterates as long as the performance increases. Finally there is a ranking with the best features. In this thesis the 3 best configurations to one previous configuration are taken into account to decide which 3 of them are pushed to the next iteration.
In table 5.7 you can see the ranking of features used in the classification. One can recognize that some features do not lead to an improvement of performance at all. There are two reasons why that could happen. First features can have no separation power at all. Secondly there are other features deliver the same information so they are not independent of each other. In words of linear algebra: The goal is to find features which are as orthogonal to each other as possible. So that they do not share any properties of the events.
The table also shows the improvement the value of the overall classification rate after the new feature was introduced. As one can see the last features improved the classification only by one percent.

Table 5.7: *Ranked Feature List*

Rank	Feature	Overall Classification Rate
1	GParameter	0.5823
2	TimeResidualFWHM	0.6702
3	SmallInertiaNormedSphere	0.6995
4	CounterEndEndTrack	0.7175
4	SmallInertia	0.7212
5	TimeResidualMeanDistance	0.7259
6	CounterTrackAll	0.7284
7	RelativeInertia	0.7314
8	QStrategyQuality	0.7332
9	HitsPerTrackLength	0.7368
10	TimeDifferenceWidth15_85	0.7377

5.4 Training and Evaluation

5.4.1 Weighting of the Training Events

Not every event in the test sample comes up with the same rate in the experiment. To deal with this the events can be weighted in the evaluation. Events with a lower rate have a smaller impact to the result as events with a higher rate.
If events are generated under real conditions in a Monte Carlo simulation the lifetime is an important impactor. The lifetime is the time the simulated processes would take in reality. As the different particles are simulated with different algorithms the samples of each simulation are combined. If one does not consider the lifetime a sample with higher lifetime dominates simulations with less lifetime.

In this thesis there is no proper weighting as there are some ingredients not known very well. For the weight one needs the flux of neutrinos through the detector, which could be approximated with the flux from other sites as [14]. The physical events are weighted with the Bartol flux, but as there is no lifetime for electron neutrinos it is not possible to generate a weight. Further for premium events the rates are not known at all in the detector.
Following the events are weighted so that there is an equal amount of electron neutrinos and muon neutrinos in each sample The differences in the energy regime can be neglected as the evaluation is done in small bins in energy. The width of the bins is chosen to be 1 GeV. In the premium events the width of a bin is effectively even smaller as the events are only out of an interval 0.1 GeV above and below a full GeV. The dependence in the zenith is neglected.

5.4.2 Confusion Matrix

Once the separation algorithm is applied to the test events one can illustrate them within a confusion matrix. The matrix shows the distribution of the different results of the separation process. So it answers the question if the events were classified correctly.
The matrix consists of nine entries arranged in a grid of three by three. The entry of one cell is the number of events with the same outcome of the classification process. The rows stand for the real class, consequently the columns stand for the reconstructed class. In the following the number of row and column are numbered from 0 upward. This leads to the next example. The class 0 event reconstructed as class 1 increases the entry in column 1 and row 0. The outer cells are the sums of the cells in the column or row. Table 5.8 shows an example.

Table 5.8: *Confusion matrix*

	reconstructed class 0	reconstructed class 1	Sum of real class
real class 0	correctly classified	wrong classified	
real class 1	wrong classified	correctly classified	
Sum of reconstructed class			

As the number of training and test events are finite, on each entry of the matrix there is an error. The errors can be seen as binomial errors, because each event has a choice of two different outcomes. Either it is correctly classified or it is wrongly classified. According to [37] the error is calculated in the following way:

$$\Delta p = u_{(1-\alpha)/2} \sqrt{\frac{p(1-p)}{n}} \tag{5.16}$$

where p is the resulting probability of the result in the specific cell. n is the number of events used. It is important to be aware that the number of events counting for the entry are only the sum of the row. This is caused as no event can switch rows. The event is either a class 1 event or a class 0 event. Further u_x is the x-Quantile of the normal distribution.
According to the consideration above the confidence interval is given with

$$P(p - \Delta p \leq p \leq p + \Delta p) = 1 - \alpha. \tag{5.17}$$

This method is only an approximation of the binomial distribution with the normal distribution. This is possible in some cases, because of the central limit theorem. It requires that $np(1-p) \geq 9$. This is true for the interesting cases shown here, where the purity and classification rate is balanced.
When the values changes so that p or 1-p get closer to 1 the requirement is no longer fulfilled. The incorrectness of the calculated values are indicated by the error bars reaching over 1 in the plots of Chapter 5.5.

If one is interested in these ranges one has to use other calculations. One possibility are the Pearson-Clopper-Values [37]:

$$p_{low} = \frac{mF_{2m,2(n-m+1),\alpha/2}}{n-m+1+mF_{2(m),2(n-m+1),\alpha/2}} \tag{5.18}$$

and

$$p_{high} = \frac{(m+1)F_{2m+1,2(n-m),1-\alpha/2}}{n-m+(1+m)F_{2(m+1),2(n-m),1-\alpha/2}} \tag{5.19}$$

with the quantiles of the F-distribution. However, in the following, only the approximative error is used as the interesting values are in the range of the central limit theorem.
Up to now there are only errors for the single entries in the inner part of the confusion matrix. The outer part values corresponding to purity and classifiaction rate are assembled quantities. Error propagation has to be used. Here Gaussian error propagation is used.
If one has got the weights of the events the values have to be modified slightly. The point value of p can be estimated as

$$p = \frac{\sum_i \omega_i}{\sum_n \omega_n} \tag{5.20}$$

where the denominator is the weighted sum of all events corresponding to the entries and the nominator is the weighted sum over all events.

5.5 Performance of the Algorithm

A visualization of the confusion matrix is used to better compare different parameters of the random decision forest. The matrix shows only the number of events in several classes. We have to look for numbers which are interesting to make a decision for the one or the other classification algorithm. First of all within one algorithm to find the best cut value of the output variable. In the case of random decision forests the percentage of trees voting for a class in the random decision forest is one example of such a variable.

5.5.1 Definitions

There are many ways of evaluating the performance of the algorithms, as there are many purposes using the algorithms. In conclusion every one has to choose the best performance for his own purpose and is looking for a way of evaluating the algorithms. In ORCA the goal is to count muon neutrinos interacting in the charged current. As the experiment is counting the track-like events, the quality parameters are developed in that direction. Firstly the number of correctly classified events has to be as big as possible. On the flip side the number of events contaminating the sample as wrongly classified events has to be as low as possible. As we will see these are two contradictory requirements. The first one is evaluated by the classification rate. It is defined by the ratio of correctly classified events of track-like events with respect to the complete number of track-like events.

$$\text{Classificationrate} = \frac{\text{Number of correctly classified track-like events}}{\text{Number of all track-like events}} \tag{5.21}$$

The latter property is evaluated by the purity defined as

$$\text{Purity} = \frac{\text{Number of correctly classified track-like events}}{\text{Number of all events classified as track-like events}} \tag{5.22}$$

The two different definitions are illustrated in figure 5.18. One has to be aware of the fact that the numbers are based on different underlying sets.

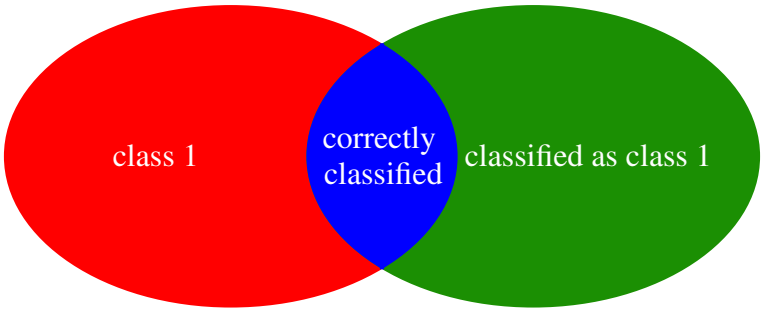

Figure 5.18: *evaluative Quantities*

In order to make a decision one has to investigate which influence is more severe to the own experiment. Is the contamination of other classes worse than the loss of events?

5.5.2 Performance Plots

The following plots are similar to receiver operating characteristic curves (ROC-curve) showing the false-positive versus the true-positive rates [29]. However, as for ORCA other values are of importance, classification rate is plotted against purity.

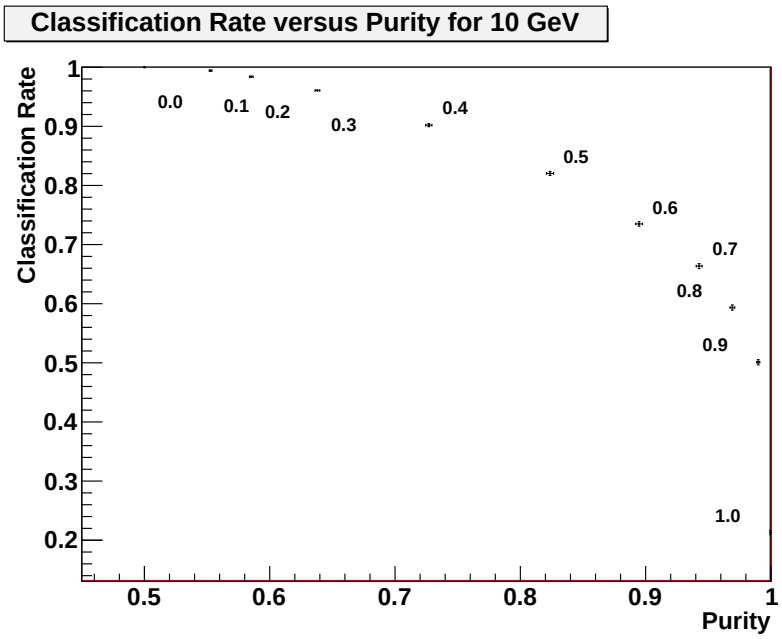

Figure 5.19: *typical plot of Quality for classifier with an output value*

One typical plot is shown in figure 5.19. Each point stands for the pair of numbers resulting from by the cut on the classifier output labeled next to the point.
The main statement is the increasing purity by decreasing classification rate and vice versa. This is justified by the next plot. Figure 5.20 illustrates the distribution of the output values for the classifier. As expected the mean of the distributions are distanced. How ever the distributions overlap, so there is no absolutely true cut. The higher the cut value the more of the lower distribution is rejected, but on the other side the more of correct distribution is rejected, too. So the purity increases at the expense of the classification rate.

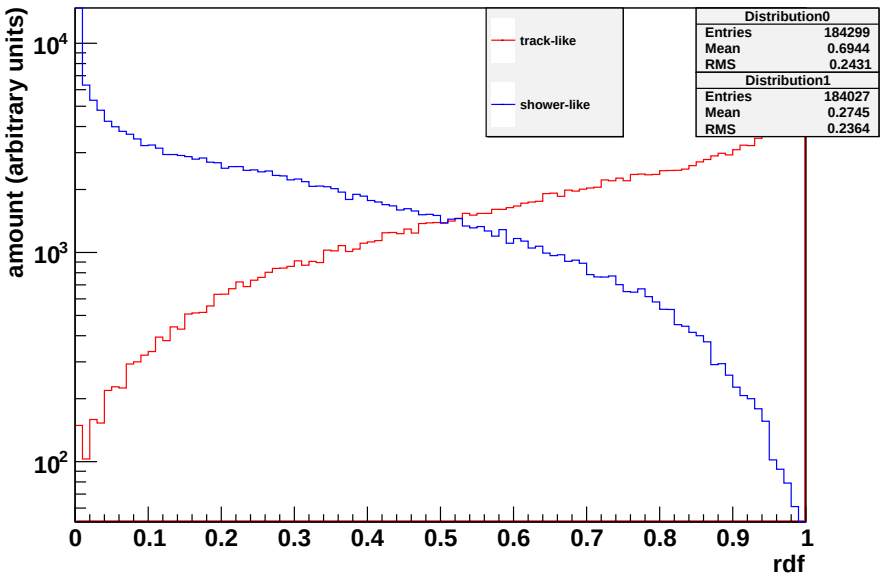

Figure 5.20: *Distribution of a classifier output value; here the distribution of the rdf outputvalue for Premium Events 25 observables*

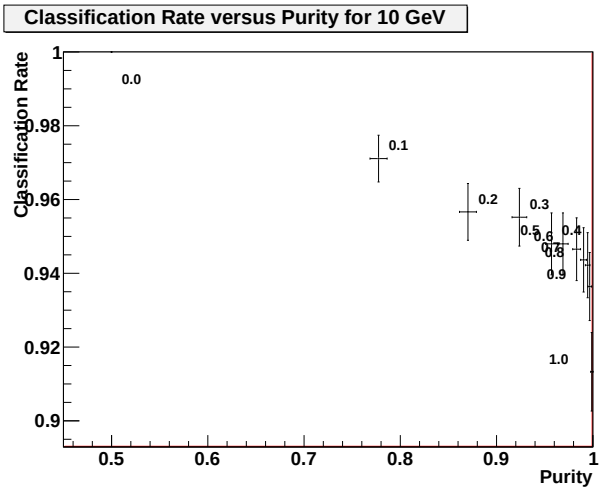

Figure 5.21: *Performance plot with physical events (without noise) at 10 GeV*

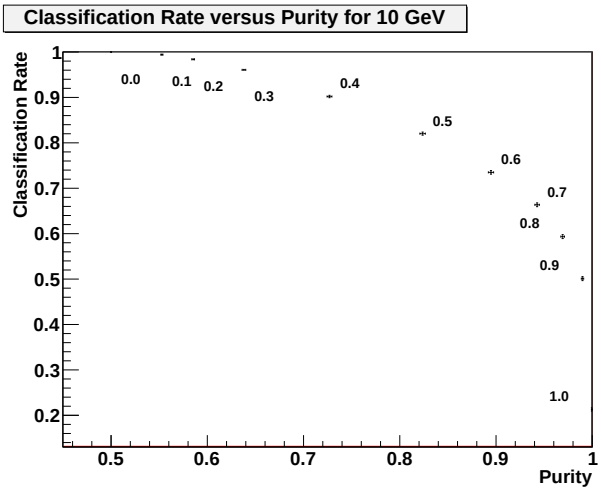

Figure 5.22: *Performance plot with physical events (with noise) at 10 GeV*

5.5.3 Performance Results

This section shows the actual results of the random decision forest. Figure 5.21 shows the case without noise. The values of purity is above 90% and for classification rate it is similar at a cut value of 0.3 and higher.

The more interesting part is the performance plot of premium events shown in figure 5.22. Here one can see the clear shape of increasing purity with decreasing classification rate. One can achieve a purity of 80 % with a classification rate of 80%. So the noise has a negative influence, but it is only on the order of ten percent.

Both plots were shown for the energy bin of 10 GeV. The whole energy range can be seen in figure 5.23.

You can see a reasonable classification is done above an energy of 8 GeV. The small number in the plot indicates the cut value of the random decision forest at this plot region again.

The values of classification rate and misidentification should be included in calculation for sensitivity.

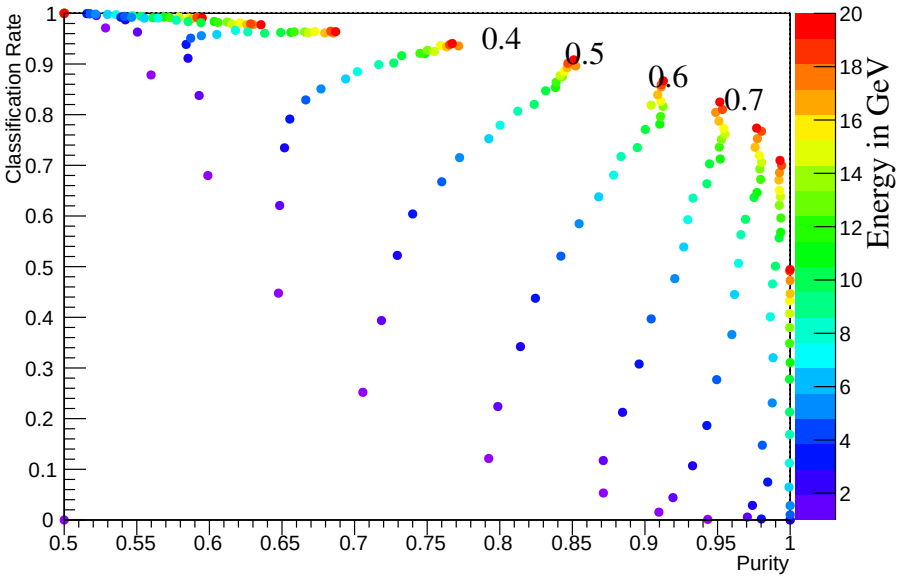

Figure 5.23: *Performance plot with premium events (number indicate the cut value in that region)*

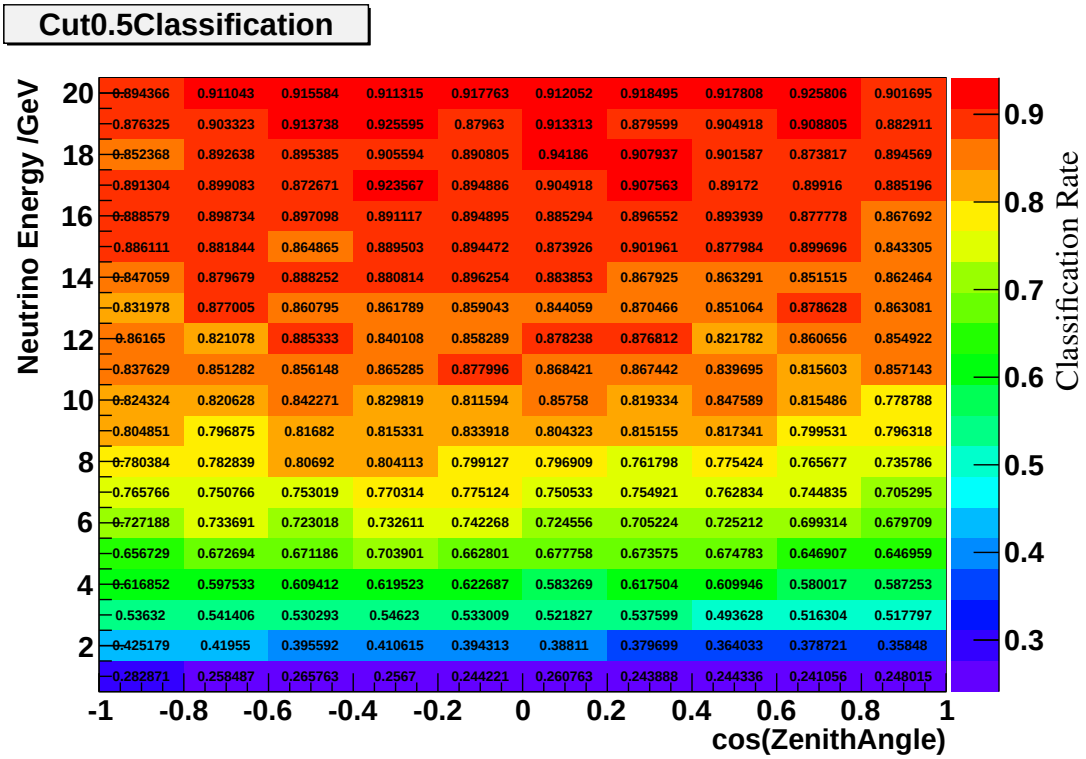

Figure 5.24: *Zenith dependence of classification rate at cut of 0.5*

So it is also interesting if the evaluative parameters are zenith dependent. The studies showed that there is no angular dependence. One exemplary plot is shown in figure 5.24. As you can see the classification performance is flat over the zenith angle, indicated by the same color code in all zenith angle bins. However a clear variation is seen with energy. The same appearance can be detected for other cuts than 0.5 and the classification rate.

Future reconstruction algorithms can also aim to the Bjorken-y of an event. To be able to deal with this the correlation between Bjorken-y and the purity is investigated.

Figures with other cut values can be found in the appendix.

Chapter 6

Conclusion and Outlook

This thesis deals with the necessary identification of event classes in ORCA, as other neutrinos than muon neutrinos would contaminate the result. They would weaken the ability to achieve the discrimination of the possible mass hierarchies.
The identification was done with a random decision forest, a well tested multi-variate analysis technique for separation. Several features have been devised to be able to perform cuts on them. The features concerning the time residuals showed the best performance. There are some of these among the top performer in the final ranking. Especially the width of the time residual distribution is a good feature.
The studies showed that one only needs to look at muon neutrinos in both currents and electron neutrinos in the charged current as the electron neutrinos in the neutral current look similar to the muon neutrinos. But it is necessary to look at electron neutrinos as shown. In this low energy regime they do not look like other shower events. It is possible that an electron comes out of the shower region and beheaves in a way like a muon. So the distributions can be regarded as an intermediate state of neutral current and charged current events of muon neutrinos.
With a set of over 30 features the forest was trained and is performing well. The result shows a purity over 80% at a classification rate over 80% at energies above 8 GeV.
Even if in this low energy regime one expects only less differences between the different classes, with the used method the identification is possible.
Preliminary results have already been used to evaluate the impact to the sensitivity to the mass hierarchy in a bachelor thesis [7]. There one can see that most information can be extracted out of the muon neutrinos. The usage of flavor identification leads to no increasing separation power for the mass hierarchy if one takes the other inaccuracies of reconstruction also into account. In conclusion to improve this fact the classification rate and purity would have to be increased.
Using the results in other studies it is also interesting if there are some dependencies in events variables others than energy. This increases the accuracy of the results. There was no big influence found in the zenith angle. But as one expects the Bjorken y has a big influence. High values lead to a low energetic muon neutrino so that such events do not differ from real shower like events.
The results of this thesis will be helpful to study the influence of several parameters, such as to the sensitivity of ORCA to the mass hierarchy.

Bibliography

[1] B. Pontecorvo. Inverse beta processes and nonconservation of lepton charge. *Sov.Phys.JETP*, 7:172–173, 1958.

[2] R. Davis, D. S. Harmer, and K. C. Hoffman. Search for neutrinos from the sun. *Phys.Rev.Lett.*, 20:1205–1209, 1968.

[3] Q.R. Ahmad et al. Direct evidence for neutrino flavor transformation from neutral current interactions in the Sudbury Neutrino Observatory. *Phys.Rev.Lett.*, 89:011301, 2002.

[4] DAYA-BAY Collaboration. Observation of electron-antineutrino disappearance at Daya Bay. *Phys.Rev.Lett.*, 108:171803, 2012.

[5] E. K. Akhmedov, S. Razzaque, and A. Y. Smirnov. Mass hierarchy, 2-3 mixing and CP-phase with Huge Atmospheric Neutrino Detectors. *JHEP*, 1302:082, 2013.

[6] KM3Net Collaboration. Km3net- opens a new window on our universe. `http://www.km3net.org`, September 2013.

[7] V. Ludwig. Elektronneutrino-untergrund bei der bestimmung der neutrinomassenhierarchie mit orca. Bachelor's thesis, FAU Erlangen Nürnberg, September 2013.

[8] C. Guinti and C. W. Kim. *Fundamentals of neutrino physics and astrophysics*. Oxford University Press, Oxford/New York, 2007.

[9] G.L. Fogli, E. Lisi, A. Marrone, D. Montanino, A. Palazzo, et al. Global analysis of neutrino masses, mixings and phases: entering the era of leptonic CP violation searches. *Phys.Rev.*, D86:013012, 2012.

[10] KamLAND Collaboration. Precision Measurement of Neutrino Oscillation Parameters with KamLAND. *Phys.Rev.Lett.*, 100:221803, 2008.

[11] Super-Kamiokande Collaboration. A Measurement of atmospheric neutrino oscillation parameters by SUPER-KAMIOKANDE I. *Phys.Rev.*, D71:112005, 2005.

[12] A. de Gouvea, J. Jenkins, and B. Kayser. Neutrino mass hierarchy, vacuum oscillations, and vanishing |U(e3)|. *Phys.Rev.*, D71:113009, 2005.

[13] C. H. Albright. Normal vs. inverted hierarchy in type i seesaw models. *Physics Letters B*, 599(34):285 – 293, 2004.

[14] M. Honda, T. Kajita, K. Kasahara, and S. Midorikawa. Improvement of low energy atmospheric neutrino flux calculation using the jam nuclear interaction model. *Phys. Rev. D*, 83:123001, Jun 2011.

[15] B. Pontecorvo. Neutrino Experiments and the Problem of Conservation of Leptonic Charge. *Sov.Phys.JETP*, 26:984–988, 1968.

[16] ANTARES Collaboration. Neutrino oscillations. http://antares.in2p3.fr/Overview/particle.html, October 2013.

[17] Adam M. Dziewonski and Don L. Anderson. Preliminary reference earth model. *Physics of the Earth and Planetary Interiors*, 25(4):297 – 356, 1981.

[18] R. Gandhi, C. Quigg, M. H. Reno, and I. Sarcevic. Ultrahigh-energy neutrino interactions. *Astropart.Phys.*, 5:81–110, 1996.

[19] J. A. Formaggio and G. P. Zeller. From ev to eev: Neutrino cross sections across energy scales. *Rev. Mod. Phys.*, 84:1307–1341, Sep 2012.

[20] KM3Net Collaboration. Km3net- opens a new window on our universe. http://www.km3net.org/images-DOM.php, August 2013.

[21] M. CIRCELLA, P. COYLE, and P. KOOIJMAN. The digital optical module (dom) of the km3net detector. *Proceedings of the 33rd International Comsic Ray Conference, Rio de Janeiro*, 2013.

[22] The KM3NeT collaboration. Expansion cone for the 3-inch pmts of the km3net optical modules. *Journal of Instrumentation*, 8(03):T03006, 2013.

[23] P. KOOIJMAN. The neutrino mass hierarchy in km3net - orca, a feasibility study. *Proceedings of the 33rd International Comsic Ray Conference, Rio de Janeiro*, 2013.

[24] S. Escoffier. The ANTARES detector: background sources and effects on detector performance. *Proceedings of the 30th International Cosmic Ray Conference*, 2007.

[25] S. Hallmann. Sensitivity of orca to the neutrino mass hierarchy. Bachelor's thesis, FAU Erlangen Nürnberg, April 2013.

[26] C. Andreopoulos et al. The GENIE Neutrino Monte Carlo Generator. *Nucl. Instrum. Meth.*, A614:87–104, 2010.

[27] S Geisselsoeder. Rdfclassify tutorial. Mar 2012. ANTARES-SOFT-2012-002.

[28] R.O. Duda, P.E. Hart, and D.G. Stork. *Pattern classification*. Wiley New York, 2001.

[29] M. Erdmann and T. Hebbeker. *Experimentalphysik 5: Moderne Methoden der Datenanalyse*. Experimentalphysik. Springer, 2013.

[30] Q. Dorosti Hasankiadeh and H. Loehner. Search for showers induced by diffuse flux of cosmic neutrinos. May 2013. ANTARES-PHYS-2012-11.

[31] R. R. Wilcox. *Introduction to Robust Estimation and Hypothesis Testing*. Academic Press, Waltham, 3. edition, 2012.

[32] E Visser and S Wagner. Studies of the performance of different track reconstruction strategies using the filteringfit track reconstruction. Apr 2013. ANTARES-SOFT-2013-002.

[33] M De Jong. Partial linearisation of the track fit problem. 2007. ANTARES-SOFT-2007-001.

[34] M. Shiozawa. Reconstruction algorithms in the super-kamiokande large water cherenkov detector. *Nuclear Instruments and Methods in Physics Research Section A: Accelerators, Spectrometers, Detectors and Associated Equipment*, 433(12):240 – 246, 1999.

[35] R. Brun and F. Rademakers. Root an object oriented data analysis framework. *Nuclear Instruments and Methods in Physics Research Section A: Accelerators, Spectrometers, Detectors and Associated Equipment*, 389(12):81 – 86, 1997. New Computing Techniques in Physics Research V.

[36] S. Geisselsöder. private communication.

[37] Joachim Hartung, Bärbel Elpelt, and Karl-Heinz Klösener. *Statistik: Lehr- und Handbuch der angewandten Statistik ; mit zahlreichen, vollständig durchgerechneten Beispielen*. Oldenbourg, München, 14. edition, 2005.

Appendix A

Reconstruction

The plots in this chapter show the accuracy of the used reconstruction algorithms.

A.1 Reconstruction with QStrategy

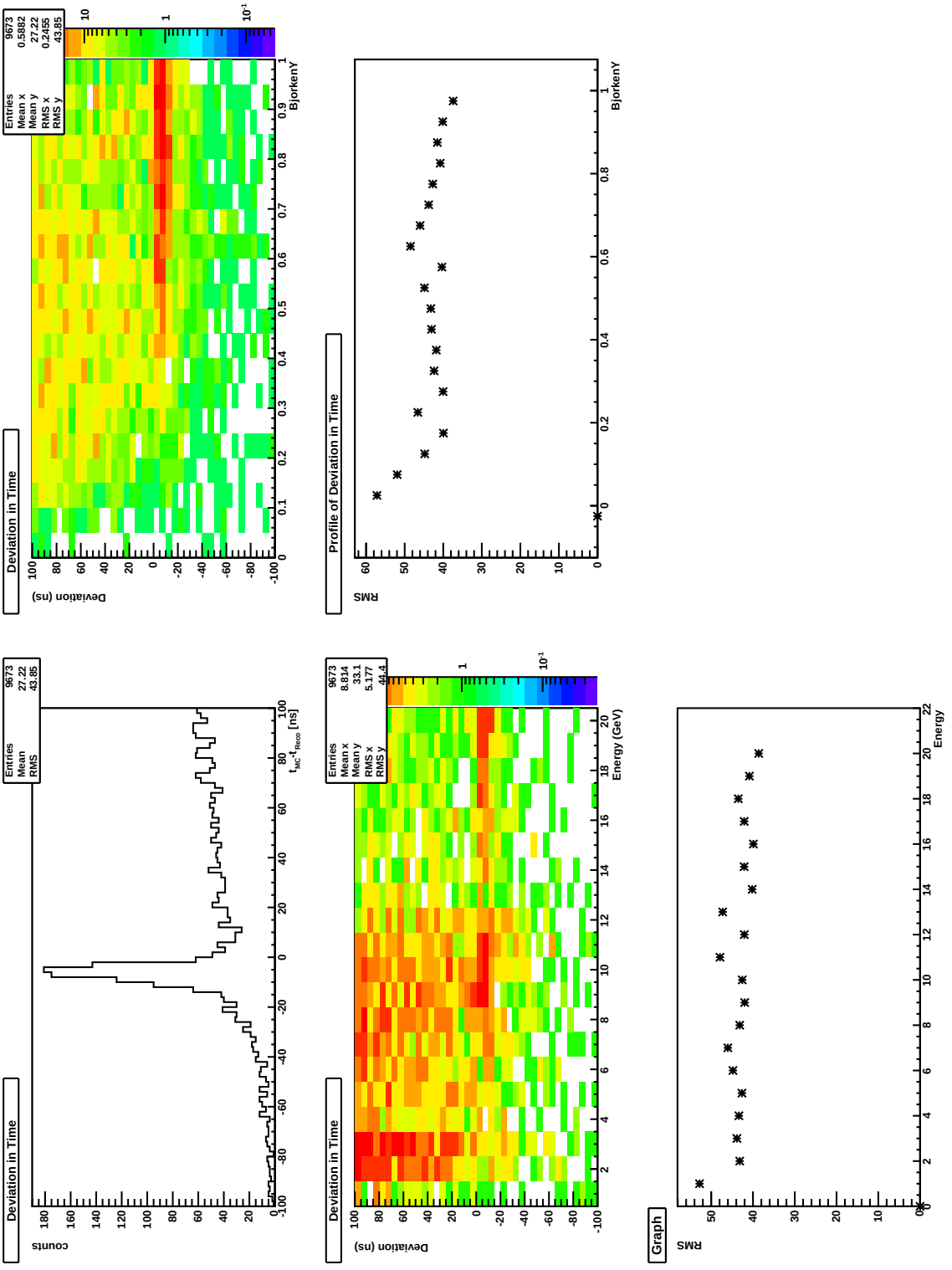

Figure A.1: *difference between the reconstructed time an the Monte Carlo time of electron neutrinos in the neutral current channel*

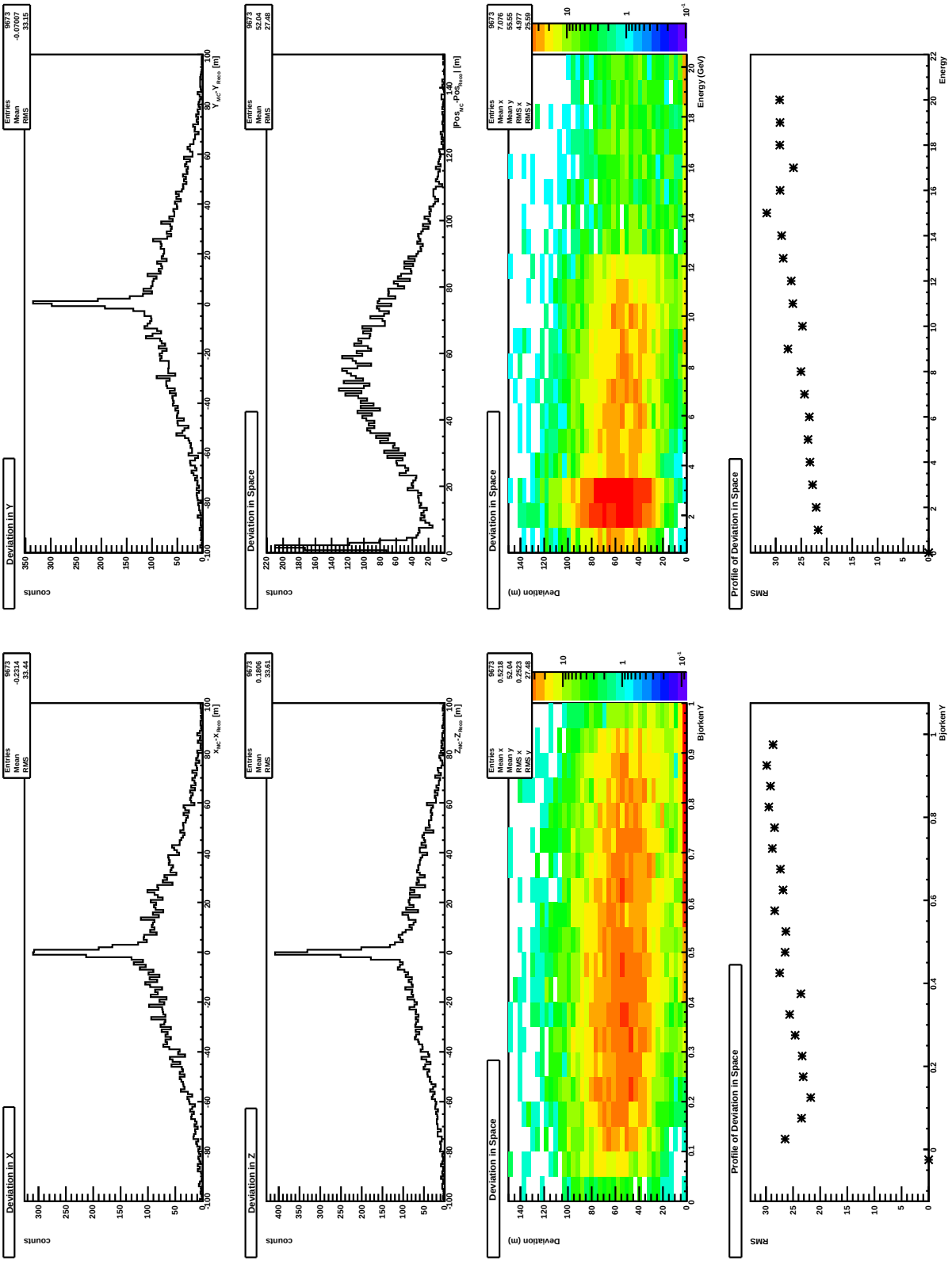

Figure A.2: *Difference between the reconstructed vertex an the Monte Carlo vertex of electron neutrinos in the neutral current channel*

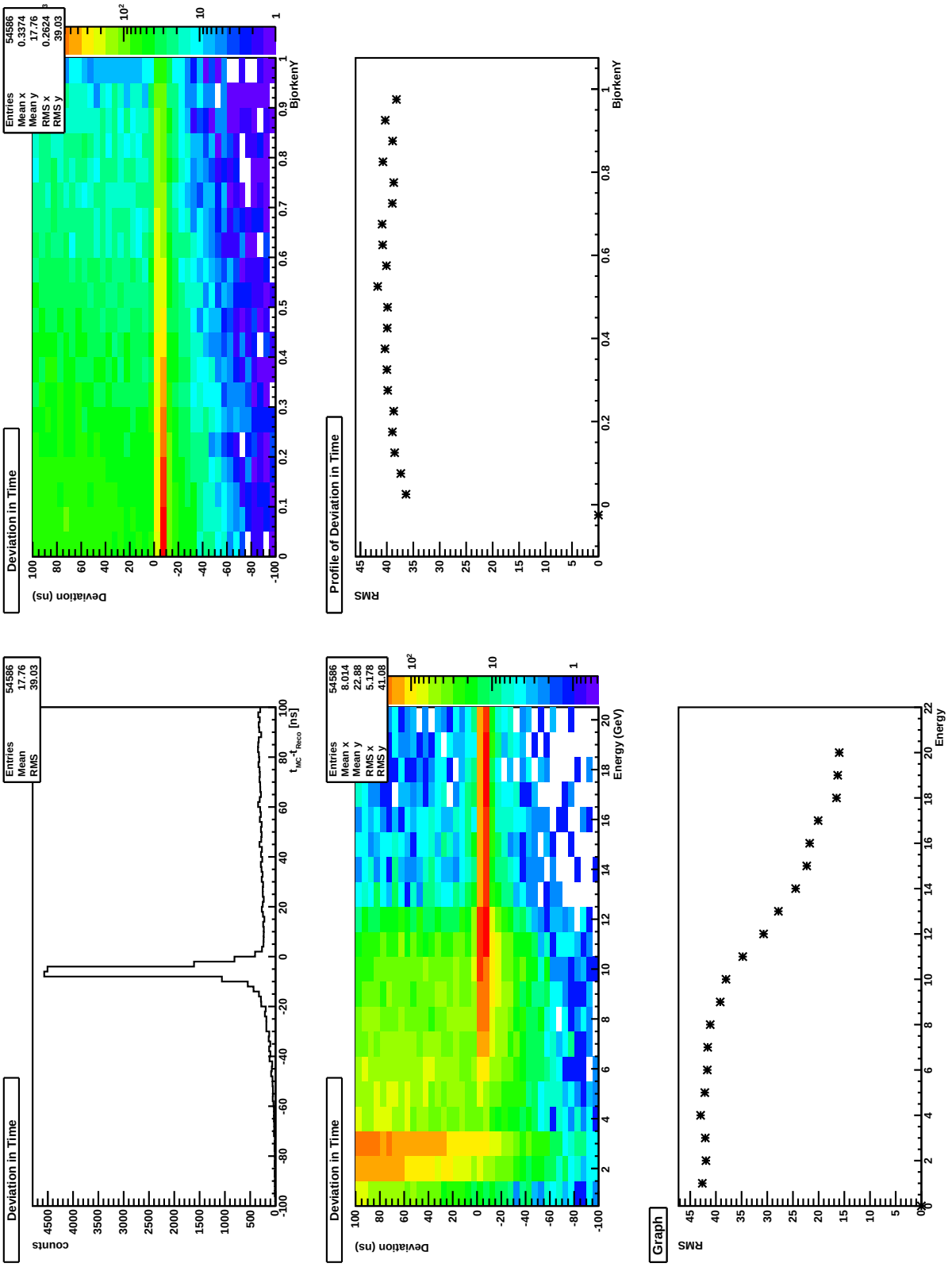

Figure A.3: *Difference between the reconstructed time an the Monte Carlo time of electron neutrinos in the charged current channel*

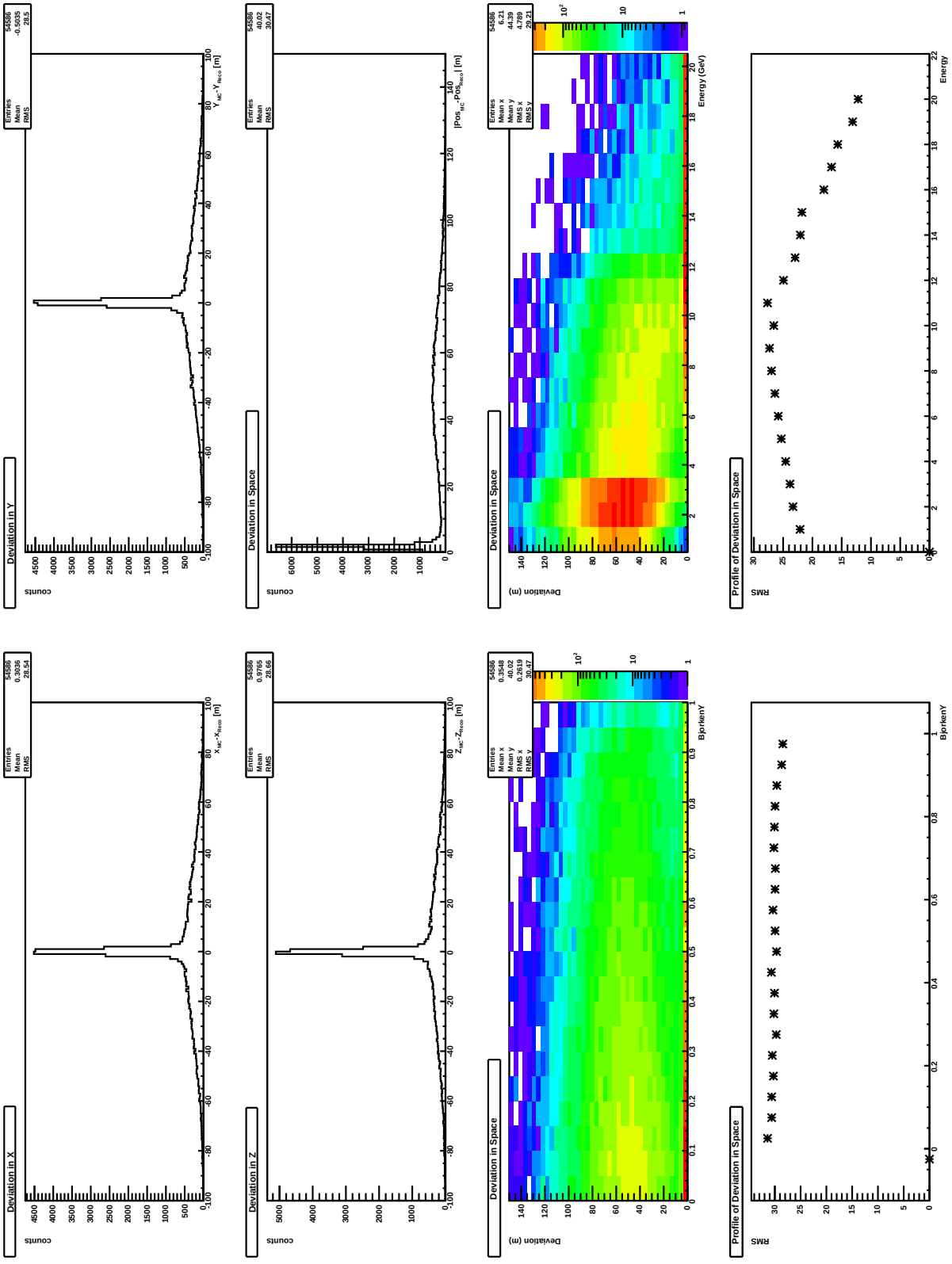

Figure A.4: *Difference between the reconstructed vertex an the Monte Carlo vertex of electron neutrinos in the charged current channel*

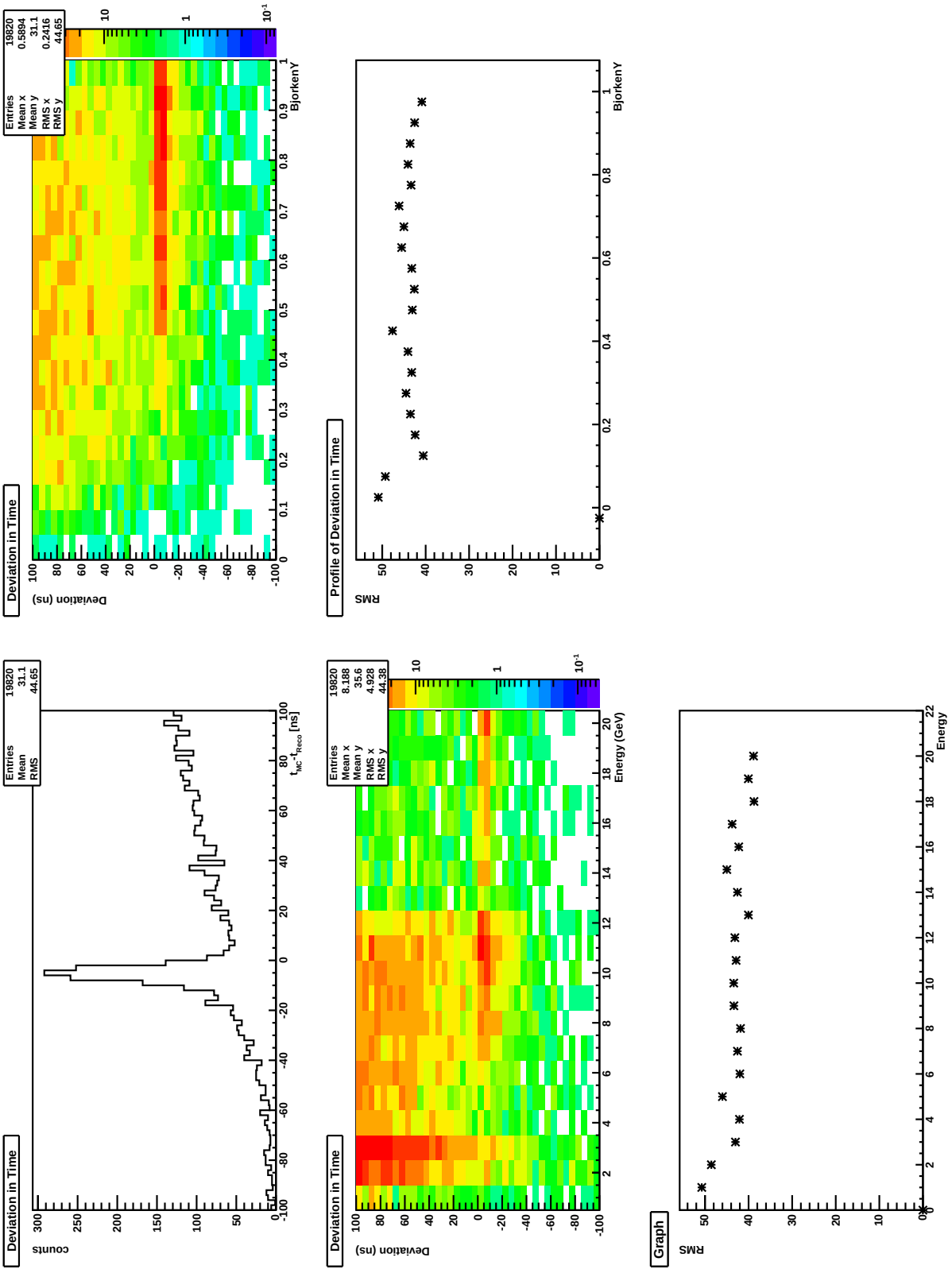

Figure A.5: *Difference between the reconstructed time an the Monte Carlo time of muon neutrinos in the neutral current channel*

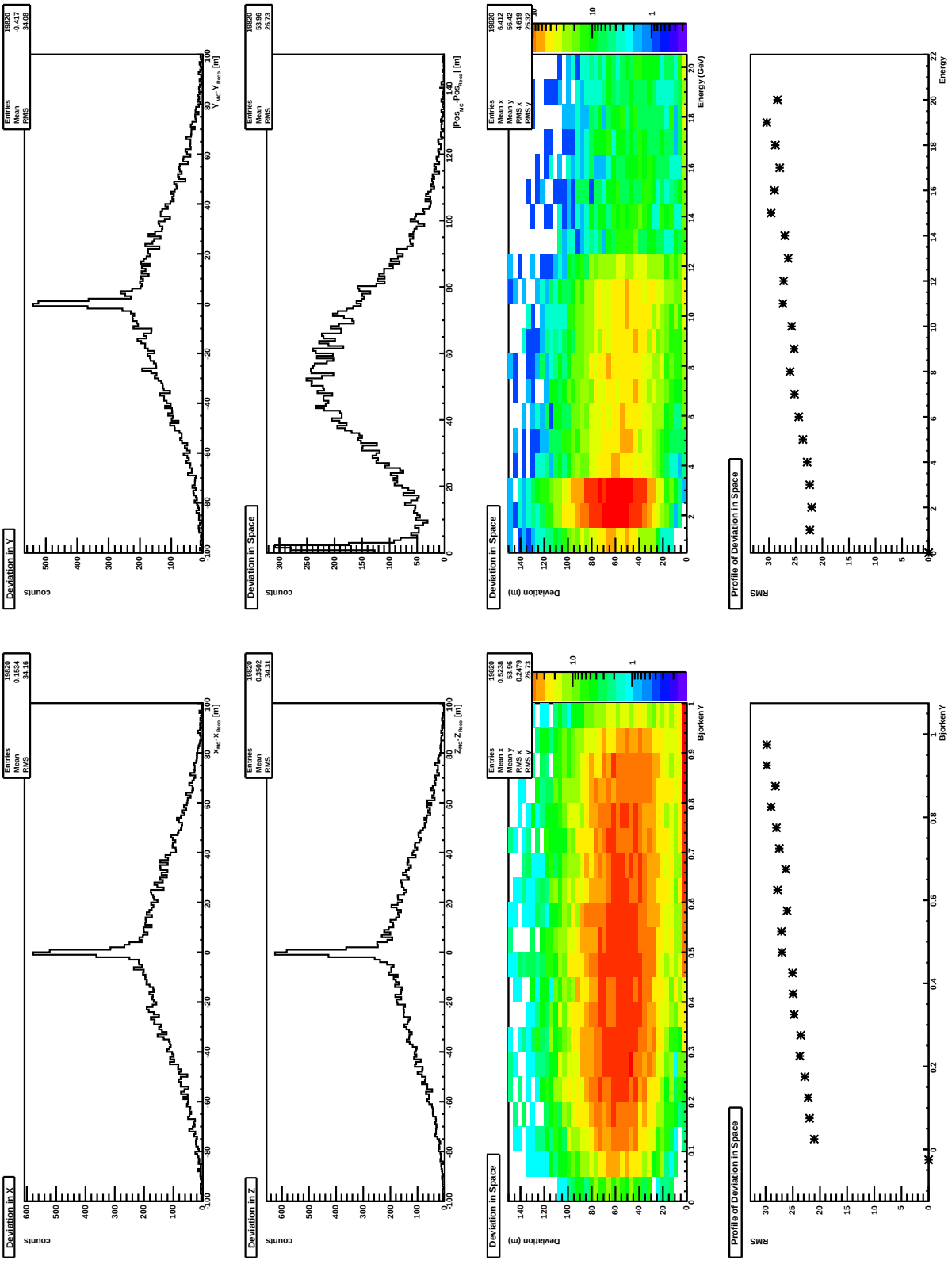

Figure A.6: *Difference between the reconstructed vertex an the Monte Carlo vertex of muon neutrinos in the neutral current channel*

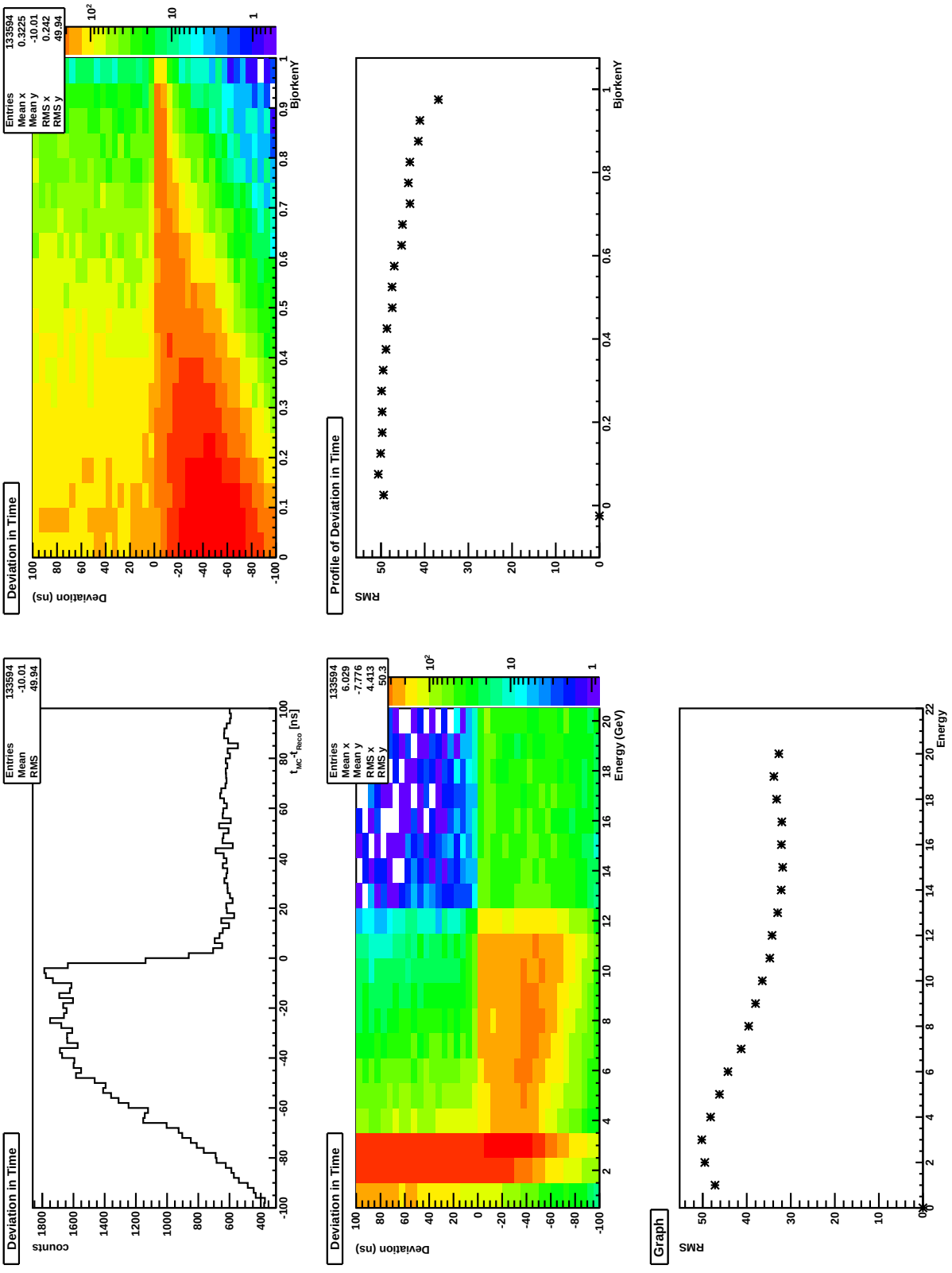

Figure A.7: *Difference between the reconstructed time an the Monte Carlo time of muon neutrinos in the charged current channel*

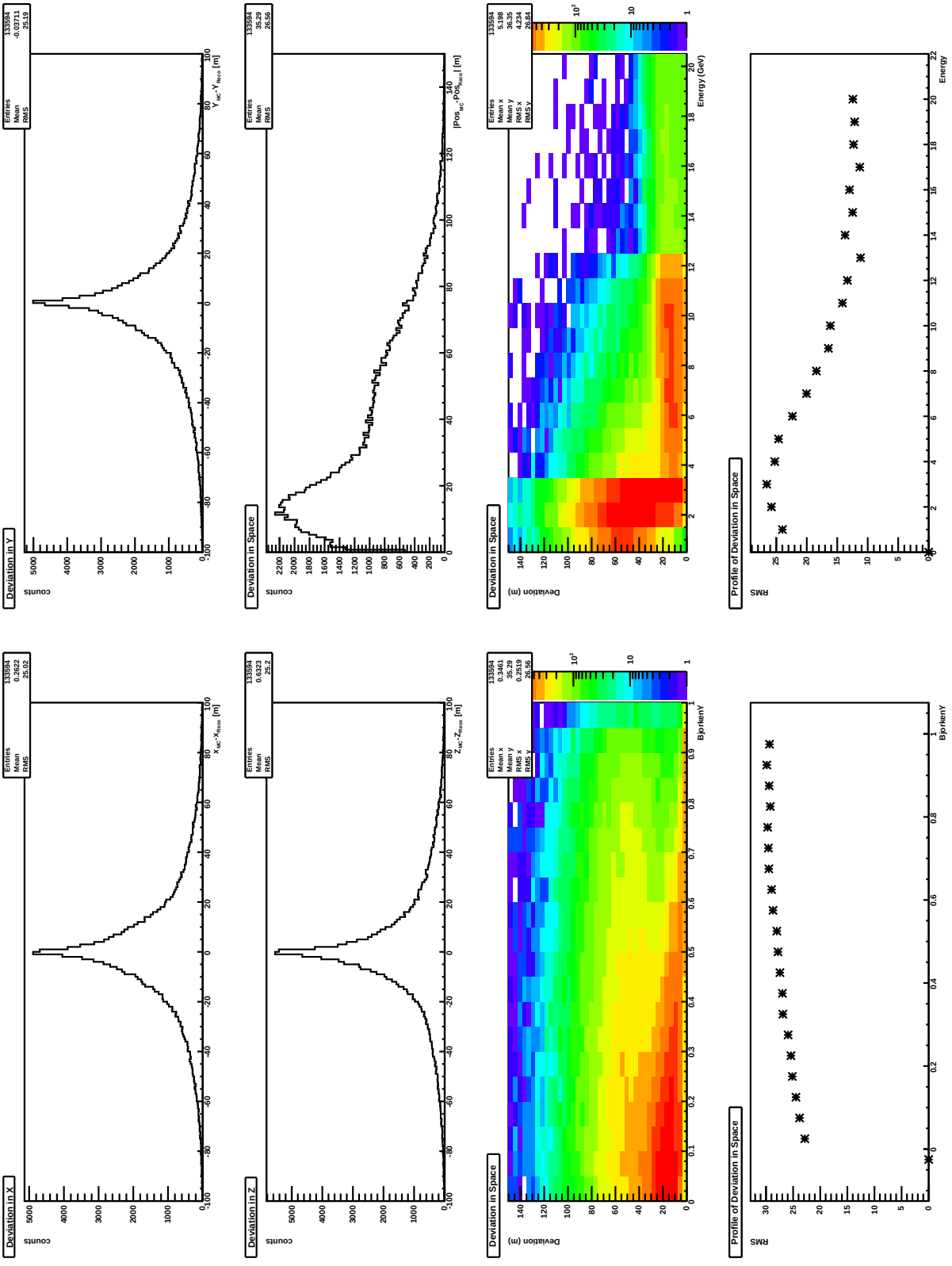

Figure A.8: *Difference between the reconstructed vertex an the Monte Carlo vertex of muon neutrinos in the charged current channel*

A.2 Reconstruction with FilteringFit

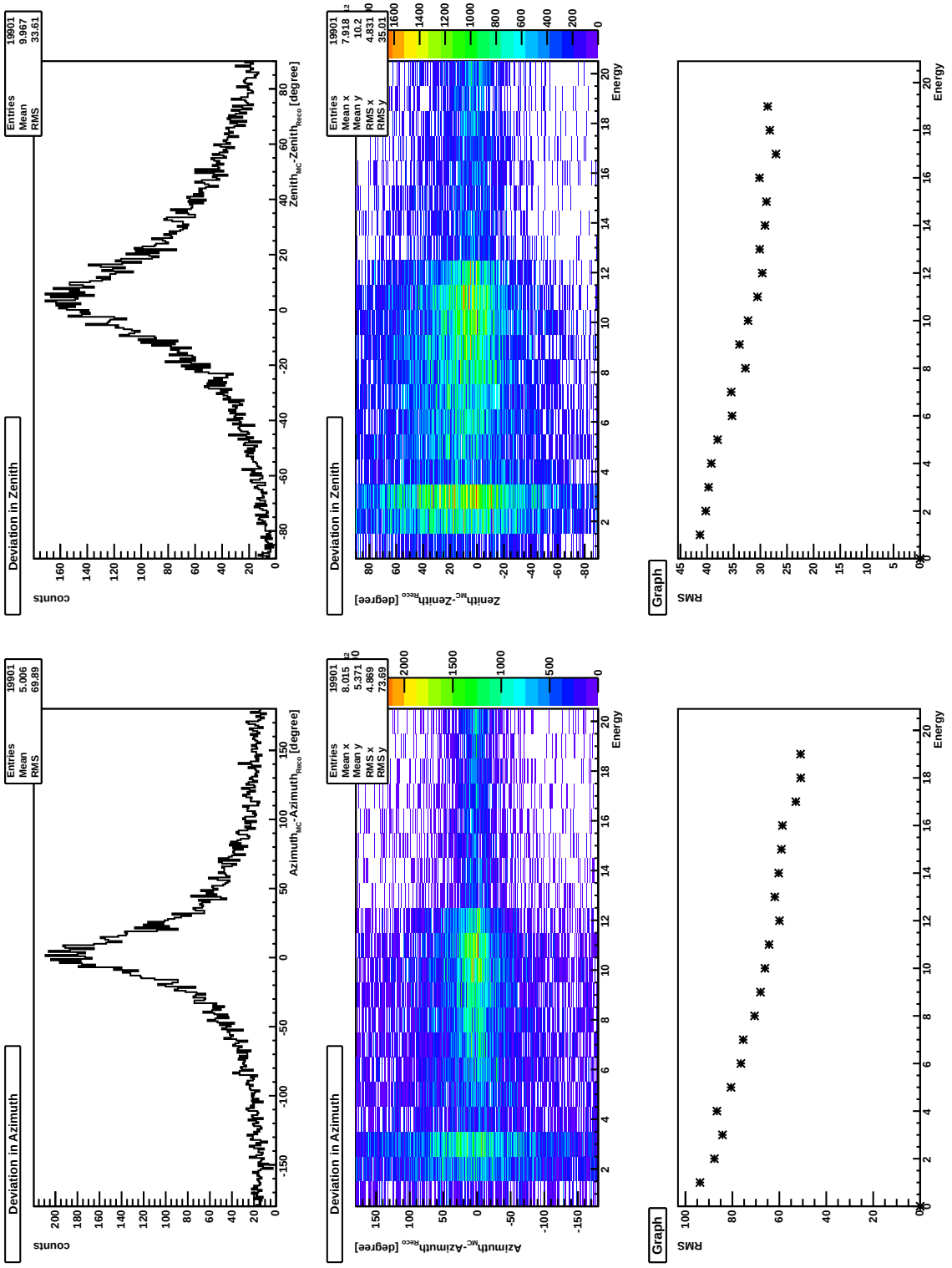

Figure A.9: *Difference between the reconstructed direction and the Monte Carlo Direction of muon neutrinos in the neutral current w.r.t. the Neutrino direction*

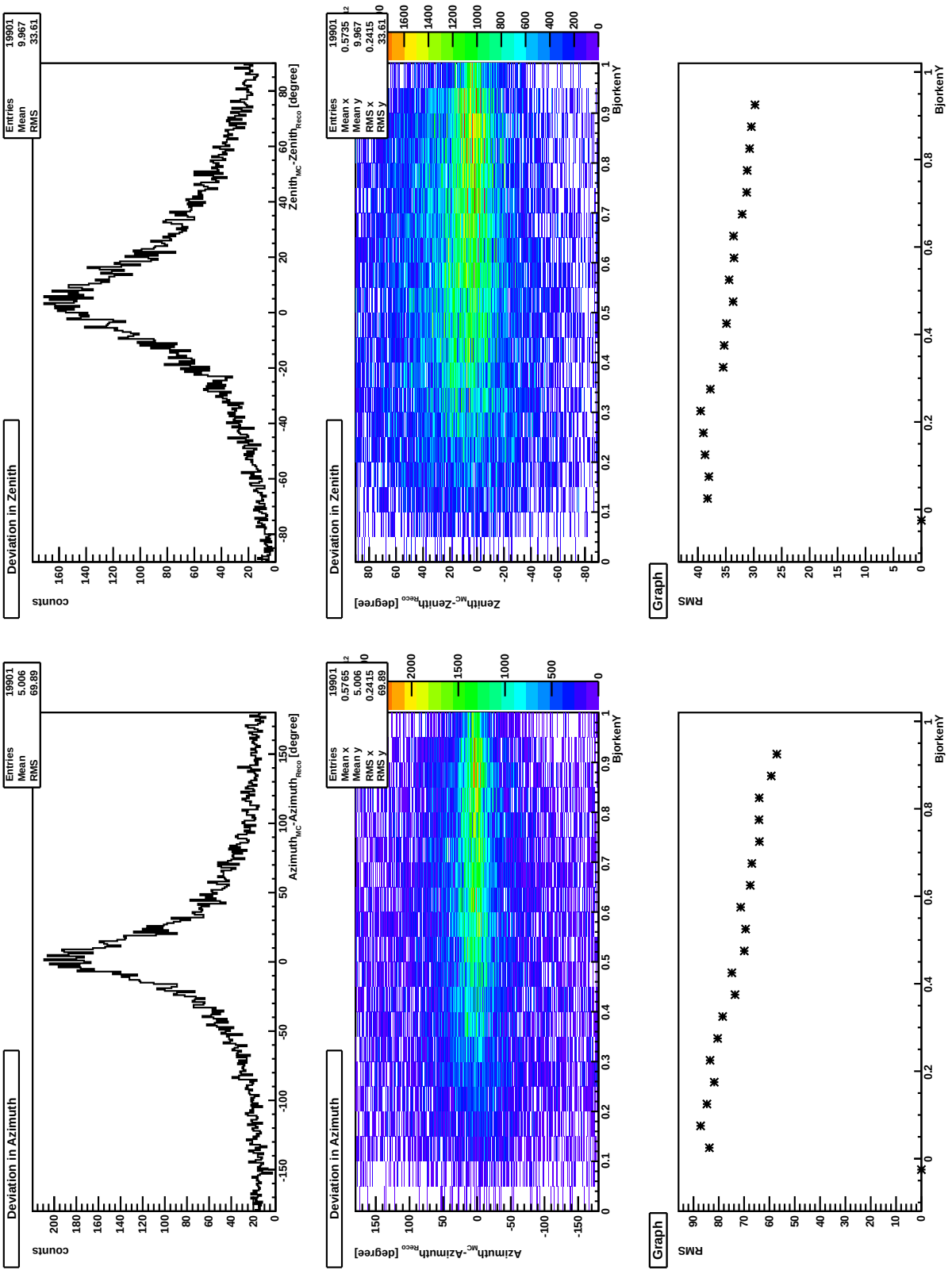

Figure A.10: *Difference between the reconstructed direction and the Monte Carlo Direction of muon neutrinos in the neutral current w.r.t. the Neutrino direction*

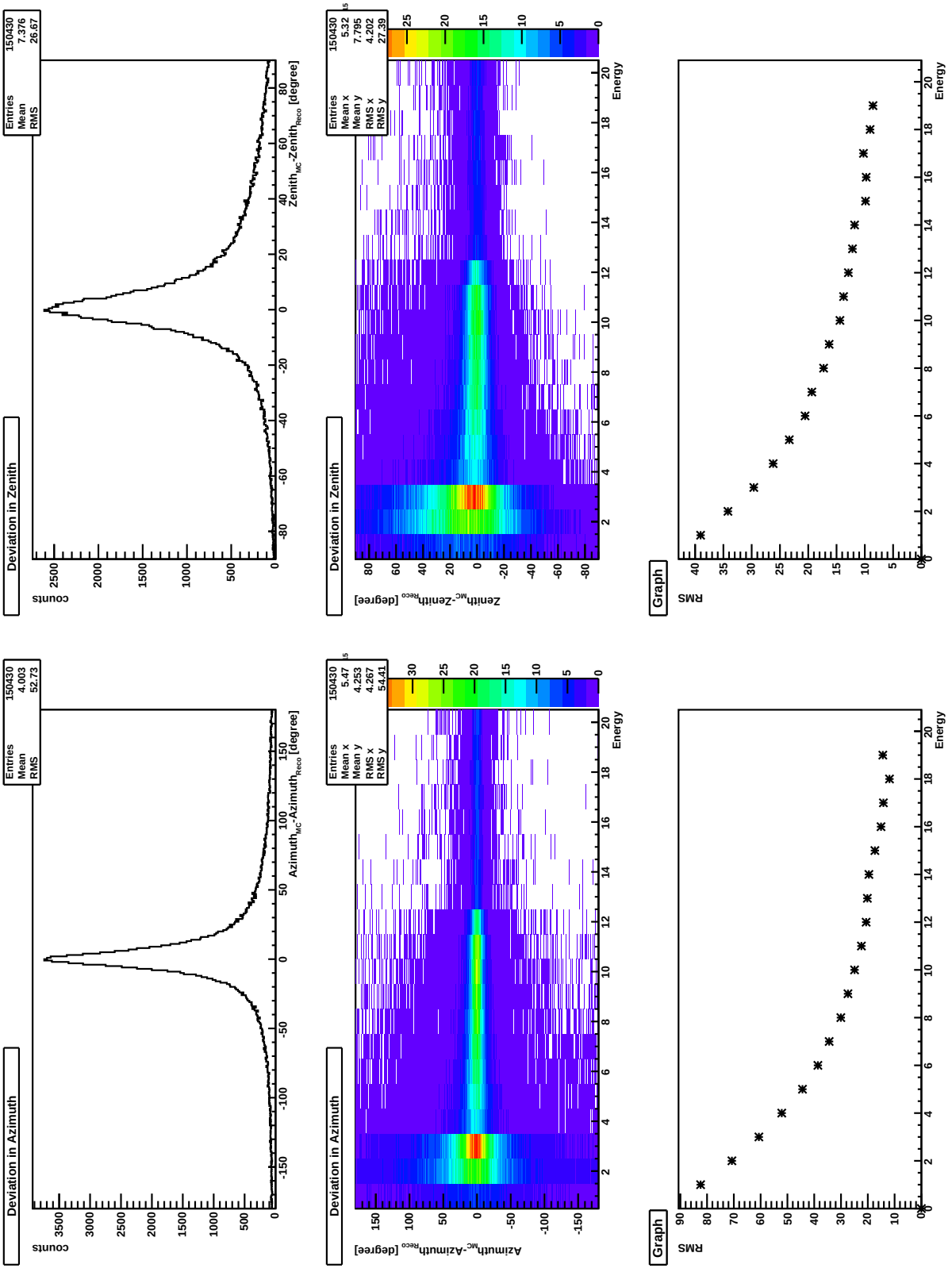

Figure A.11: *Difference between the reconstructed direction and the Monte Carlo Direction of muon neutrinos in the charged current w.r.t. the Neutrino direction*

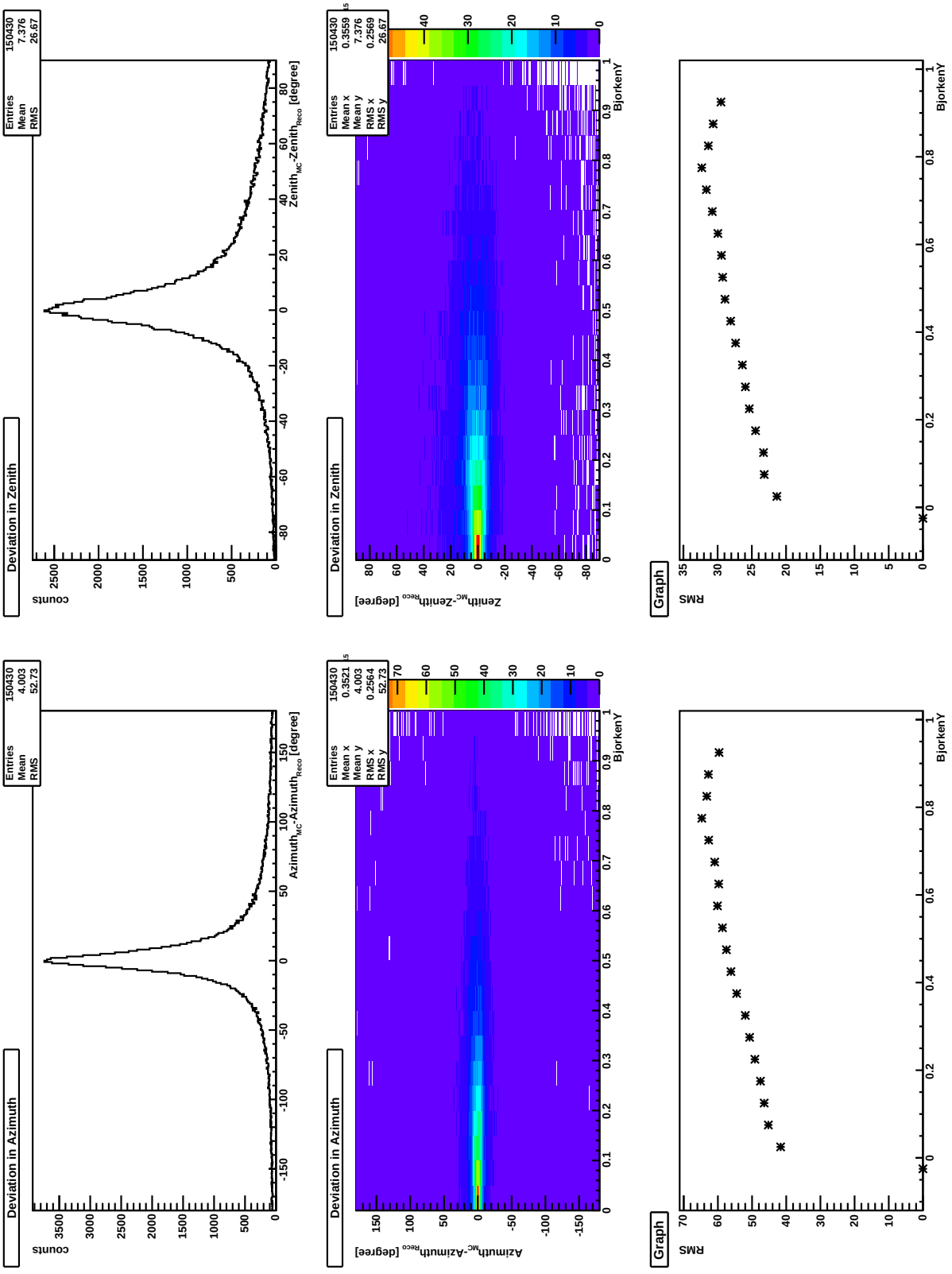

Figure A.12: *Difference between the reconstructed direction and the Monte Carlo Direction of muon neutrinos in the charged current w.r.t. the Neutrino direction*

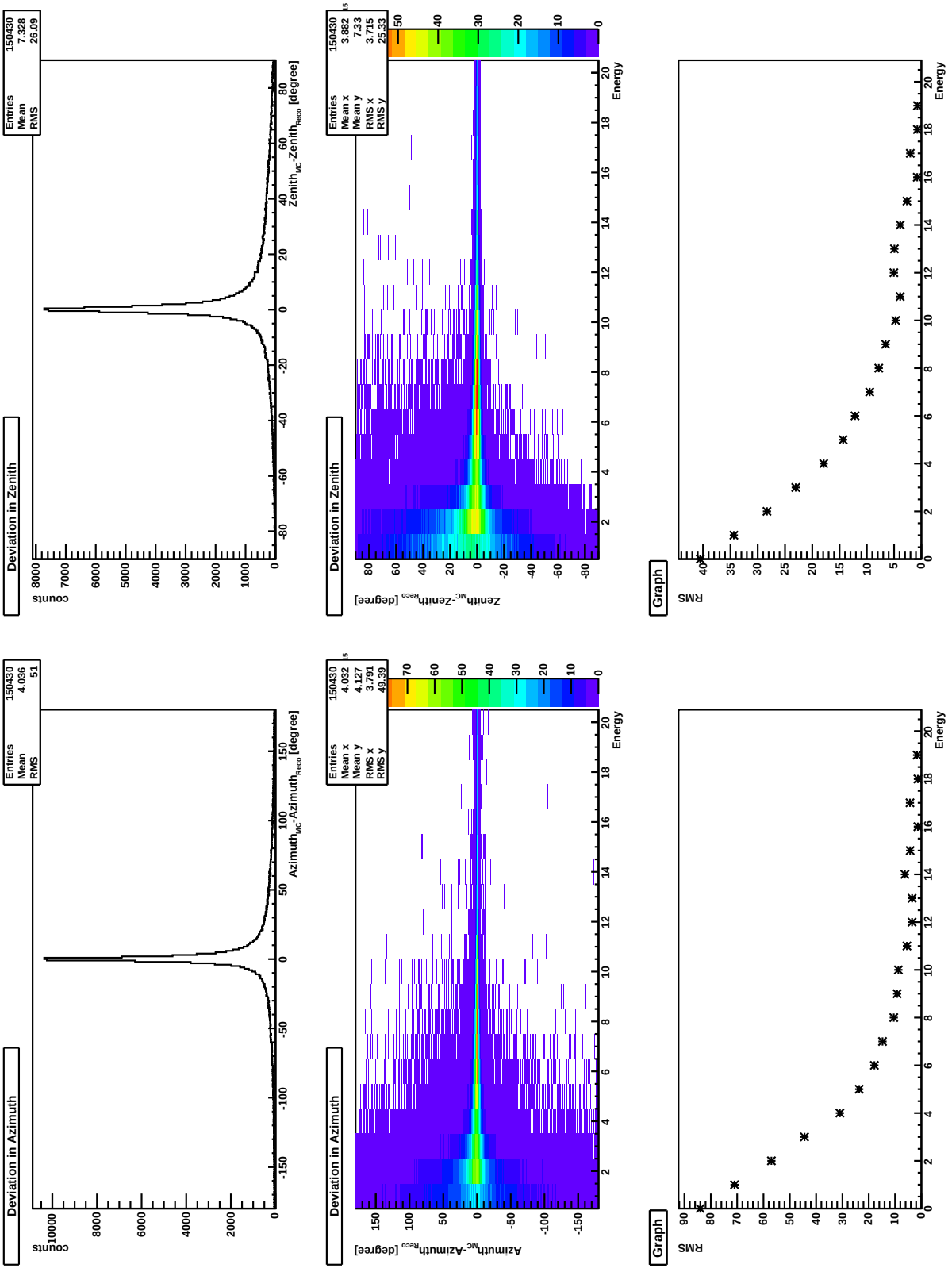

Figure A.13: *Difference between the reconstructed direction and the Monte Carlo Direction of muon neutrinos in the charged current w.r.t. the outgoing muon direction*

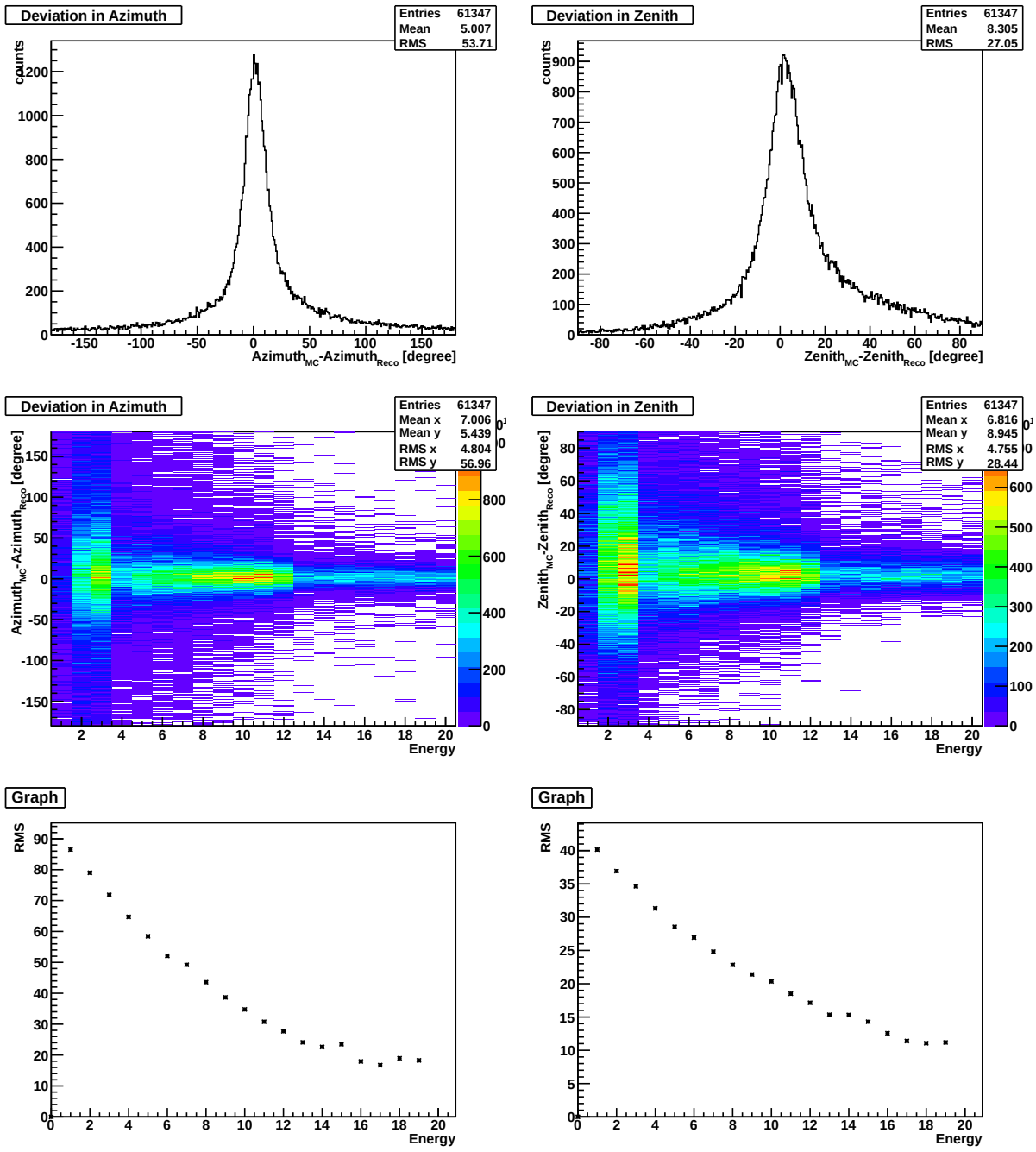

Figure A.14: *Difference between the reconstructed direction and the Monte Carlo Direction of electron neutrinos in the charged current w.r.t. the Neutrino direction*

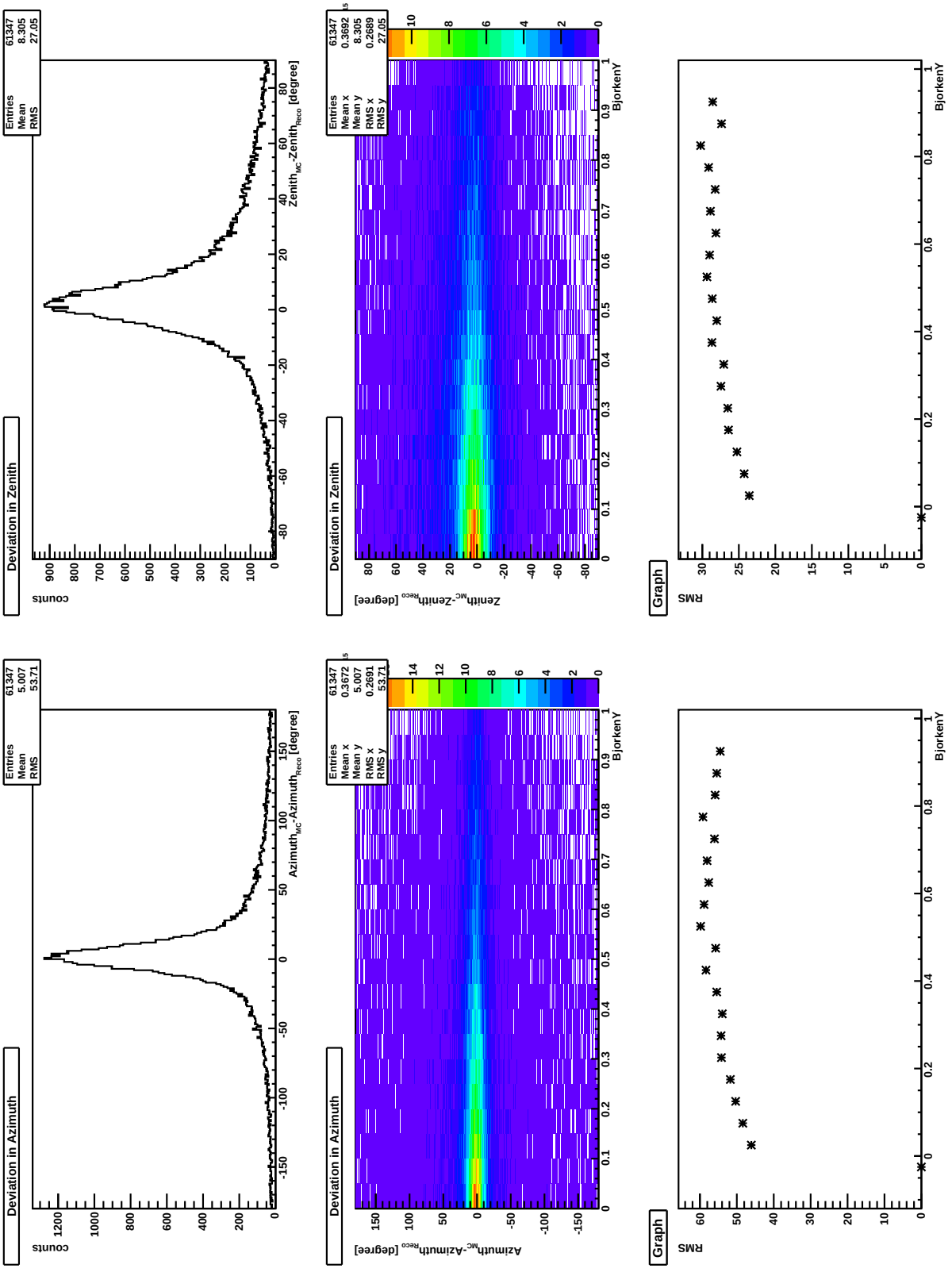

Figure A.15: *Difference between the reconstructed direction and the Monte Carlo Direction of electron neutrinos in the charged current w.r.t. the Neutrino direction*

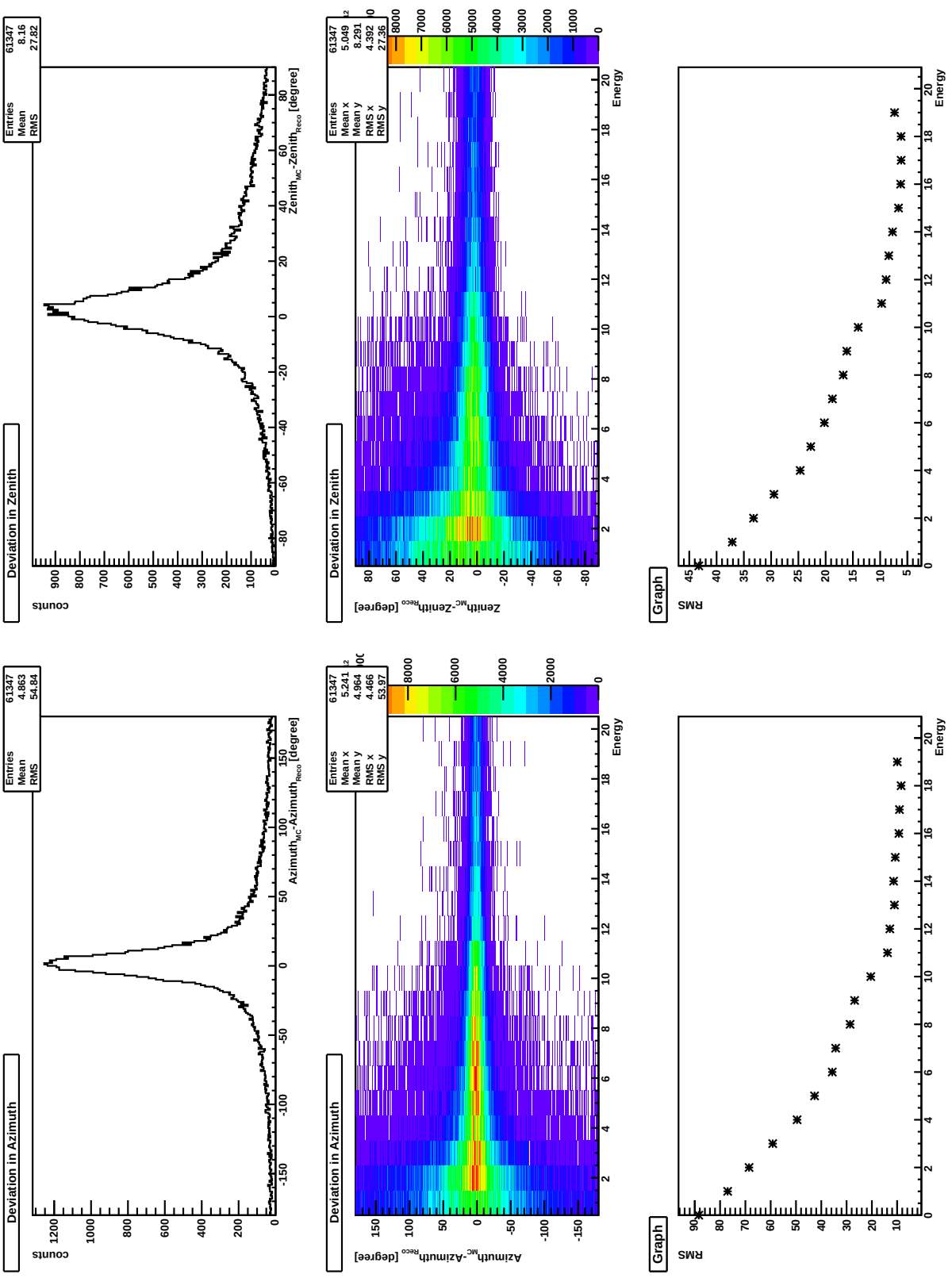

Figure A.16: *Difference between the reconstructed direction and the Monte Carlo Direction of electron neutrinos in the neutral current w.r.t. the Neutrino direction*

Appendix B

Features

B.1 List of Features

Inertia
BigInertia
BigInertiaNormedSphere
RelativeInertia
RelativeInertiaNormedSphere
SmallInertia
SmallInertiaNormedSphere
MiddleInertia
MiddleInertiaNormedSphere
Reconstruction
FilteringFitrlogl
QStrategyChi2
QStrategyQuality
Number of Events
PulseCountCharge
PulseCountNone
Ratios
CounterEndAll
CounterEndEndTrack
CounterStartAll
CounterStartStartEnd
CounterStartStartTrack
CounterTrackAll
Time Differences
TimeDifferenceFWHM
TimeDifferenceMaximum
TimeDifferenceMean
TimeDifferenceMedian
TimeDifferenceMinimum
TimeDifferenceRMS

TimeDifferenceWidth15_85
Time Residuals
GParameter
TimeResidualFWHM
TimeResidualMaximum
TimeResidualMean
TimeResidualMeanDistance
TimeResidualMedian
TimeResidualMinimum
TimeResidualRMS
TimeResidualSum
TimeResidualWidth15_85

B.2 Histograms of Features

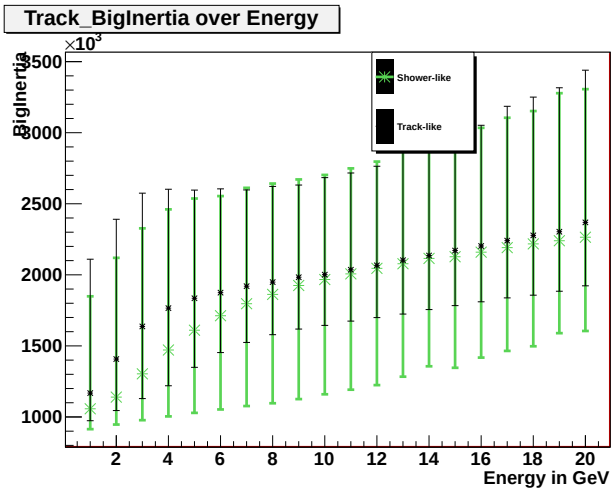

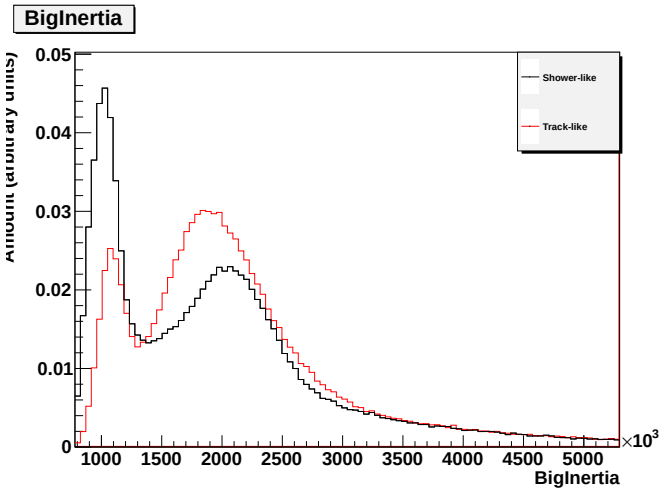

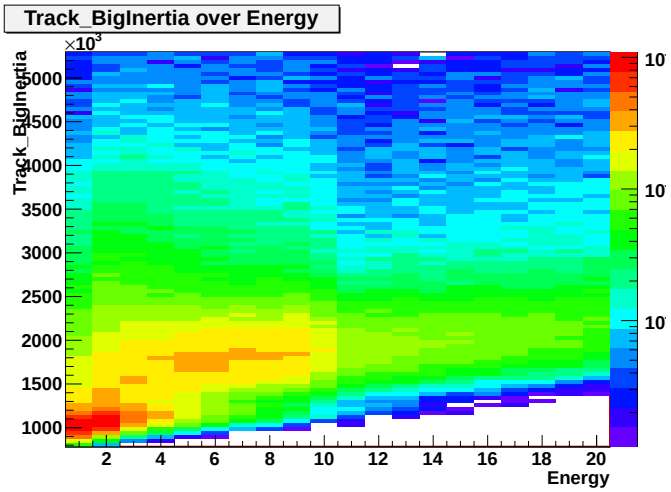

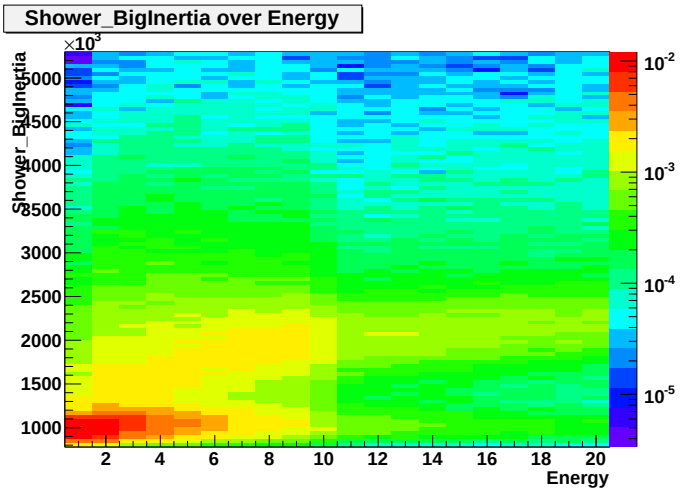

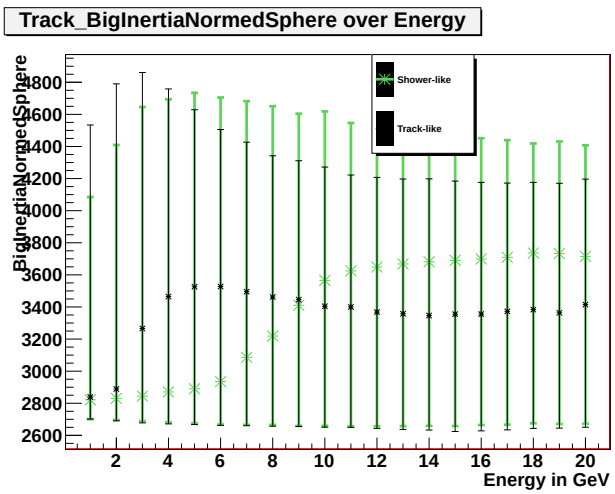

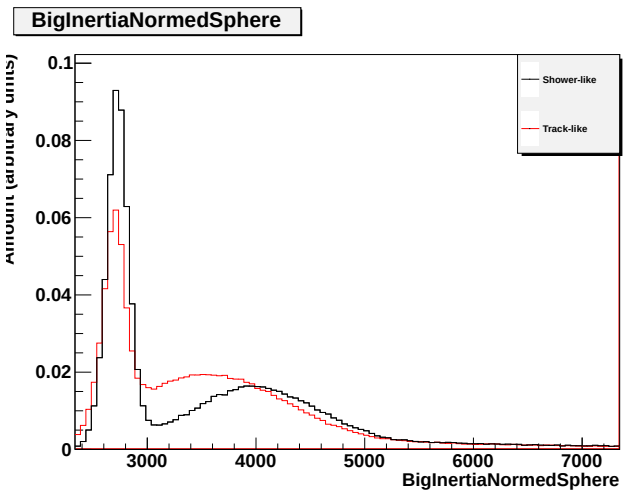

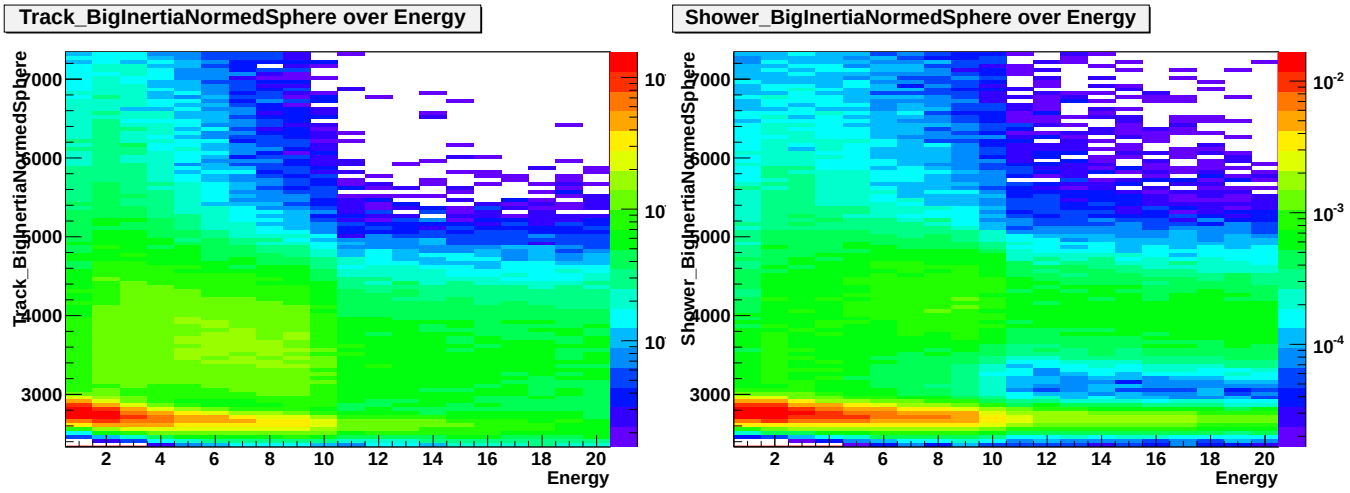
Track_BigInertiaNormedSphere over Energy
Track_BigInertiaNormedSphere
Energy
Shower_BigInertiaNormedSphere over Energy
Shower_BigInertiaNormedSphere
Energy

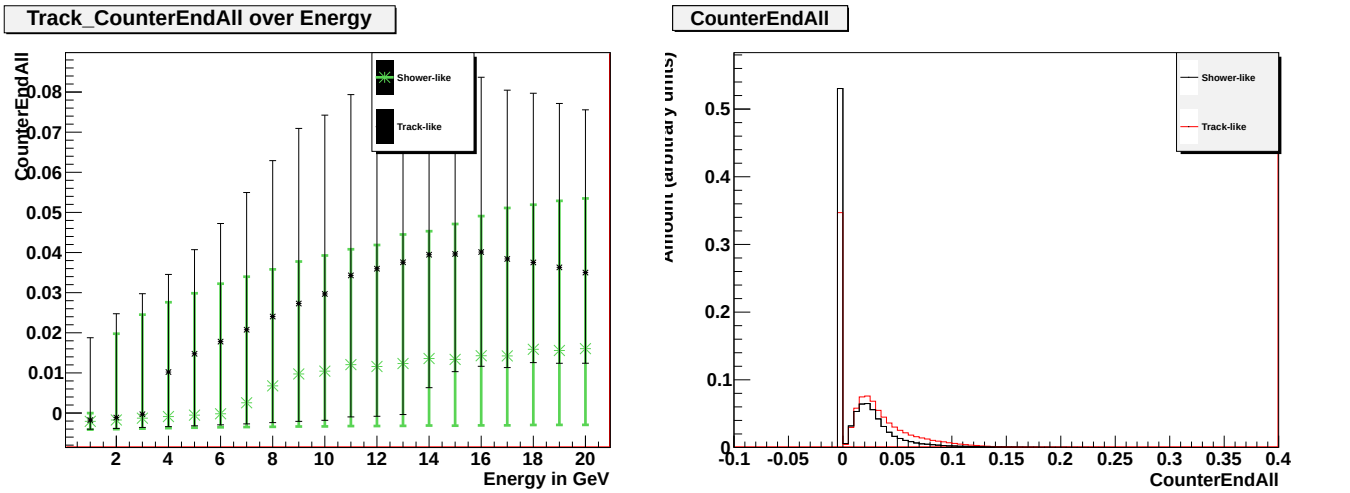
Track_CounterEndAll over Energy
CounterEndAll
Shower-like
Track-like
Energy in GeV
CounterEndAll
Shower-like
Track-like
CounterEndAll

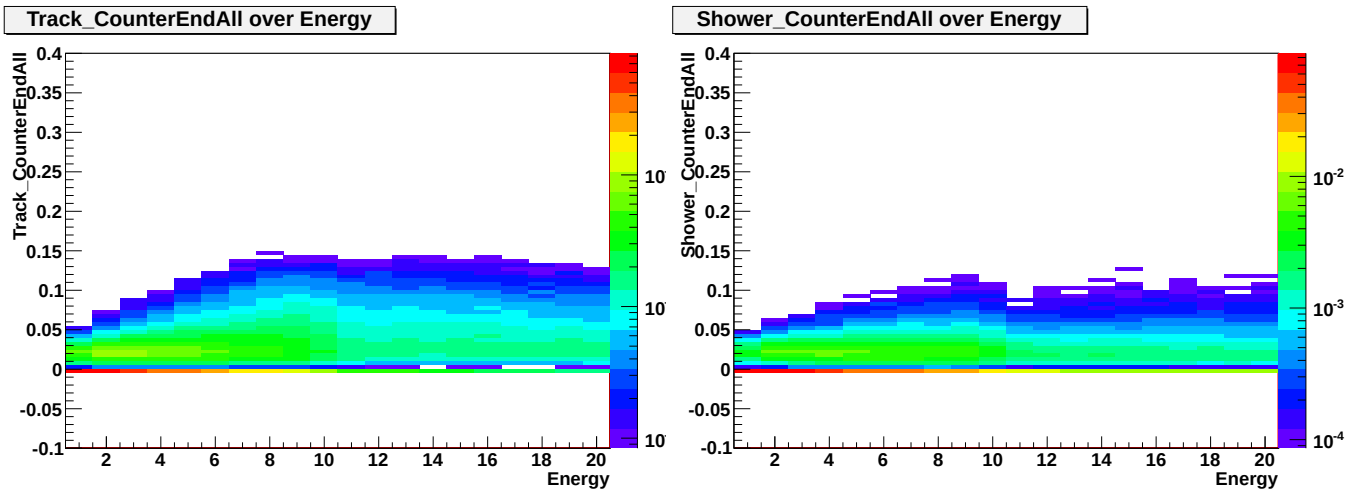
Track_CounterEndAll over Energy
Track_CounterEndAll
Energy
Shower_CounterEndAll over Energy
Shower_CounterEndAll
Energy

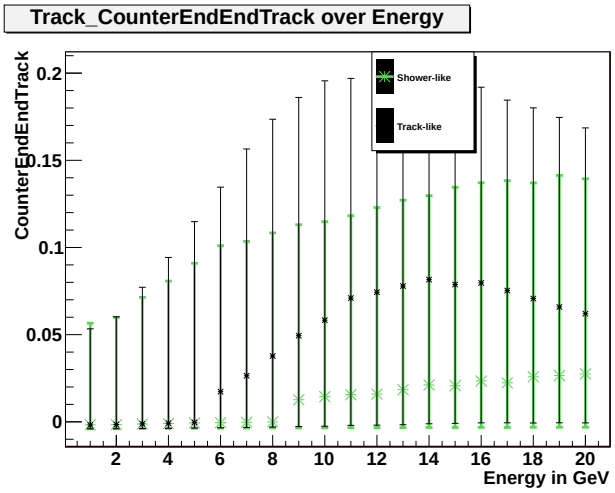
Track_CounterEndEndTrack over Energy
CounterEndEndTrack
Energy in GeV
Shower-like
Track-like

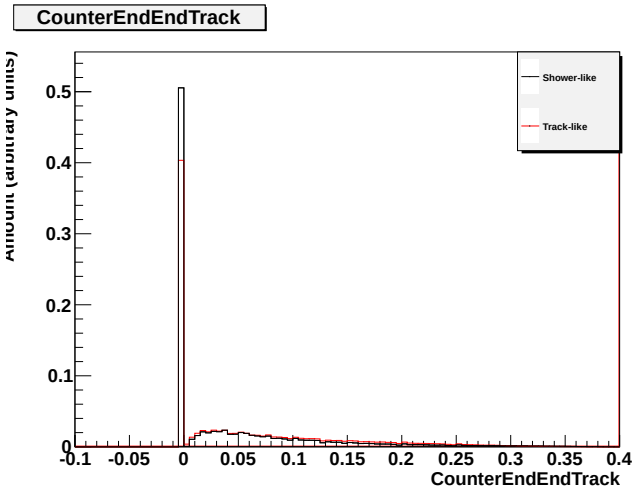
CounterEndEndTrack
Amount (arbitrary units)
CounterEndEndTrack
Shower-like
Track-like

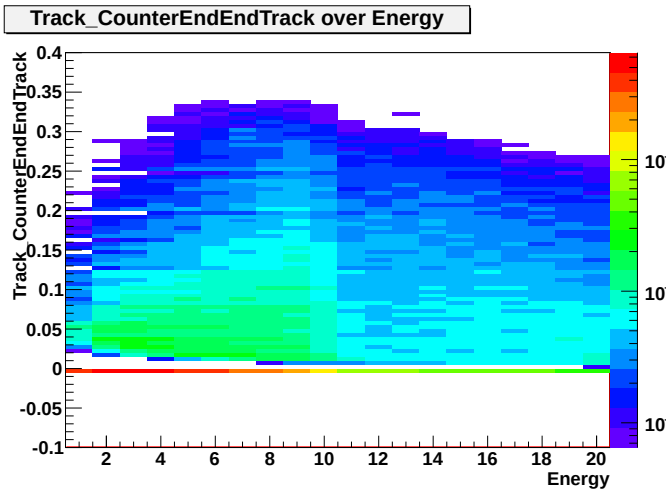
Track_CounterEndEndTrack over Energy
Track_CounterEndEndTrack
Energy

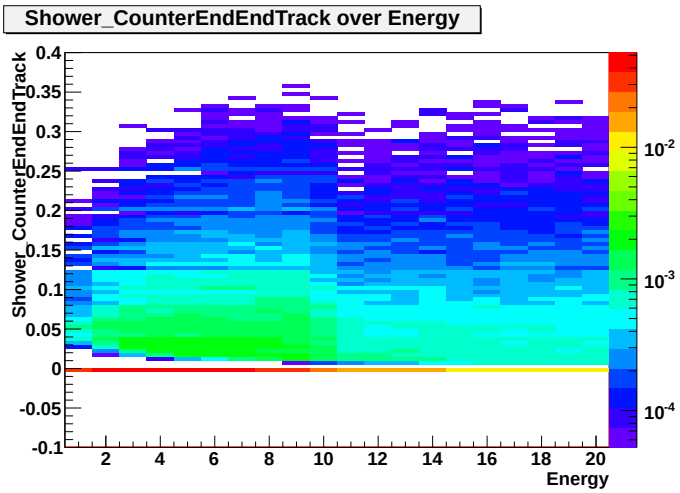
Shower_CounterEndEndTrack over Energy
Shower_CounterEndEndTrack
Energy

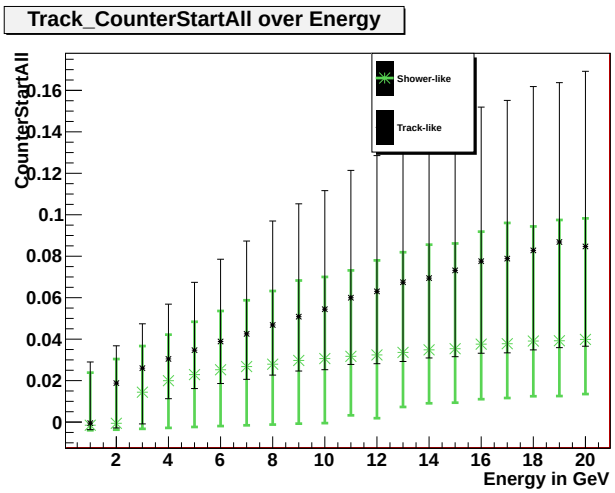
Track_CounterStartAll over Energy
CounterStartAll
Energy in GeV
Shower-like
Track-like

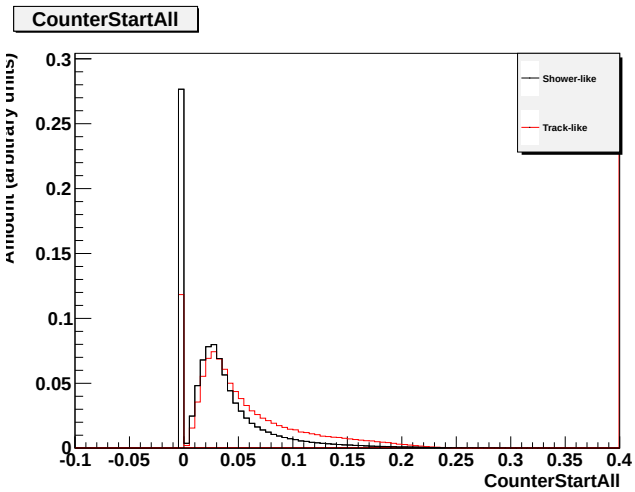
CounterStartAll
Amount (arbitrary units)
CounterStartAll
Shower-like
Track-like

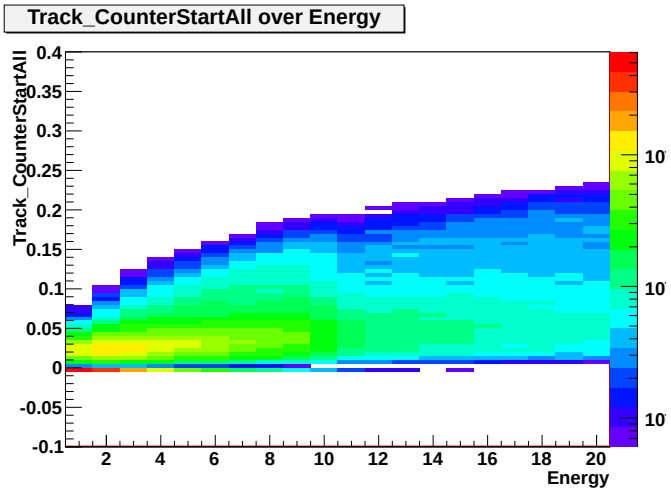
Track_CounterStartAll over Energy
Track_CounterStartAll
Energy

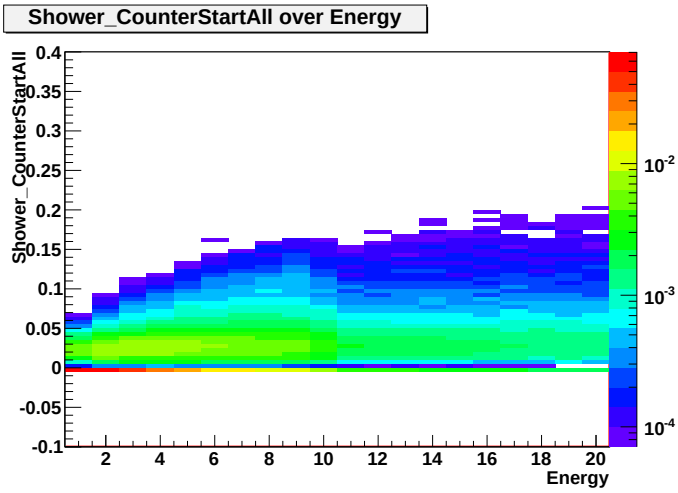
Shower_CounterStartAll over Energy
Shower_CounterStartAll
Energy

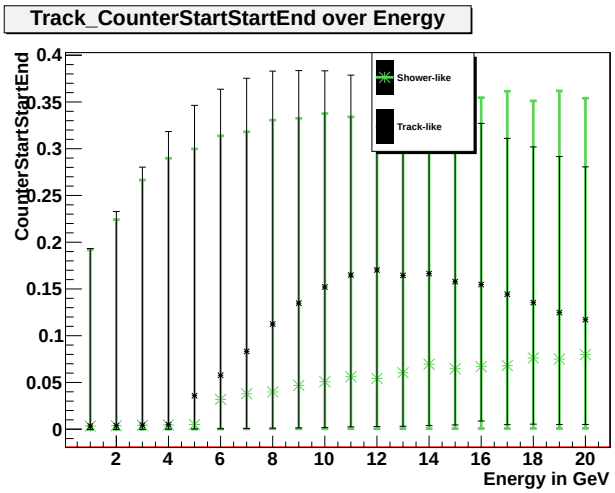
Track_CounterStartStartEnd over Energy
CounterStartStartEnd
Shower-like
Track-like
Energy in GeV

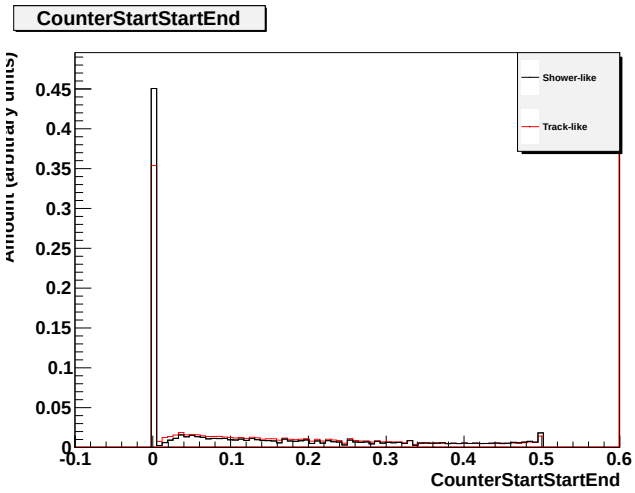
CounterStartStartEnd
Shower-like
Track-like
CounterStartStartEnd

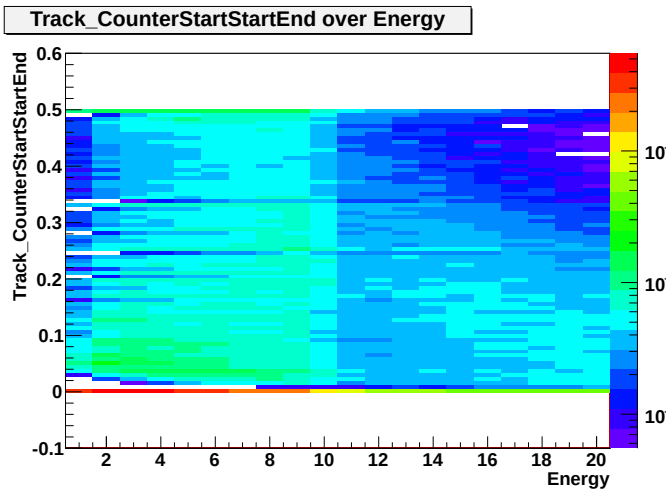
Track_CounterStartStartEnd over Energy
Track_CounterStartStartEnd
Energy

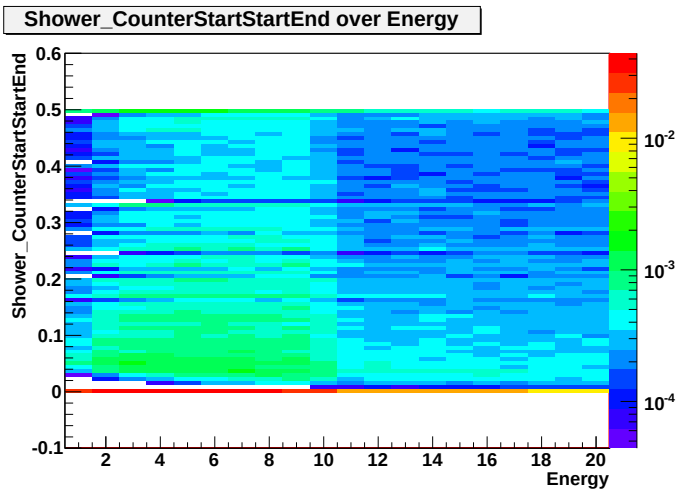
Shower_CounterStartStartEnd over Energy
Shower_CounterStartStartEnd
Energy

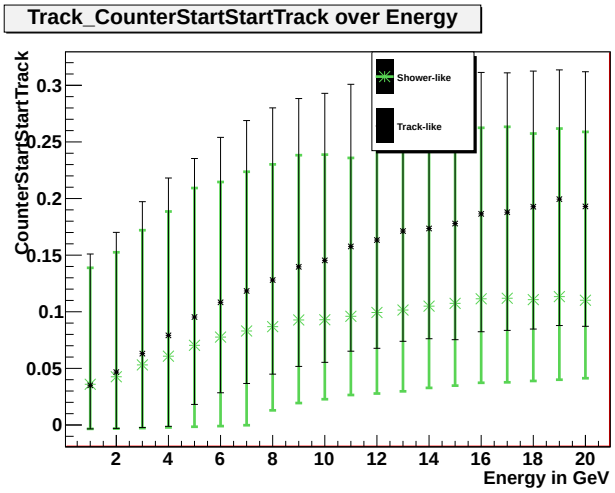
Track_CounterStartStartTrack over Energy
CounterStartStartTrack
Energy in GeV
Shower-like
Track-like

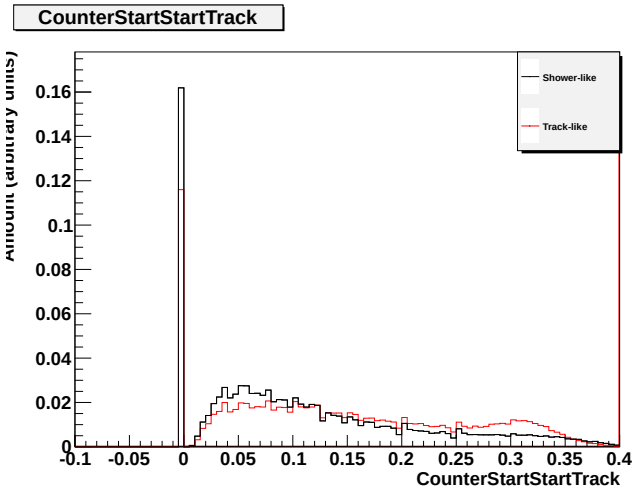
CounterStartStartTrack
Amount (arbitrary units)
CounterStartStartTrack
Shower-like
Track-like

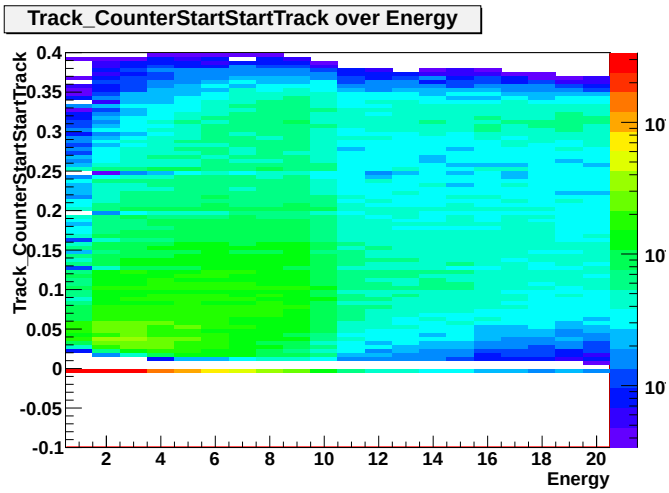
Track_CounterStartStartTrack over Energy
Track_CounterStartStartTrack
Energy

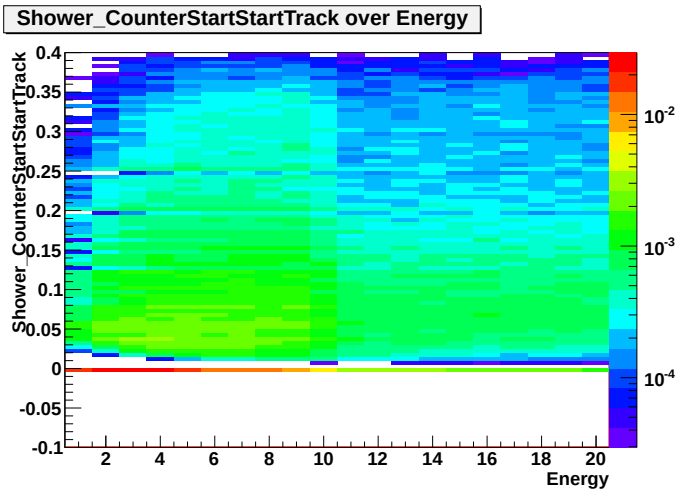
Shower_CounterStartStartTrack over Energy
Shower_CounterStartStartTrack
Energy

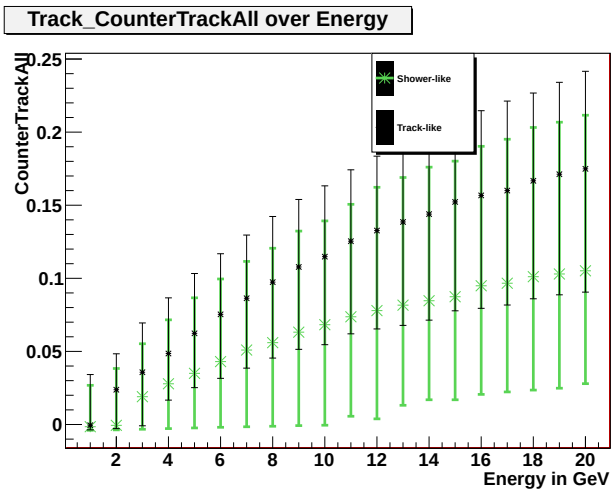
Track_CounterTrackAll over Energy
CounterTrackAll
Energy in GeV
Shower-like
Track-like

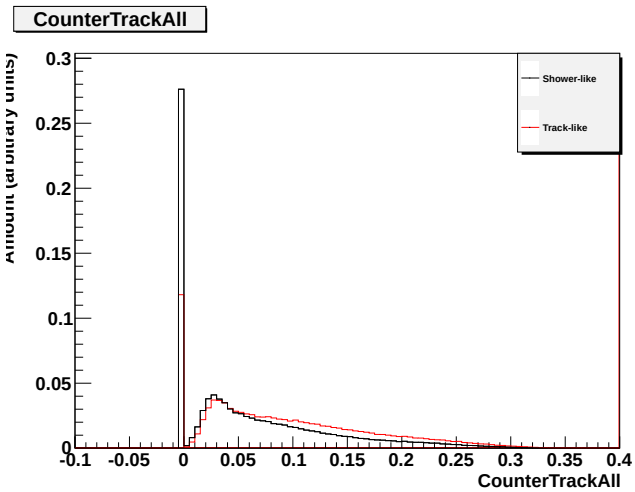
CounterTrackAll
Amount (arbitrary units)
CounterTrackAll
Shower-like
Track-like

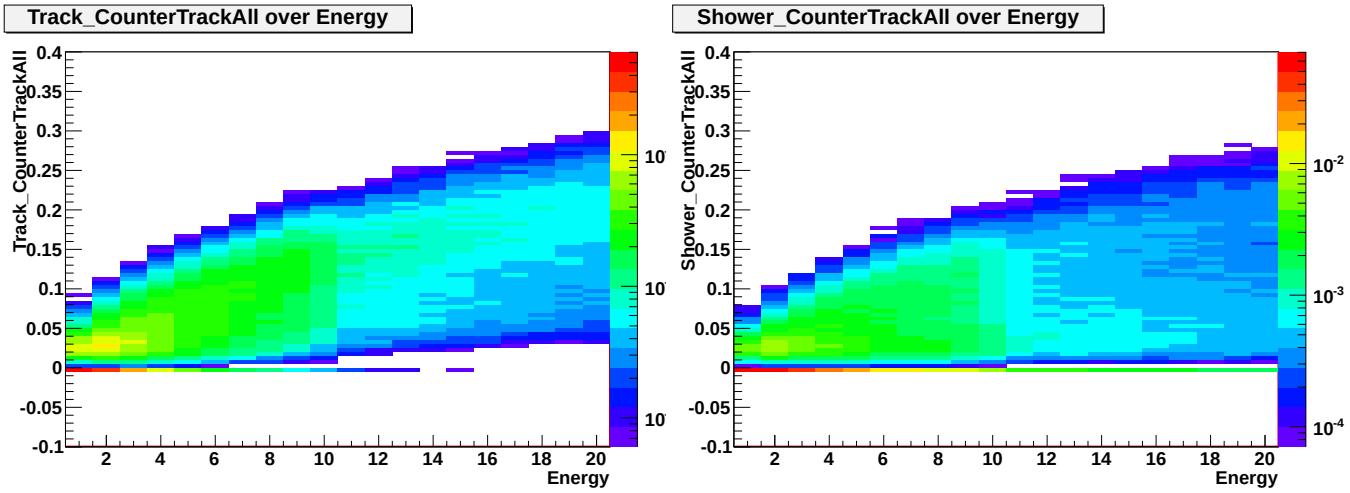
Track_CounterTrackAll over Energy
Track_CounterTrackAll
Energy
Shower_CounterTrackAll over Energy
Shower_CounterTrackAll
Energy

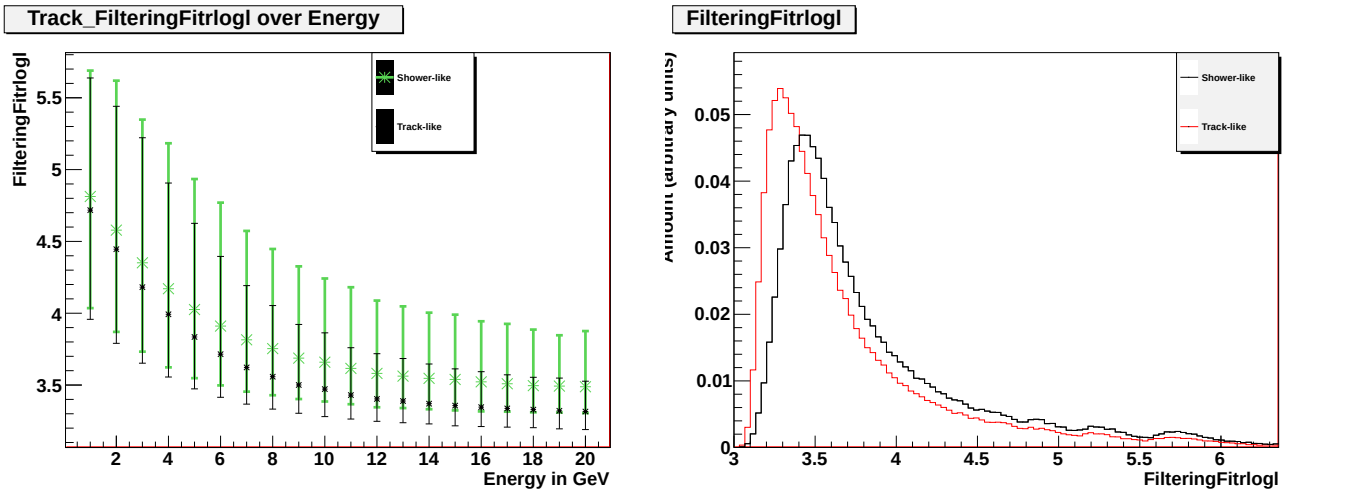
Track_FilteringFitrlogl over Energy
FilteringFitrlogl
Energy in GeV
Shower-like
Track-like
FilteringFitrlogl
Shower-like
Track-like
FilteringFitrlogl

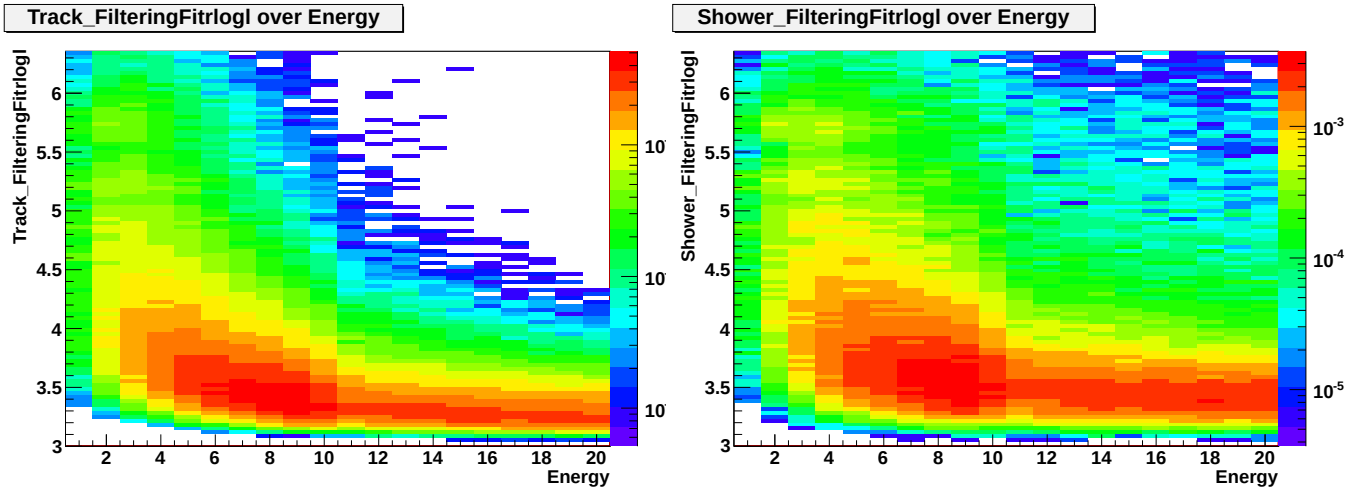
Track_FilteringFitrlogl over Energy
Track_FilteringFitrlogl
Energy
Shower_FilteringFitrlogl over Energy
Shower_FilteringFitrlogl
Energy

Track_GParameter over Energy

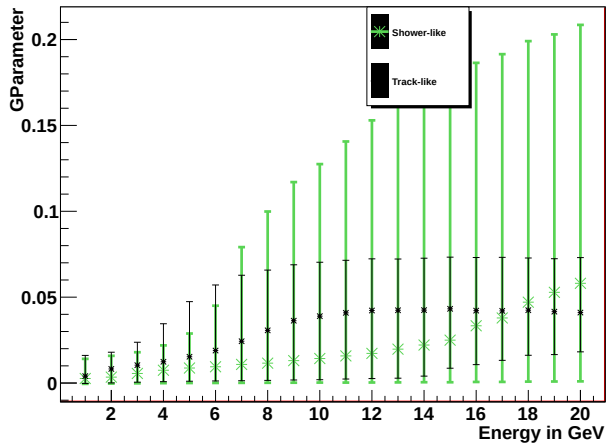

GParameter

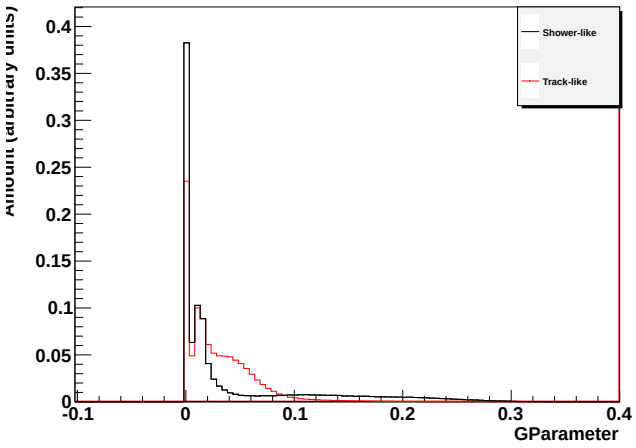

Track_GParameter over Energy

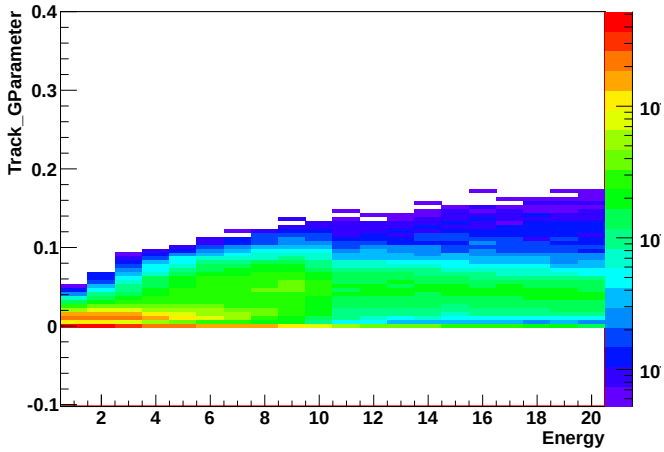

Shower_GParameter over Energy

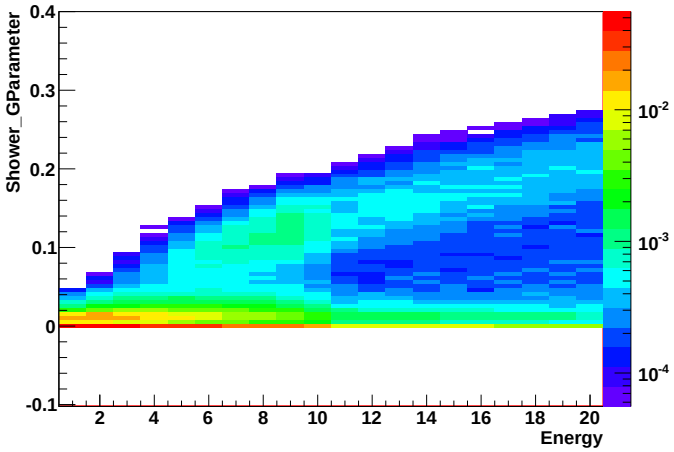

Track_HR over Energy

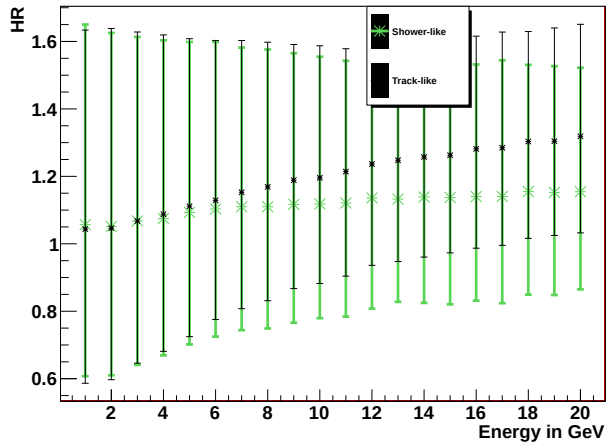

HR

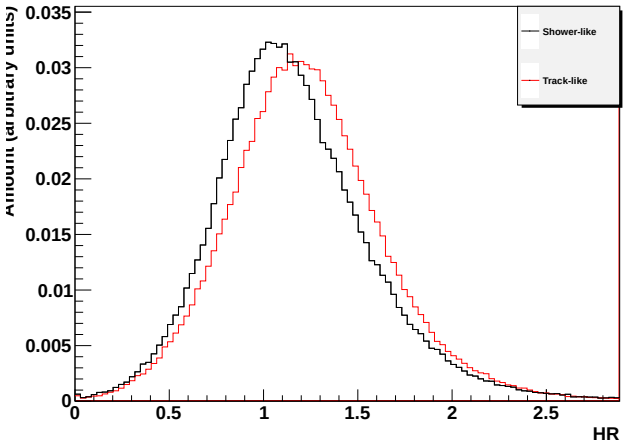

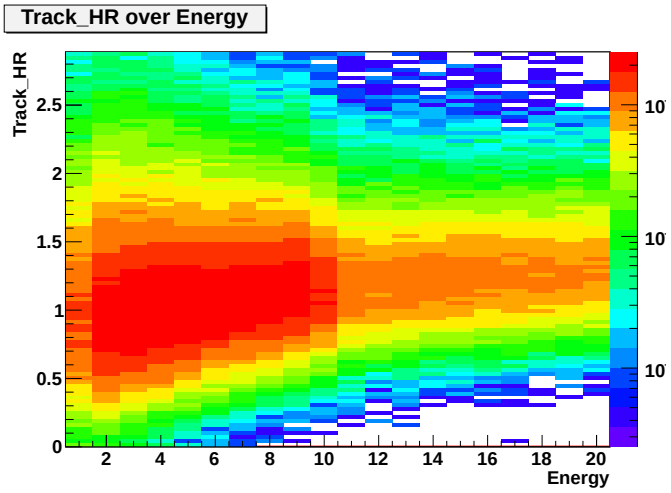
Track_HR over Energy
Track_HR
Energy

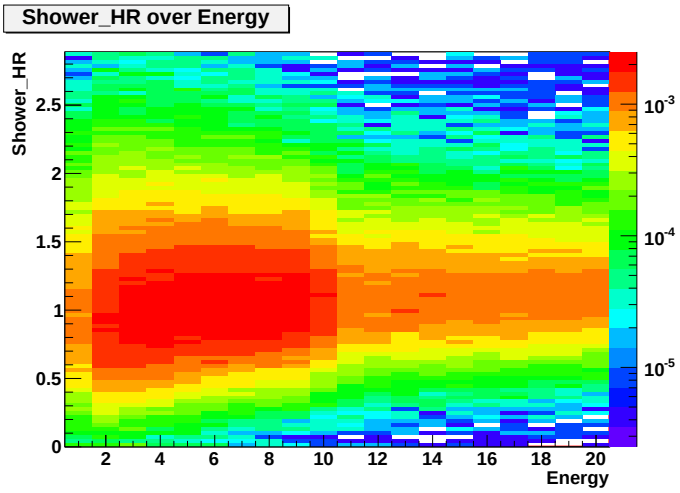
Shower_HR over Energy
Shower_HR
Energy

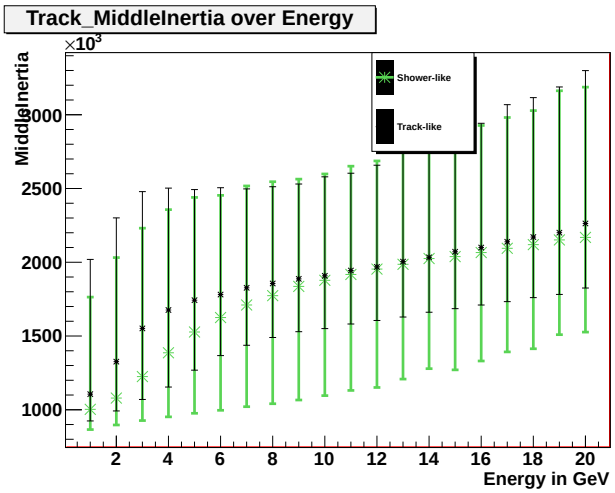
Track_MiddleInertia over Energy
MiddleInertia
Shower-like
Track-like
Energy in GeV

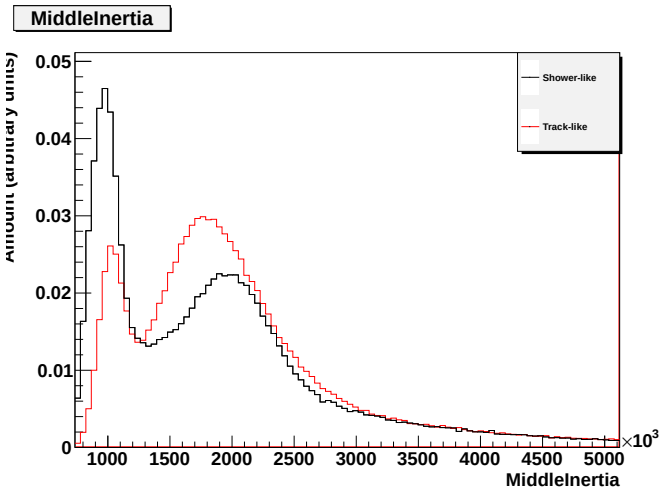
MiddleInertia
Shower-like
Track-like
MiddleInertia

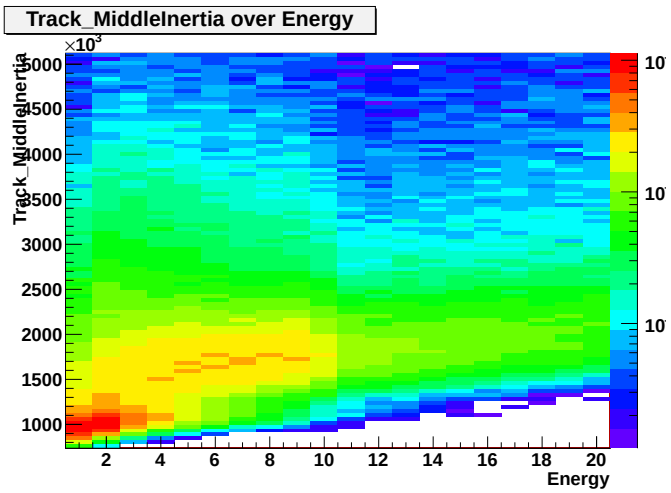
Track_MiddleInertia over Energy
Track_MiddleInertia
Energy

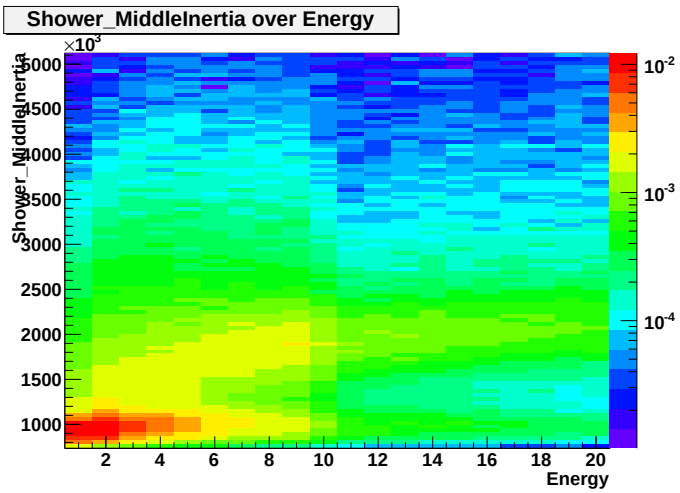
Shower_MiddleInertia over Energy
Shower_MiddleInertia
Energy

Track_MiddleInertiaNormedSphere over Energy

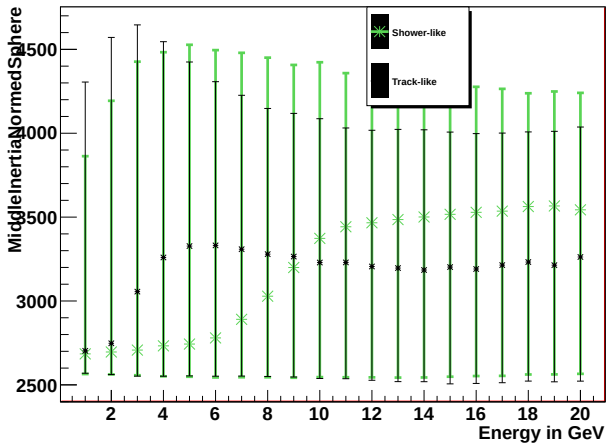

MiddleInertiaNormedSphere

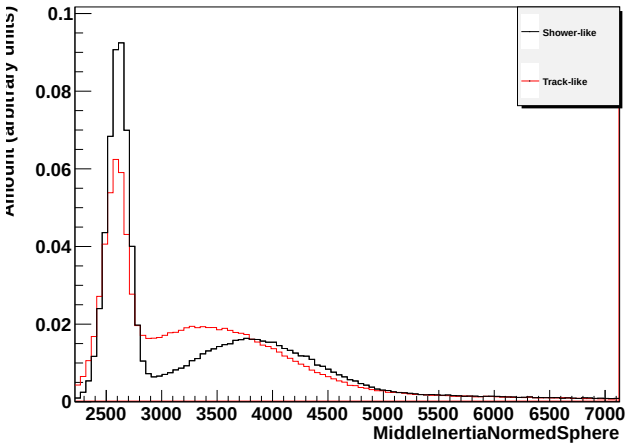

Track_MiddleInertiaNormedSphere over Energy

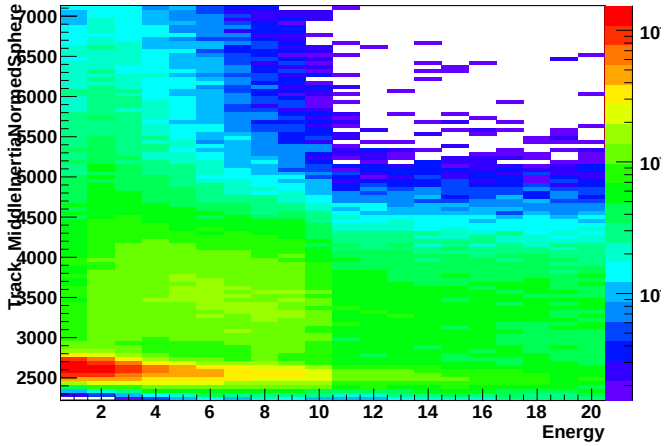

Shower_MiddleInertiaNormedSphere over Energy

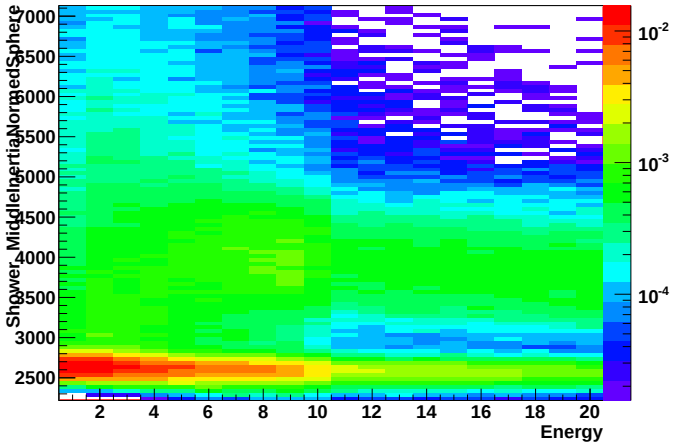

Track_PulseCountCharge over Energy

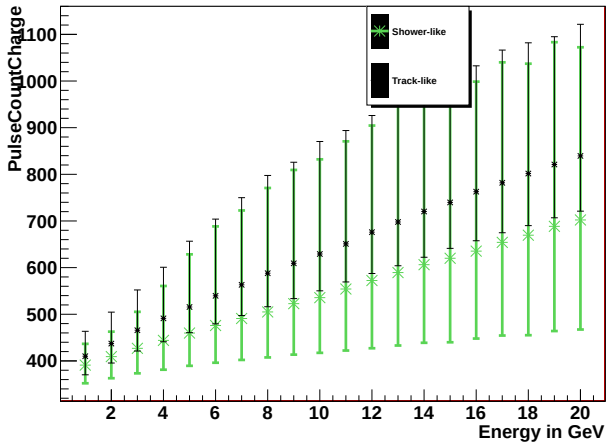

PulseCountCharge

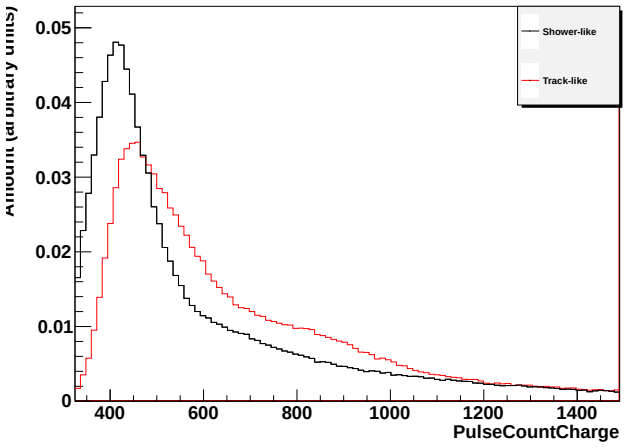

Track_PulseCountCharge over Energy

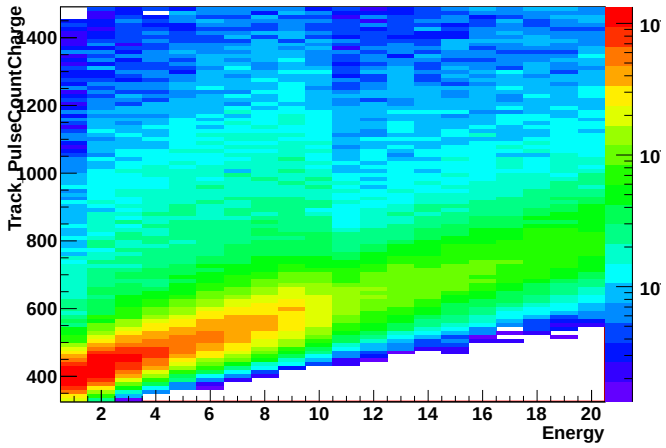

Shower_PulseCountCharge over Energy

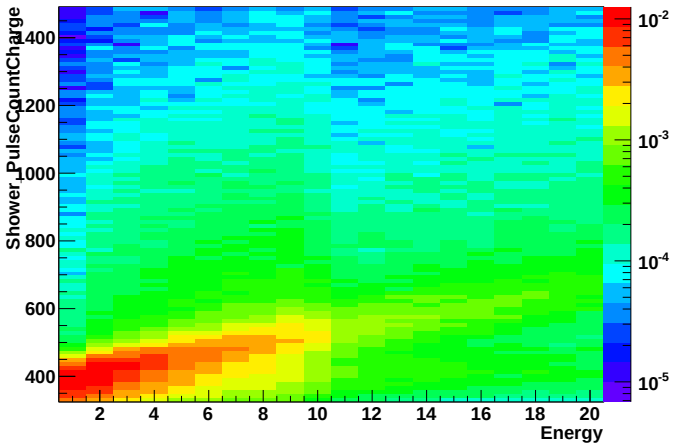

Track_PulseCountNone over Energy

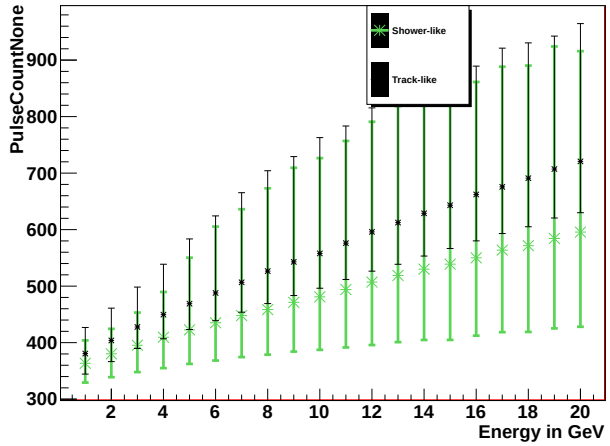

PulseCountNone

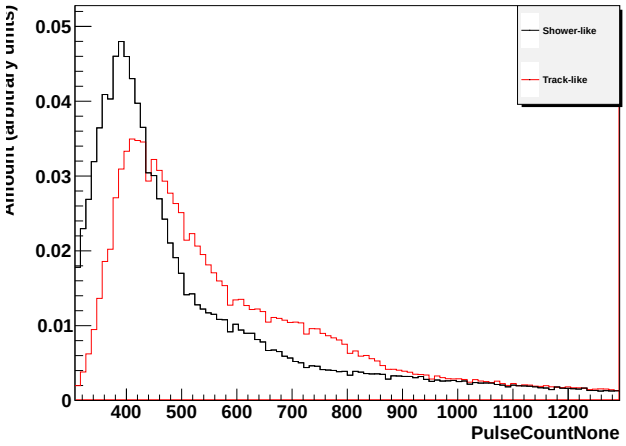

Track_PulseCountNone over Energy

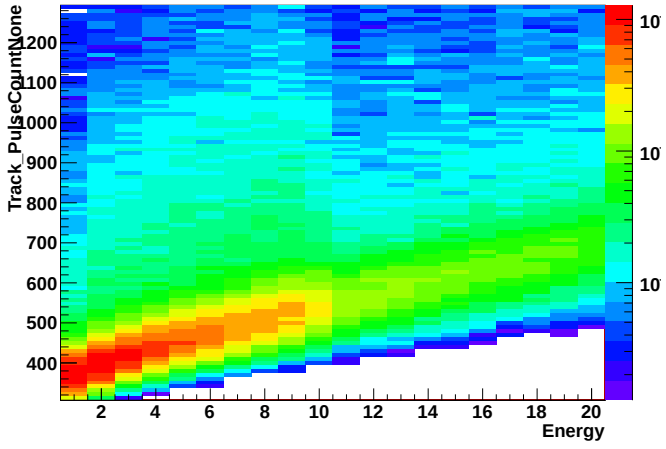

Shower_PulseCountNone over Energy

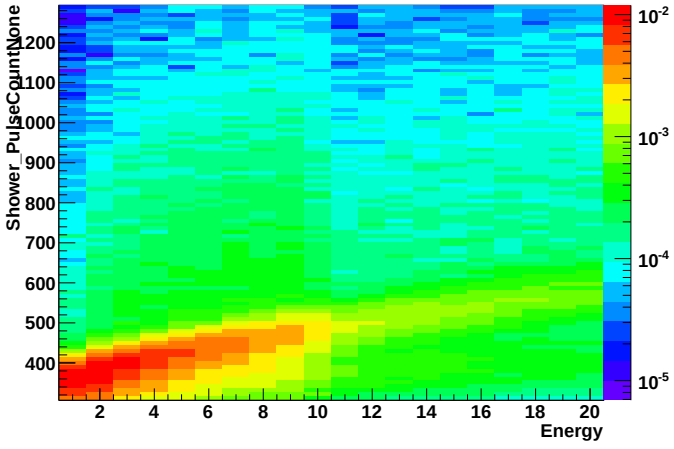

Track_QStrategyChi2 over Energy

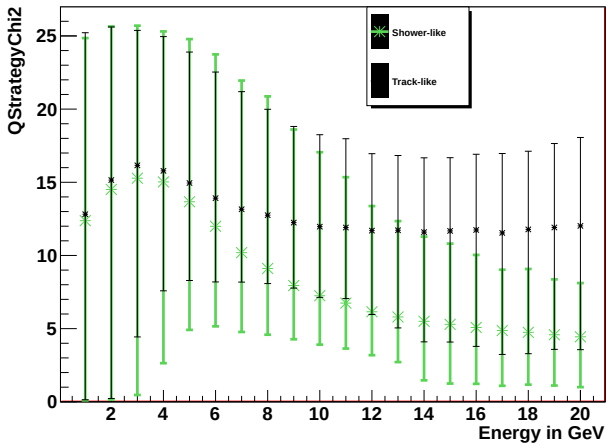

QStrategyChi2

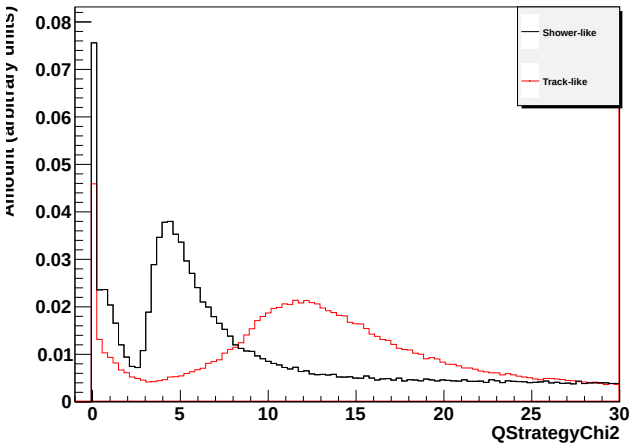

Track_QStrategyChi2 over Energy

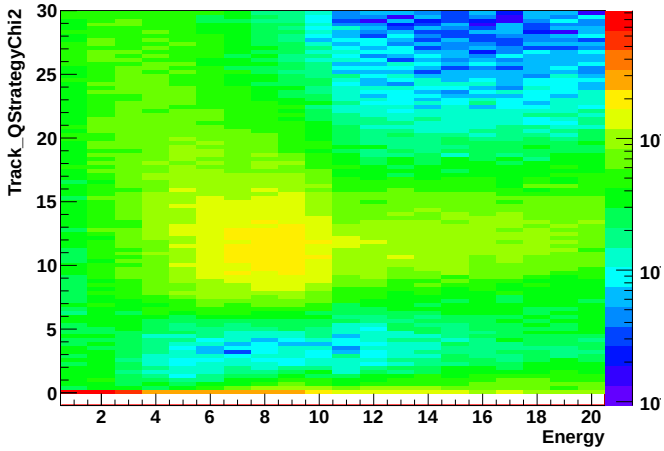

Shower_QStrategyChi2 over Energy

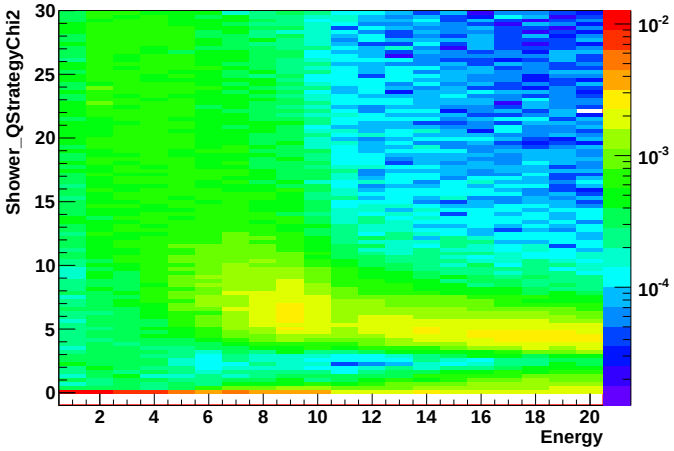

Track_QStrategyQuality over Energy

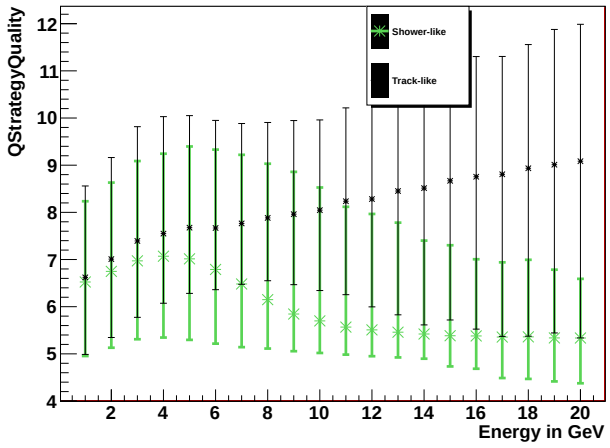

QStrategyQuality

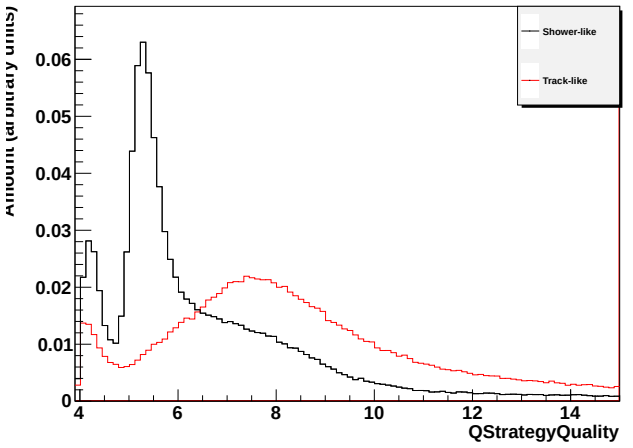

Track_QStrategyQuality over Energy

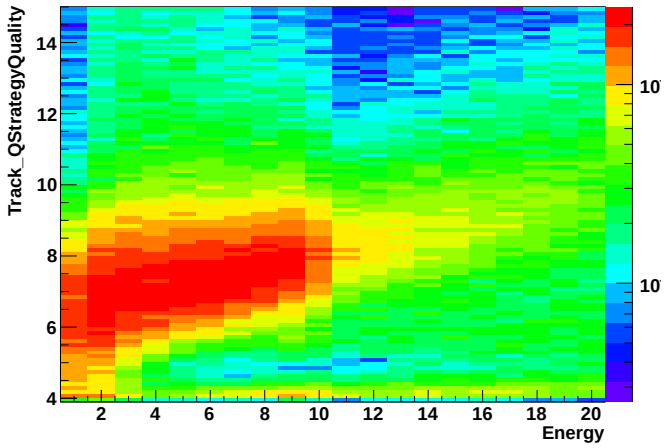

Shower_QStrategyQuality over Energy

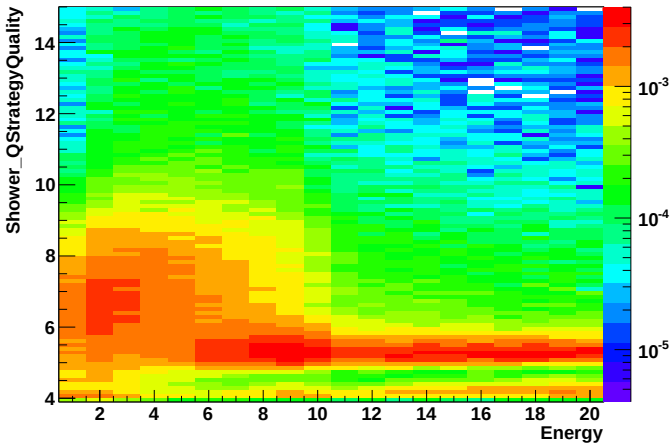

Track_RelativeInertia over Energy

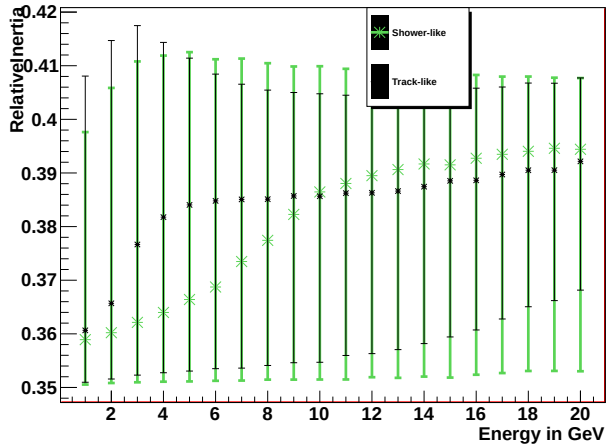

RelativeInertia

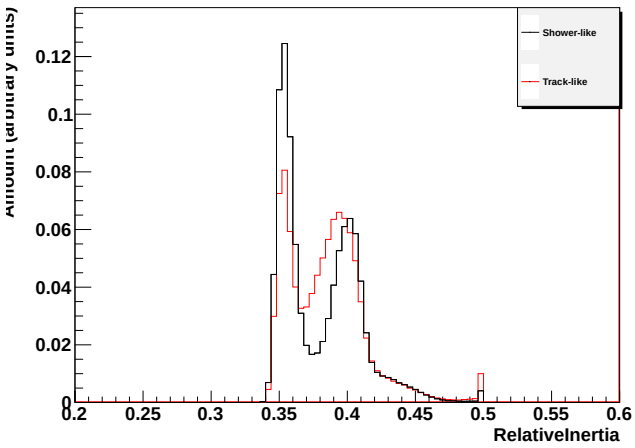

Track_RelativeInertia over Energy

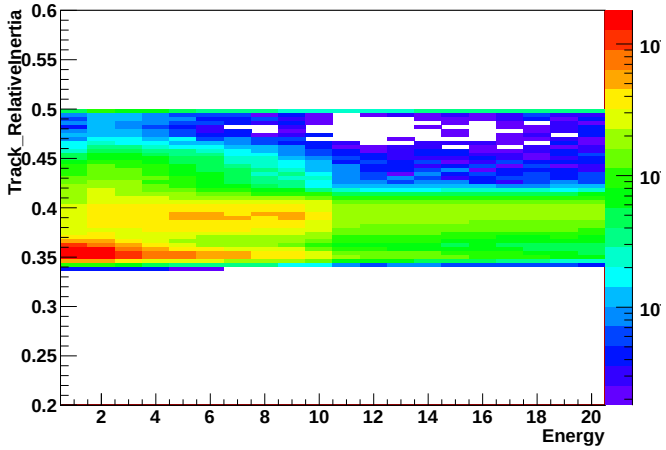

Shower_RelativeInertia over Energy

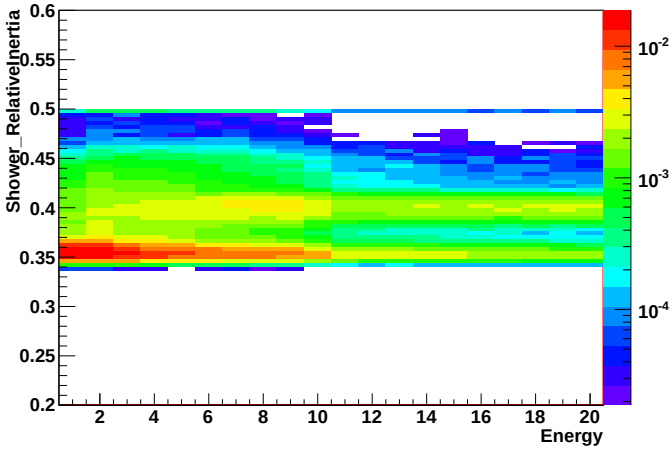

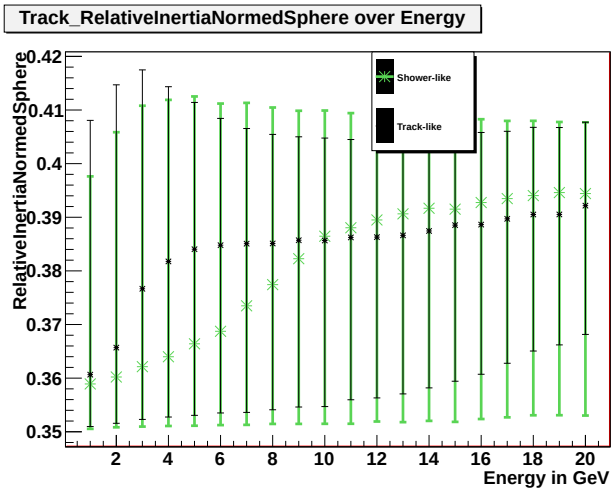
Track_RelativeInertiaNormedSphere over Energy
RelativeInertiaNormedSphere
Energy in GeV
Shower-like
Track-like

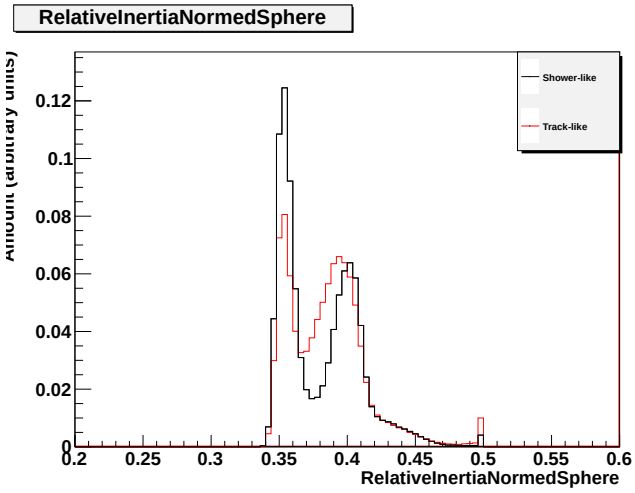
RelativeInertiaNormedSphere
Amount (arbitrary units)
RelativeInertiaNormedSphere
Shower-like
Track-like

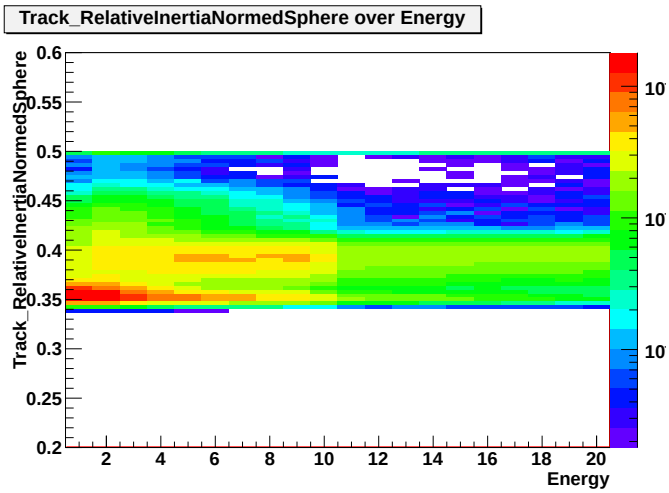
Track_RelativeInertiaNormedSphere over Energy
Track_RelativeInertiaNormedSphere
Energy

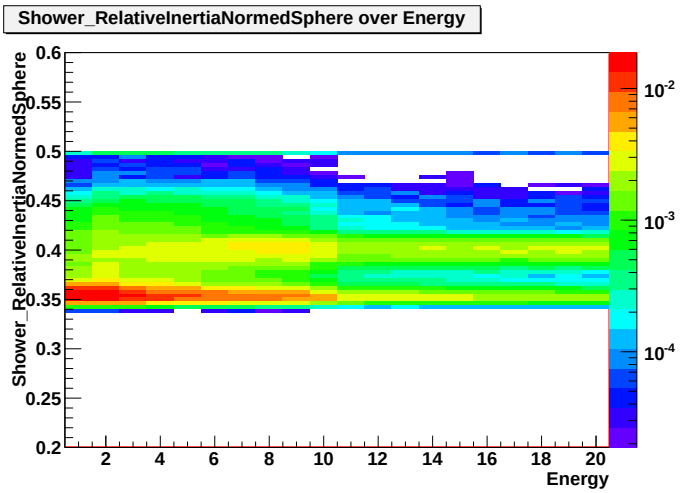
Shower_RelativeInertiaNormedSphere over Energy
Shower_RelativeInertiaNormedSphere
Energy

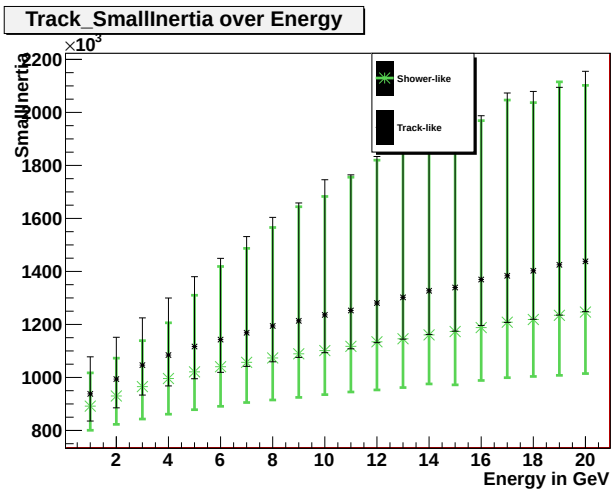
Track_SmallInertia over Energy
SmallInertia
Energy in GeV
Shower-like
Track-like

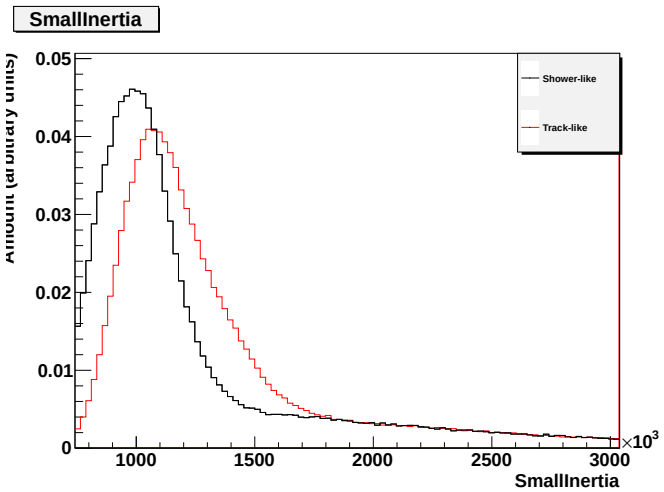
SmallInertia
Amount (arbitrary units)
SmallInertia
Shower-like
Track-like

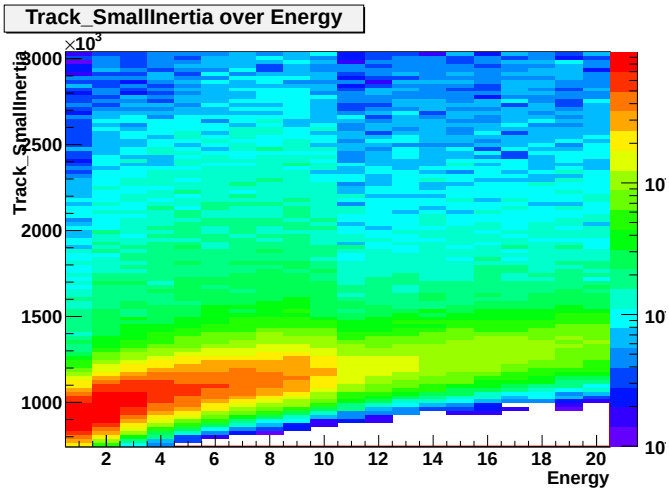
Track_SmallInertia over Energy
×10^3
Track_SmallInertia
Energy

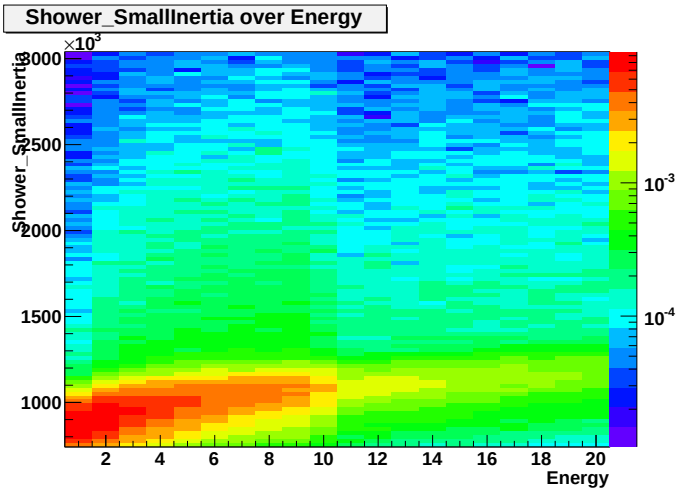
Shower_SmallInertia over Energy
×10^3
Shower_SmallInertia
Energy

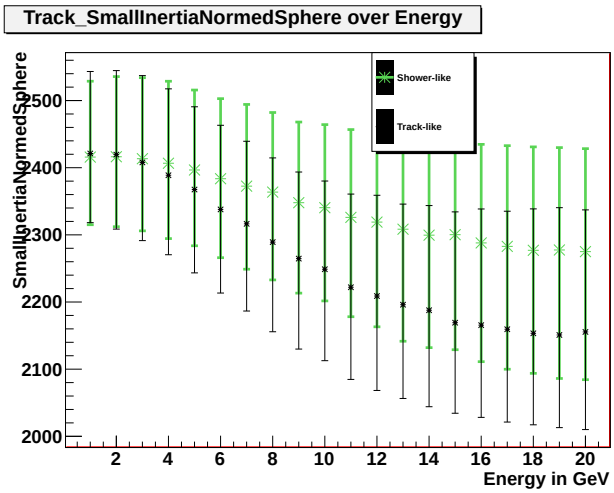
Track_SmallInertiaNormedSphere over Energy
SmallInertiaNormedSphere
Shower-like
Track-like
Energy in GeV

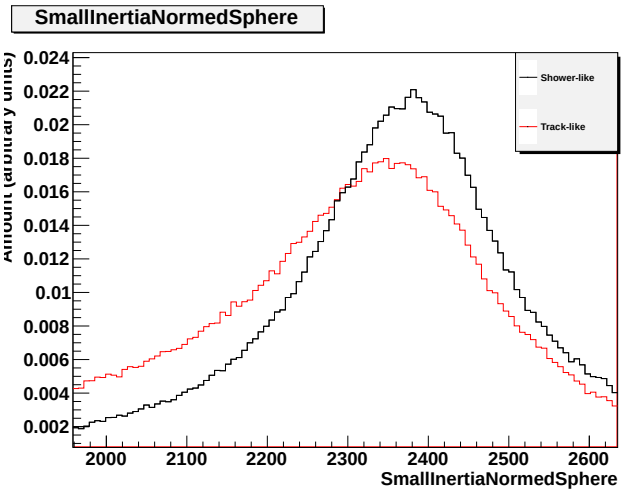
SmallInertiaNormedSphere
Shower-like
Track-like
SmallInertiaNormedSphere

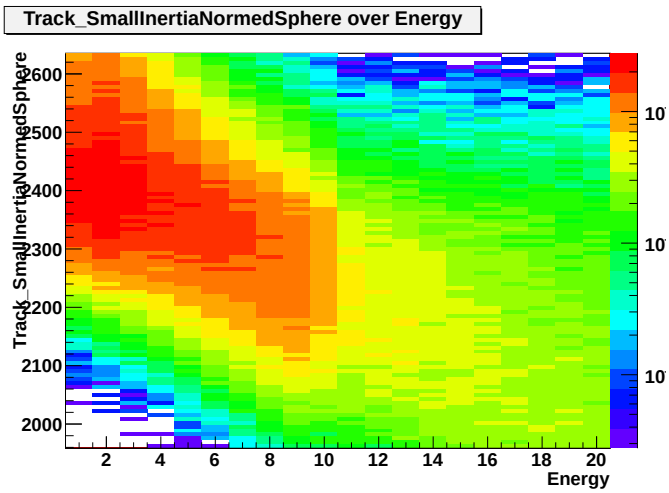
Track_SmallInertiaNormedSphere over Energy
Track_SmallInertiaNormedSphere
Energy

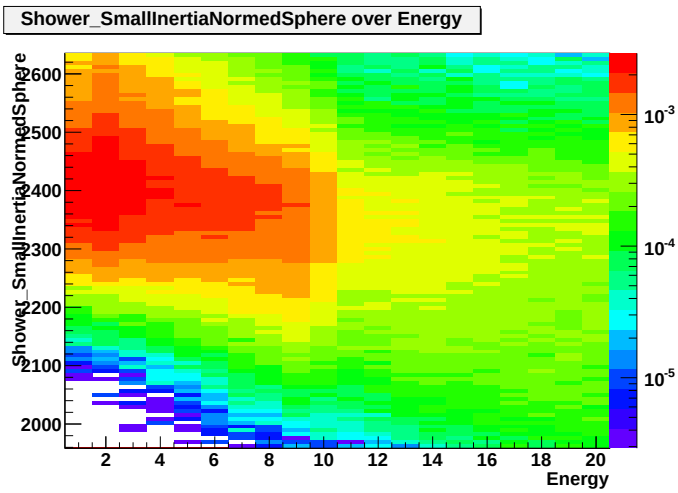
Shower_SmallInertiaNormedSphere over Energy
Shower_SmallInertiaNormedSphere
Energy

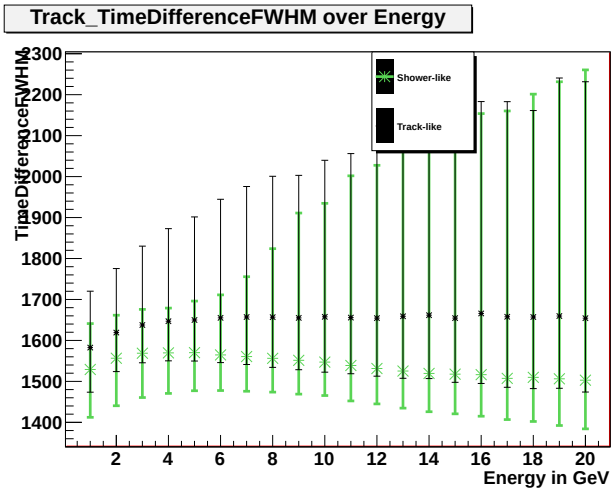
Track_TimeDifferenceFWHM over Energy
TimeDifferenceFWHM
Shower-like
Track-like
Energy in GeV

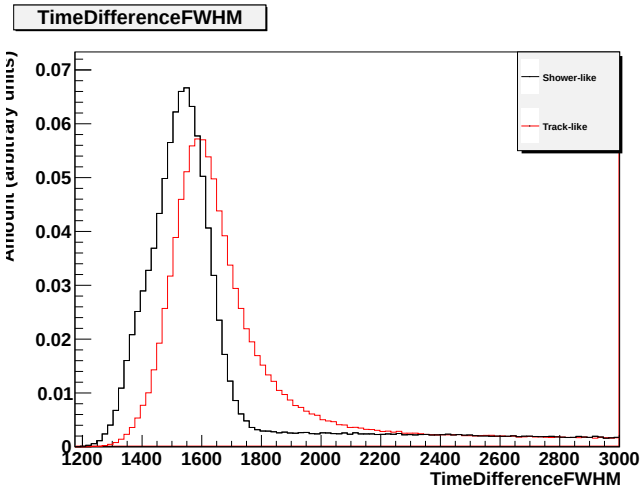
TimeDifferenceFWHM
Amount (arbitrary units)
Shower-like
Track-like
TimeDifferenceFWHM

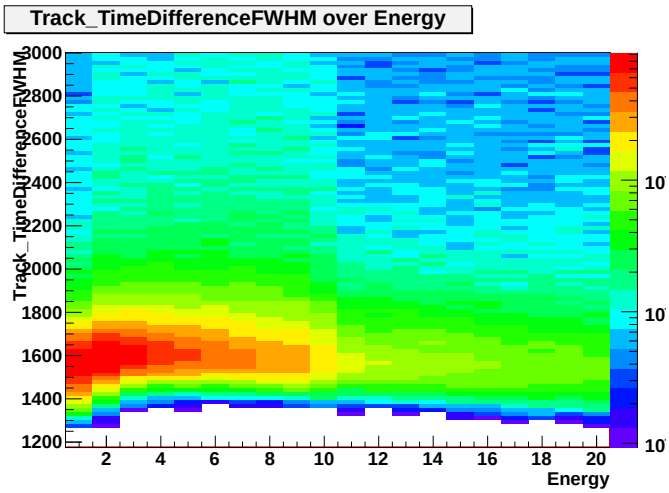
Track_TimeDifferenceFWHM over Energy
Track_TimeDifferenceFWHM
Energy

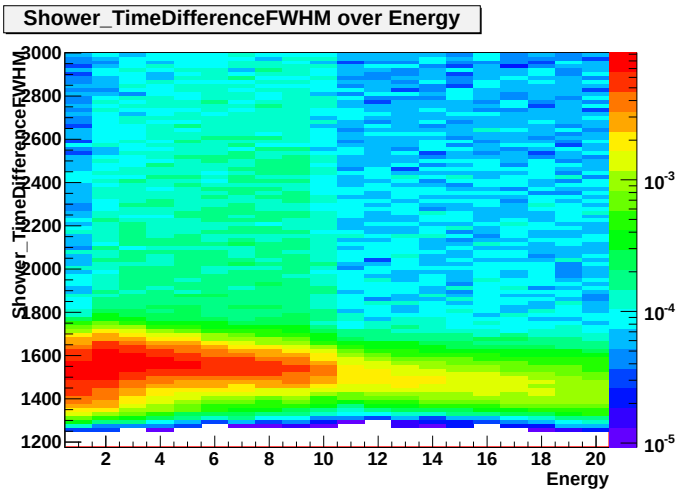
Shower_TimeDifferenceFWHM over Energy
Shower_TimeDifferenceFWHM
Energy

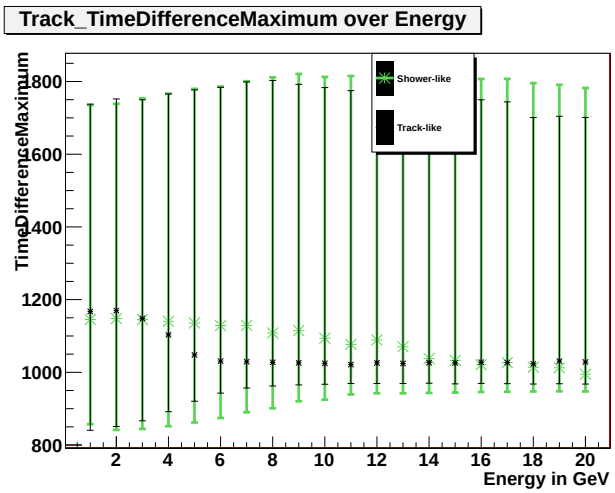
Track_TimeDifferenceMaximum over Energy
TimeDifferenceMaximum
Shower-like
Track-like
Energy in GeV

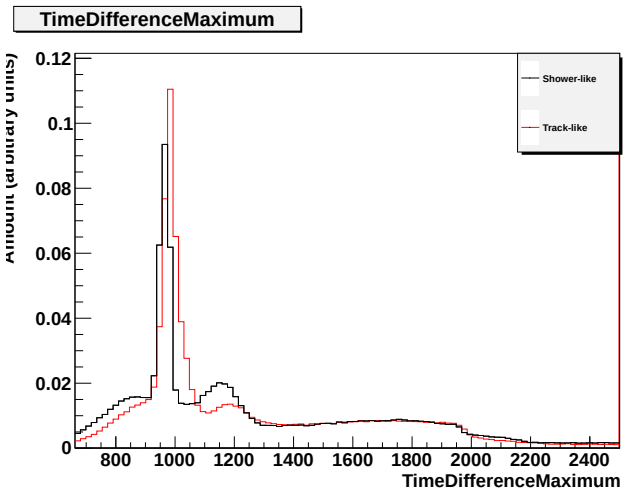
TimeDifferenceMaximum
Amount (arbitrary units)
Shower-like
Track-like
TimeDifferenceMaximum

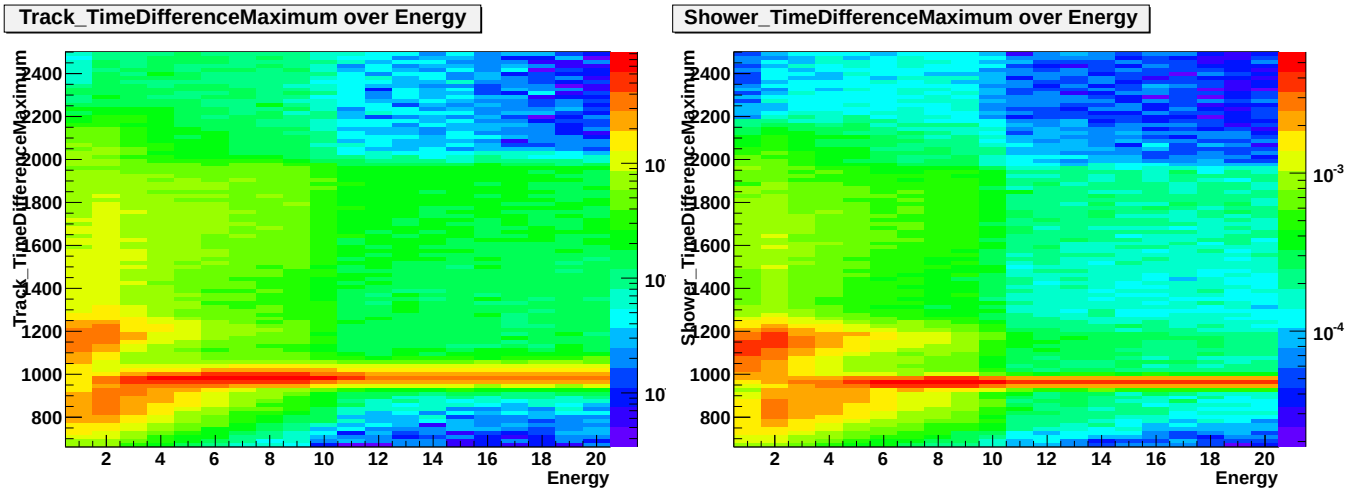
Track_TimeDifferenceMaximum over Energy
Track_TimeDifferenceMaximum
Energy
Shower_TimeDifferenceMaximum over Energy
Shower_TimeDifferenceMaximum
Energy

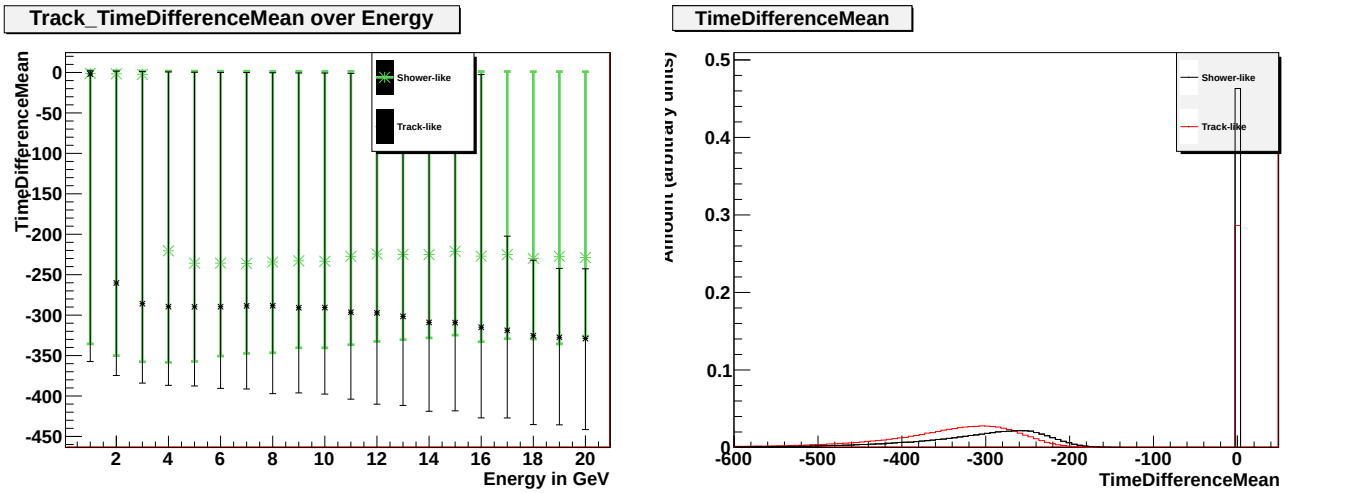
Track_TimeDifferenceMean over Energy
TimeDifferenceMean
Energy in GeV
Shower-like
Track-like
TimeDifferenceMean
Amount (arbitrary units)
TimeDifferenceMean
Shower-like
Track-like

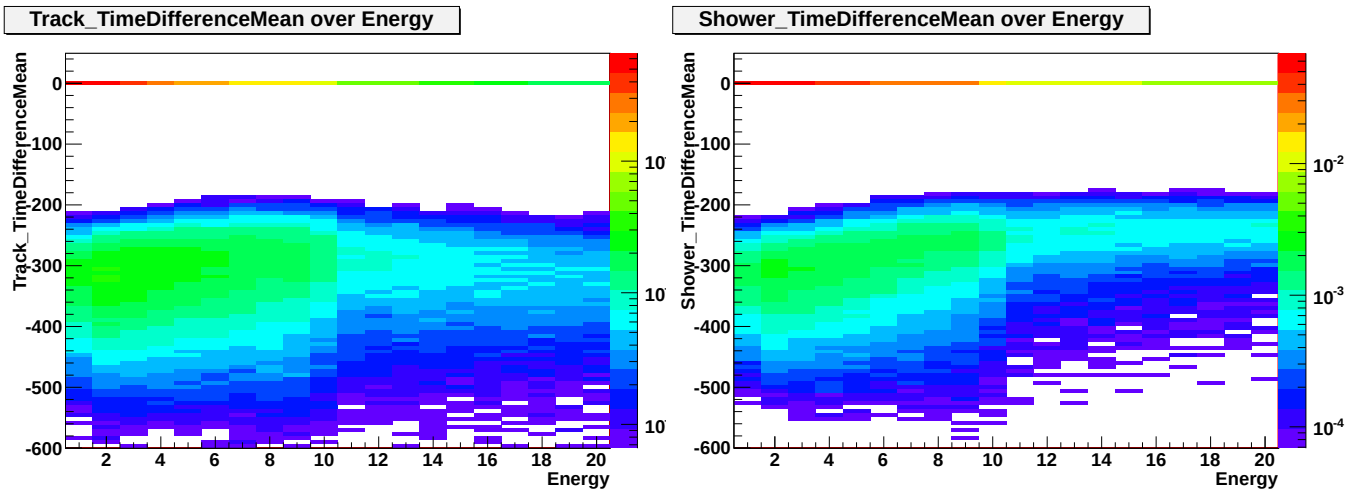
Track_TimeDifferenceMean over Energy
Track_TimeDifferenceMean
Energy
Shower_TimeDifferenceMean over Energy
Shower_TimeDifferenceMean
Energy

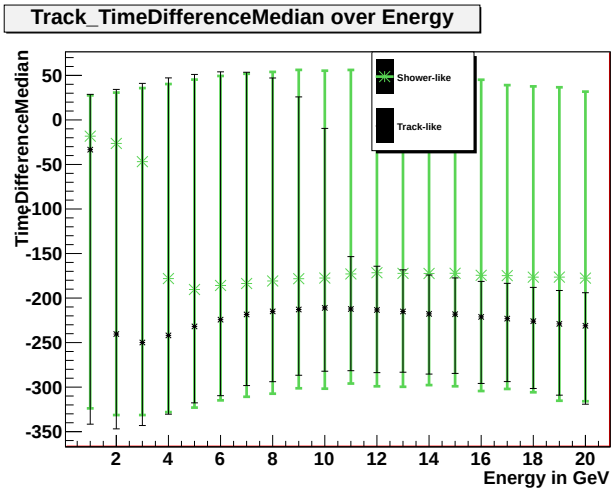
Track_TimeDifferenceMedian over Energy
TimeDifferenceMedian
Energy in GeV
Shower-like
Track-like

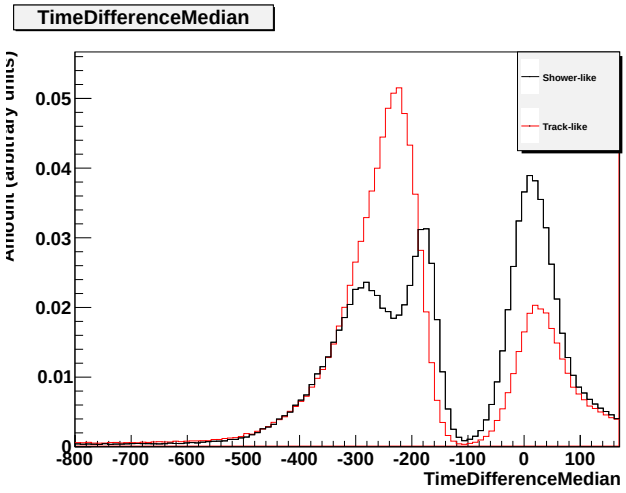
TimeDifferenceMedian
Amount (arbitrary units)
TimeDifferenceMedian
Shower-like
Track-like

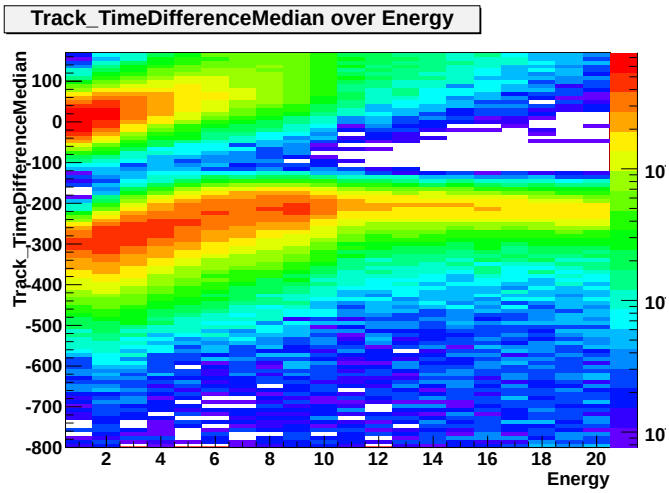
Track_TimeDifferenceMedian over Energy
Track_TimeDifferenceMedian
Energy

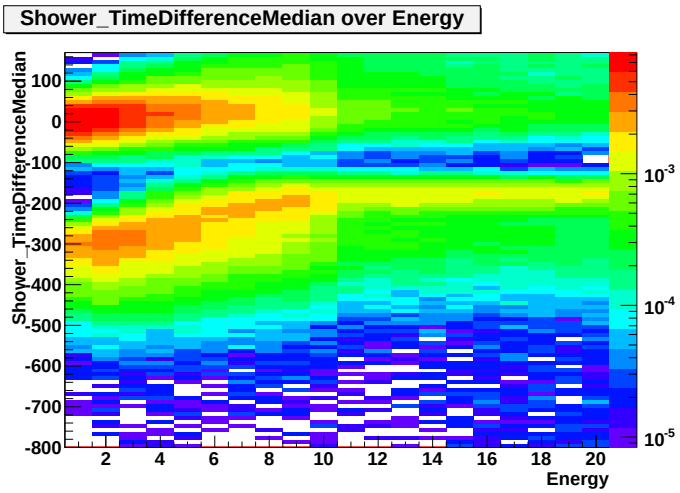
Shower_TimeDifferenceMedian over Energy
Shower_TimeDifferenceMedian
Energy

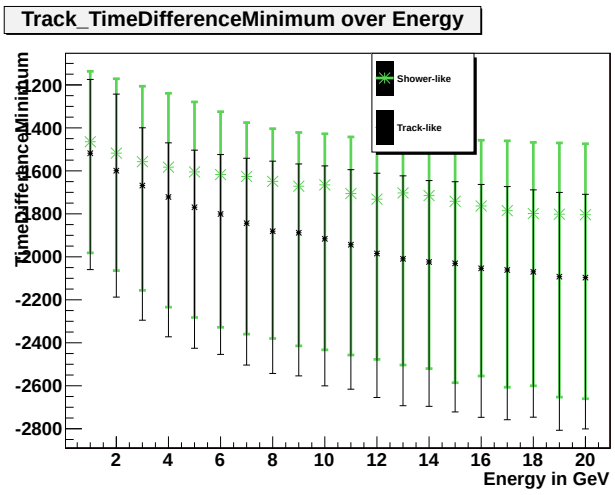
Track_TimeDifferenceMinimum over Energy
TimeDifferenceMinimum
Energy in GeV
Shower-like
Track-like

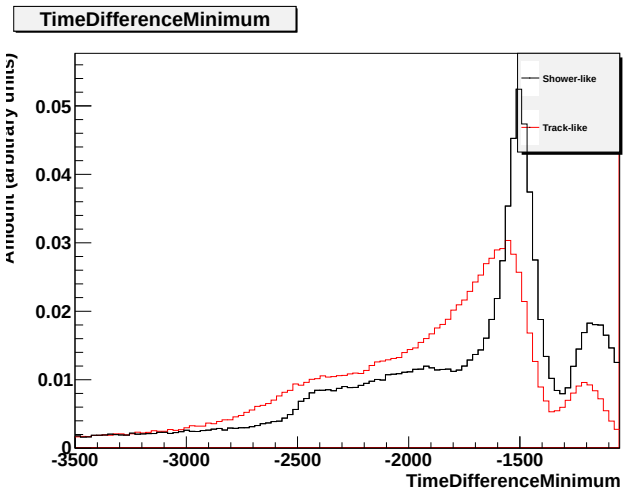
TimeDifferenceMinimum
Amount (arbitrary units)
TimeDifferenceMinimum
Shower-like
Track-like

Track_TimeDifferenceMinimum over Energy

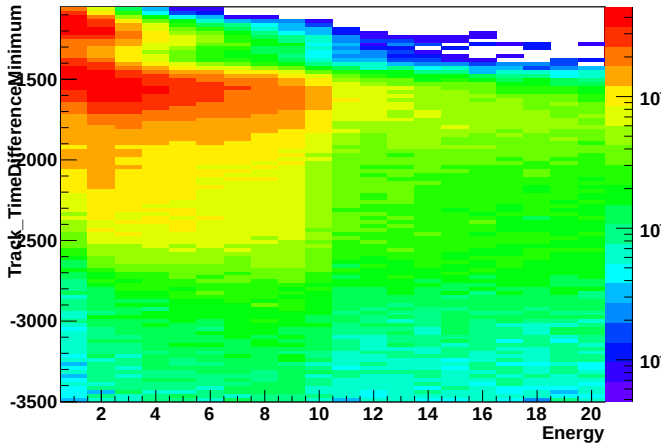

Shower_TimeDifferenceMinimum over Energy

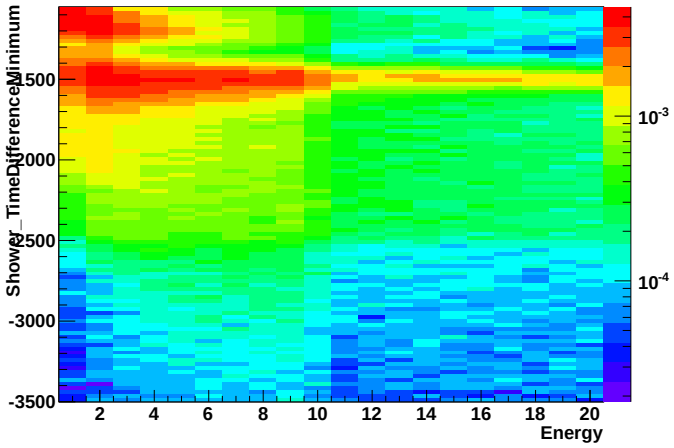

Track_TimeDifferenceRMS over Energy

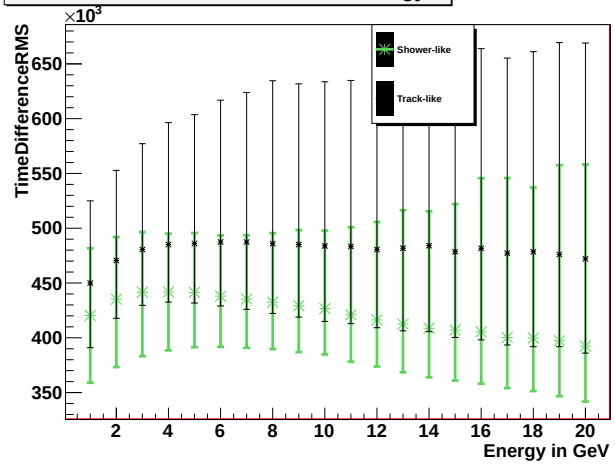

TimeDifferenceRMS

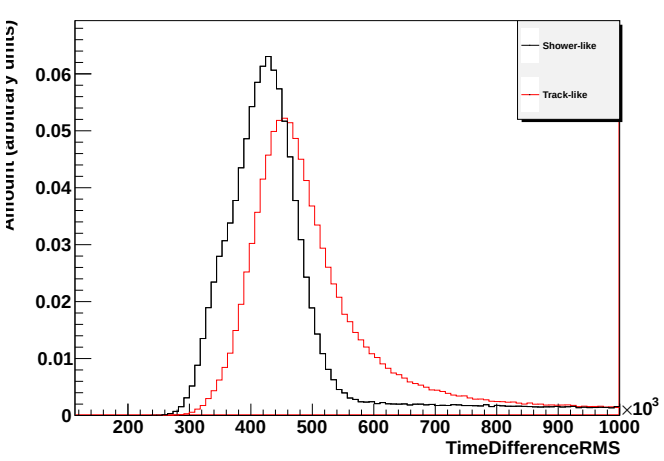

Track_TimeDifferenceRMS over Energy

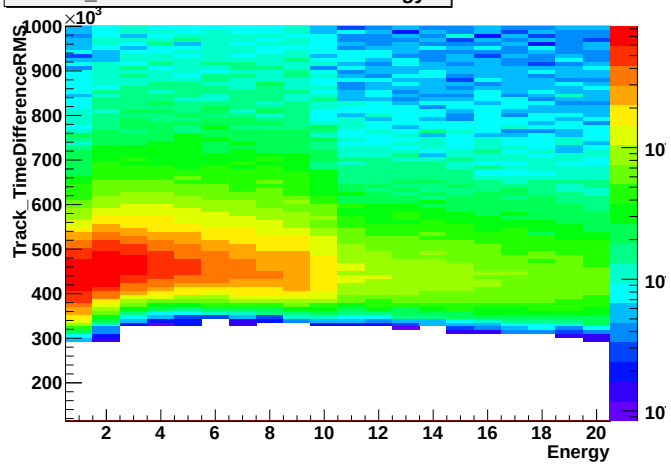

Shower_TimeDifferenceRMS over Energy

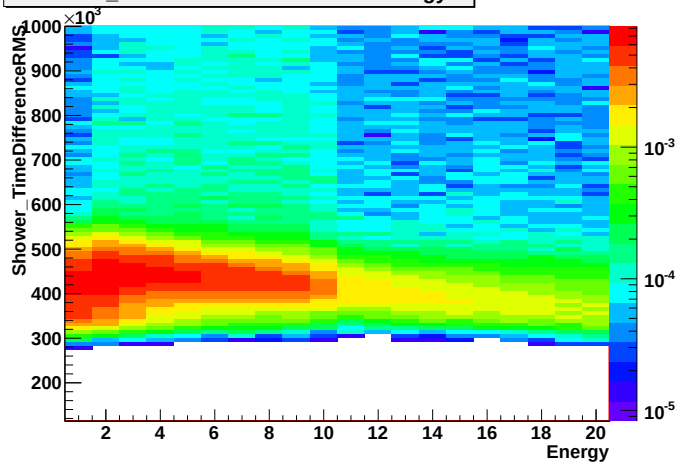

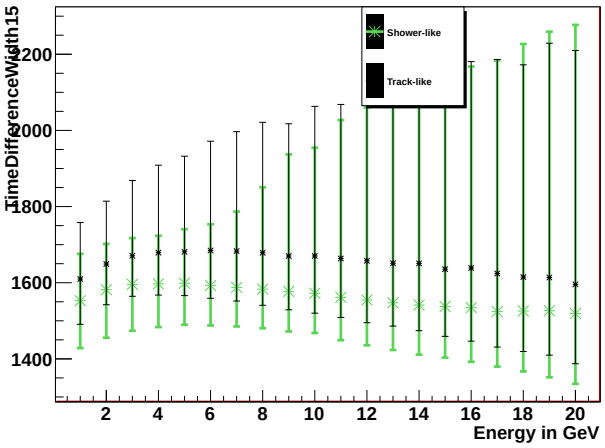

Track_TimeDifferenceWidth15_85 over Energy

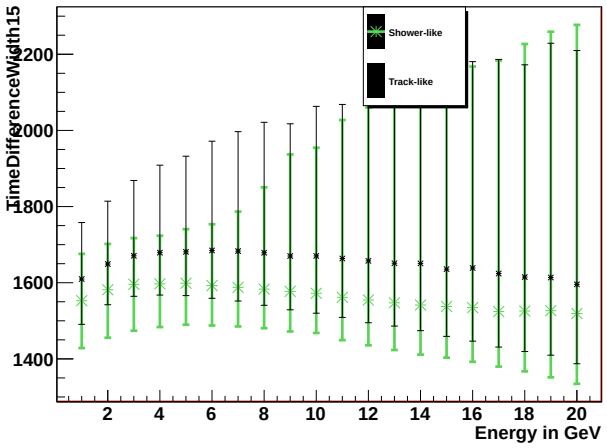

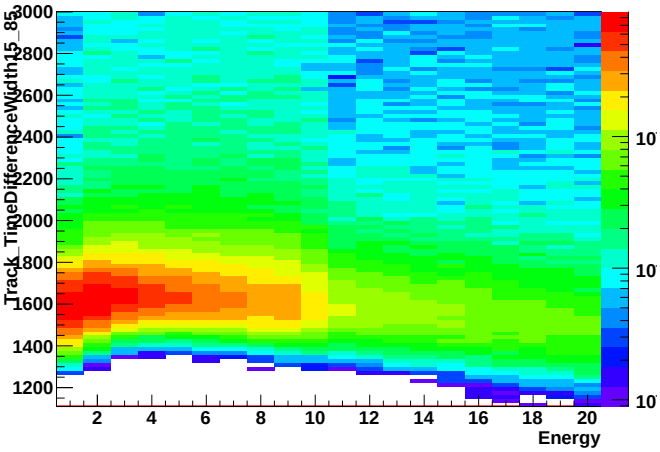

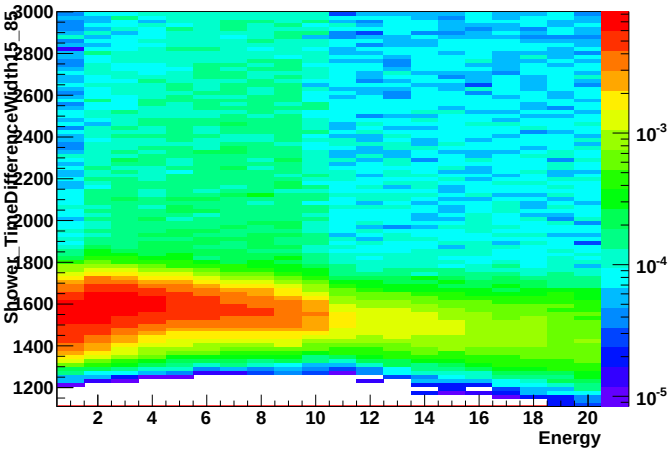

Track_TimeResidualFWHM over Energy

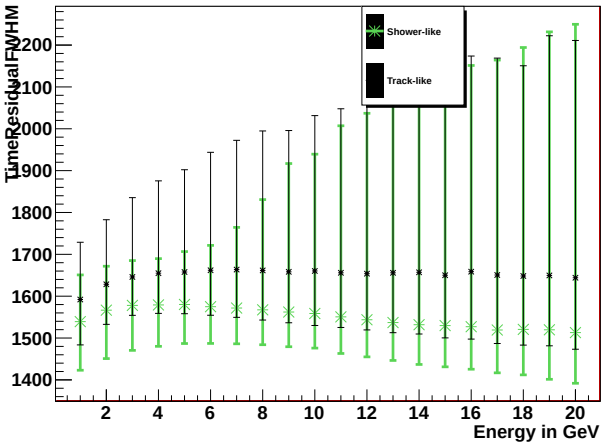

TimeResidualFWHM

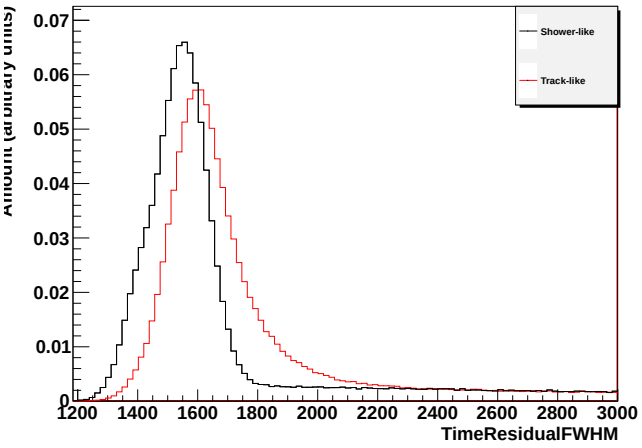

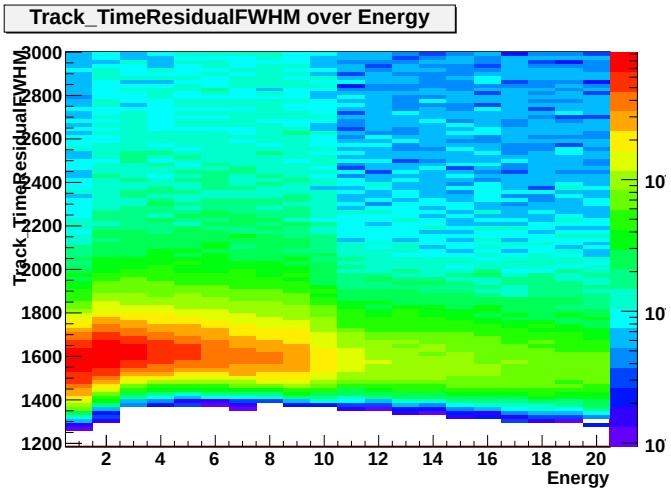
Track_TimeResidualFWHM over Energy
Track_TimeResidualFWHM
Energy

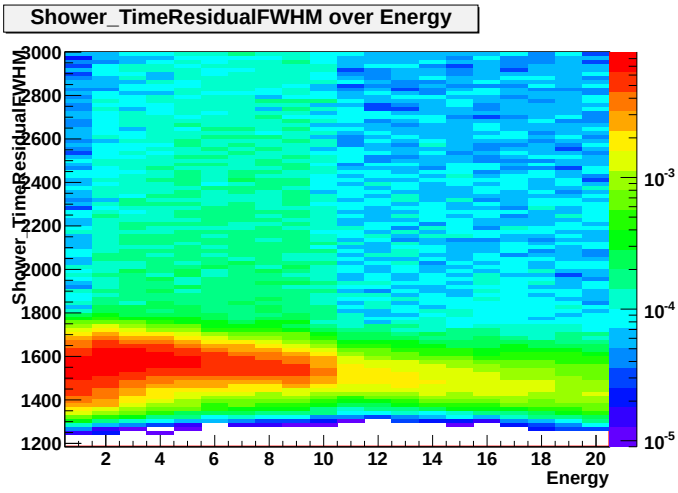
Shower_TimeResidualFWHM over Energy
Shower_TimeResidualFWHM
Energy

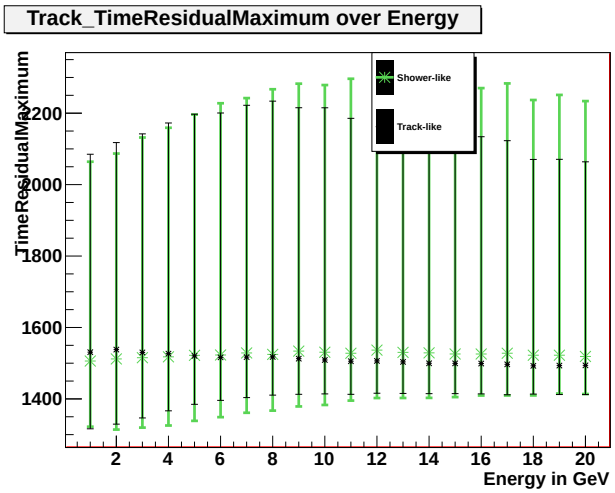
Track_TimeResidualMaximum over Energy
TimeResidualMaximum
Shower-like
Track-like
Energy in GeV

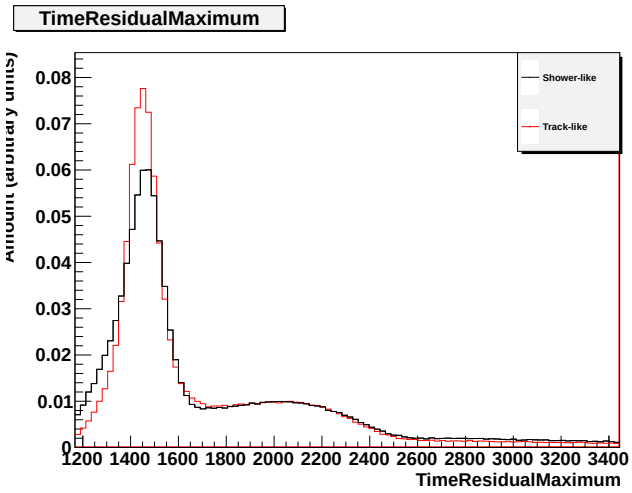
TimeResidualMaximum
Shower-like
Track-like
TimeResidualMaximum

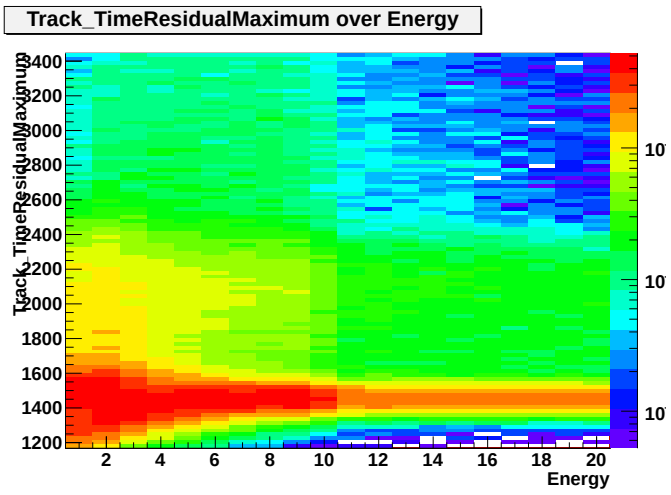
Track_TimeResidualMaximum over Energy
Track_TimeResidualMaximum
Energy

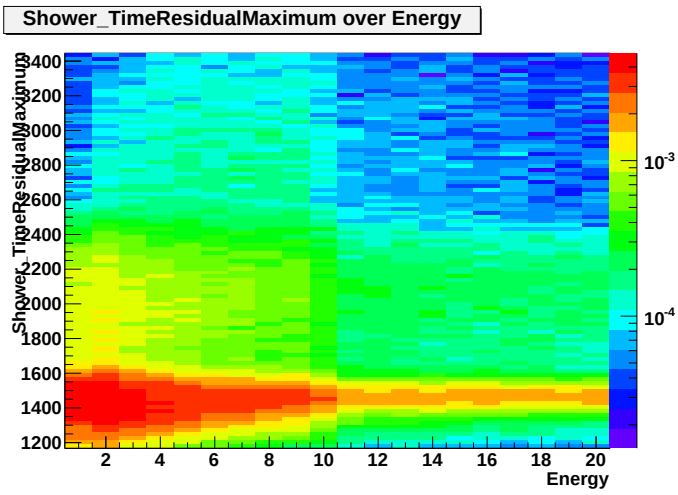
Shower_TimeResidualMaximum over Energy
Shower_TimeResidualMaximum
Energy

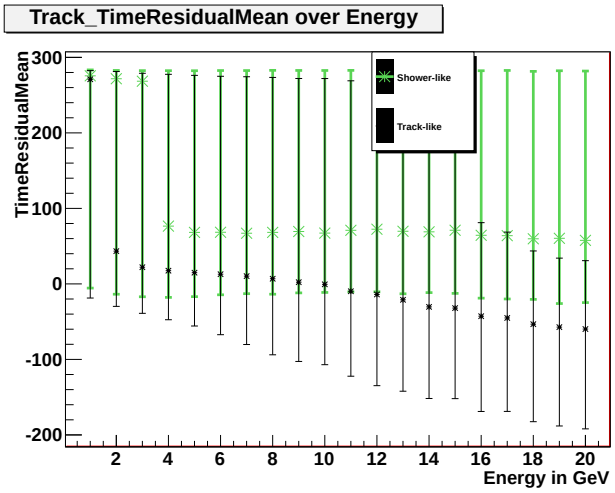
Track_TimeResidualMean over Energy
TimeResidualMean
Energy in GeV
Shower-like
Track-like

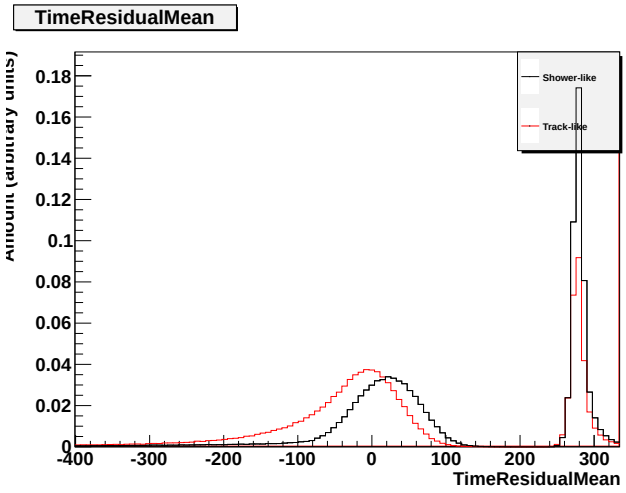
TimeResidualMean
Amount (arbitrary units)
Shower-like
Track-like

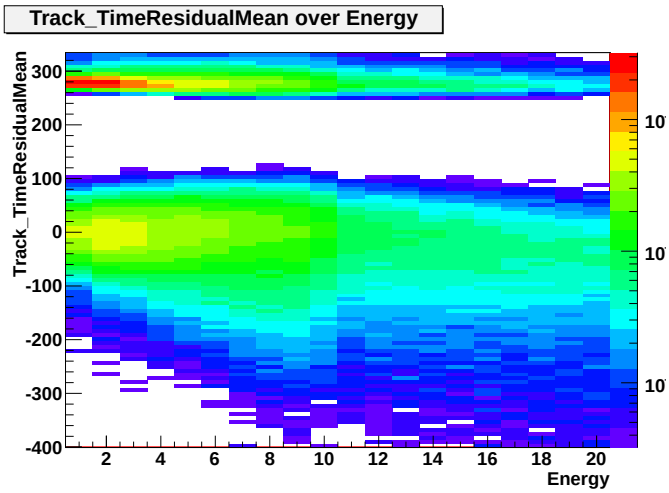
Track_TimeResidualMean over Energy
Track_TimeResidualMean
Energy

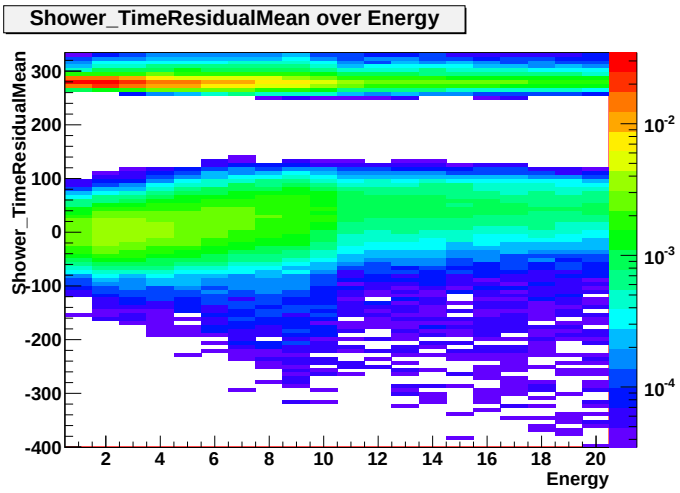
Shower_TimeResidualMean over Energy
Shower_TimeResidualMean
Energy

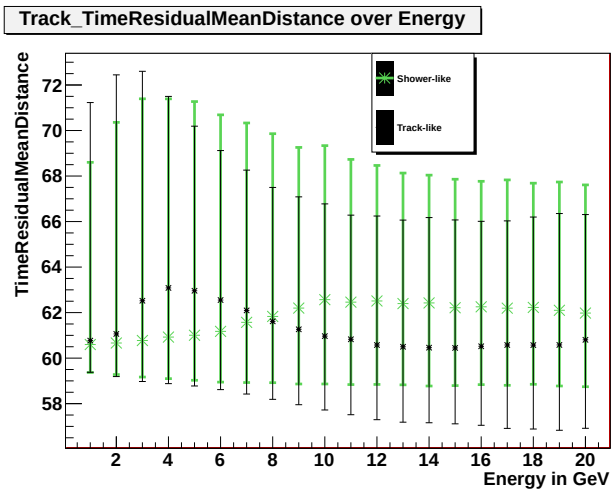
Track_TimeResidualMeanDistance over Energy
TimeResidualMeanDistance
Energy in GeV
Shower-like
Track-like

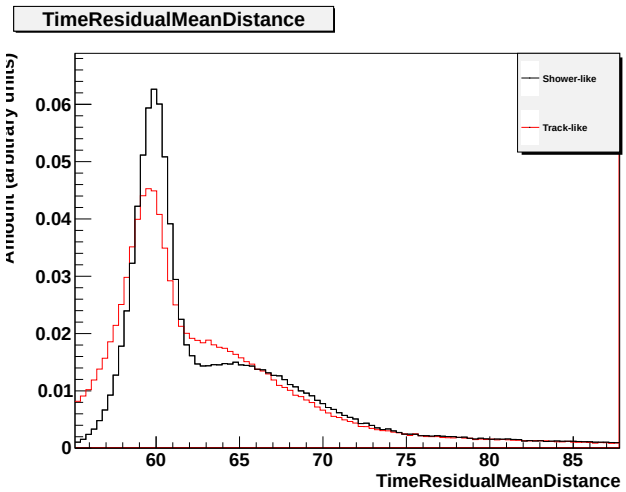
TimeResidualMeanDistance
Amount (arbitrary units)
TimeResidualMeanDistance
Shower-like
Track-like

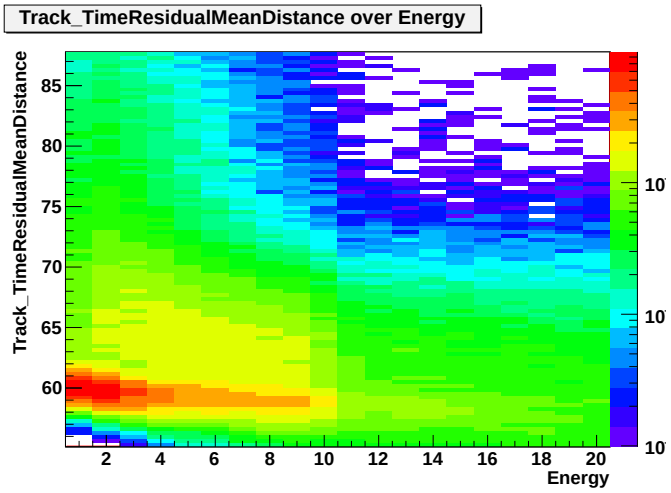
Track_TimeResidualMeanDistance over Energy
Track_TimeResidualMeanDistance
Energy

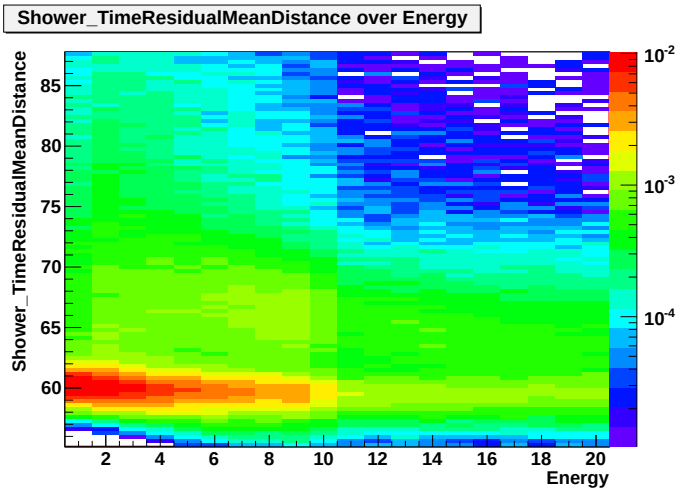
Shower_TimeResidualMeanDistance over Energy
Shower_TimeResidualMeanDistance
Energy

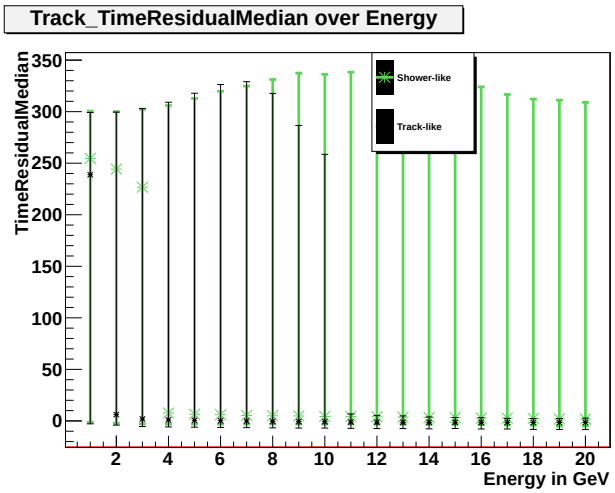
Track_TimeResidualMedian over Energy
TimeResidualMedian
Shower-like
Track-like
Energy in GeV

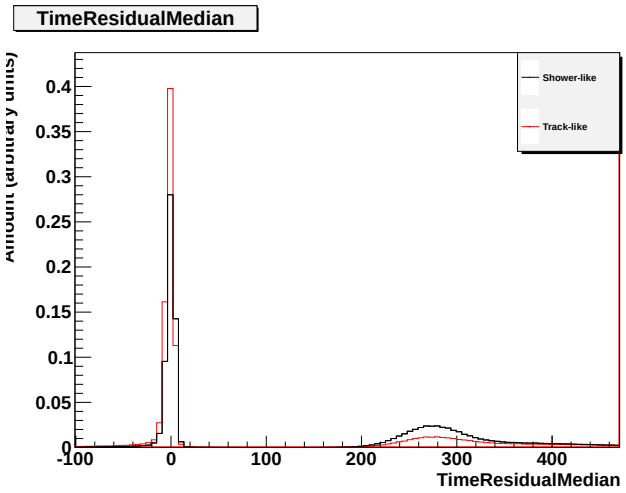
TimeResidualMedian
Shower-like
Track-like
TimeResidualMedian

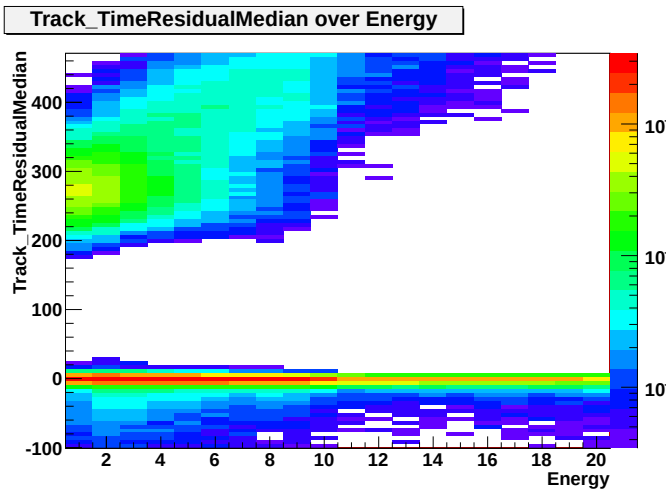
Track_TimeResidualMedian over Energy
Track_TimeResidualMedian
Energy

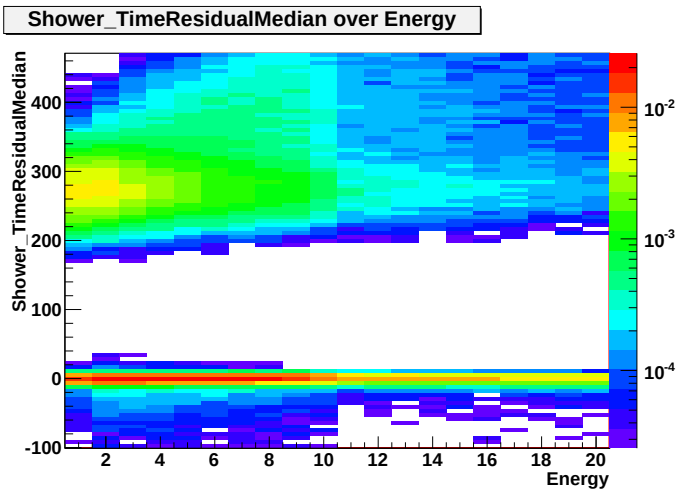
Shower_TimeResidualMedian over Energy
Shower_TimeResidualMedian
Energy

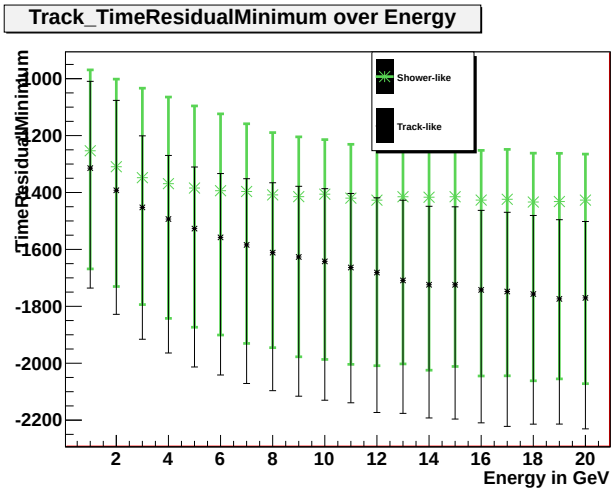
Track_TimeResidualMinimum over Energy
TimeResidualMinimum
Energy in GeV
Shower-like
Track-like

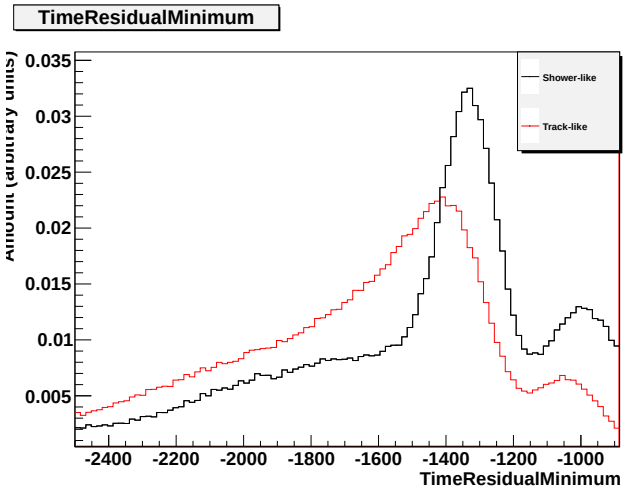
TimeResidualMinimum
Amount (arbitrary units)
TimeResidualMinimum
Shower-like
Track-like

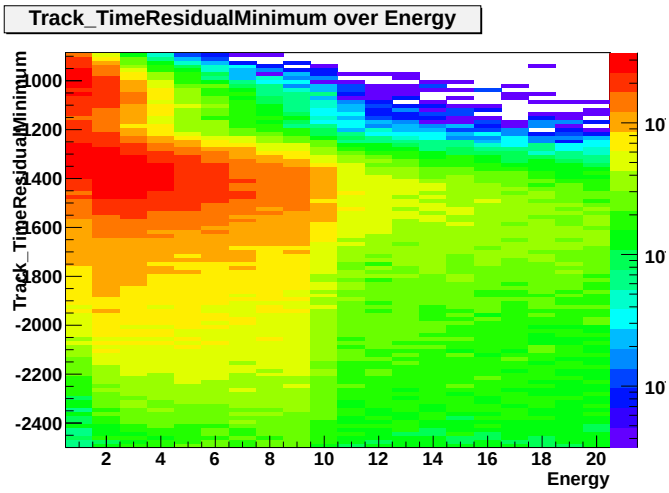
Track_TimeResidualMinimum over Energy
Track_TimeResidualMinimum
Energy

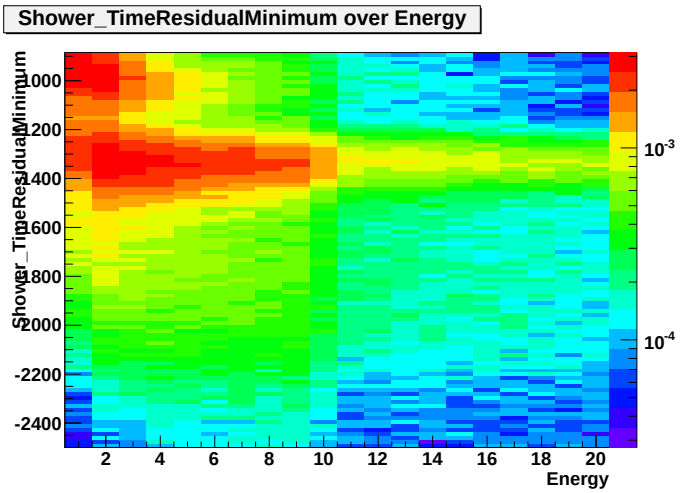
Shower_TimeResidualMinimum over Energy
Shower_TimeResidualMinimum
Energy

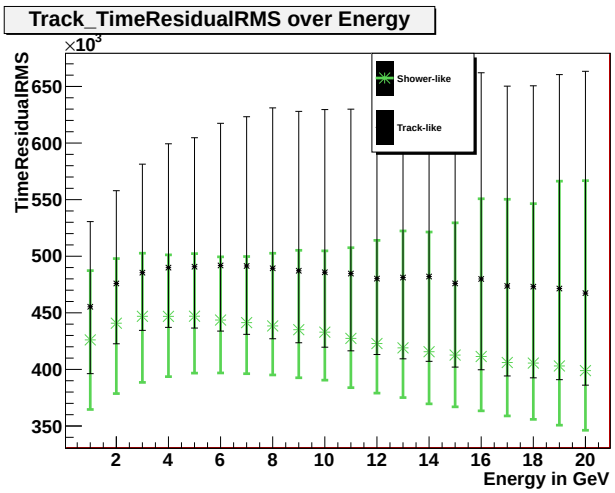
Track_TimeResidualRMS over Energy
TimeResidualRMS
Energy in GeV
Shower-like
Track-like

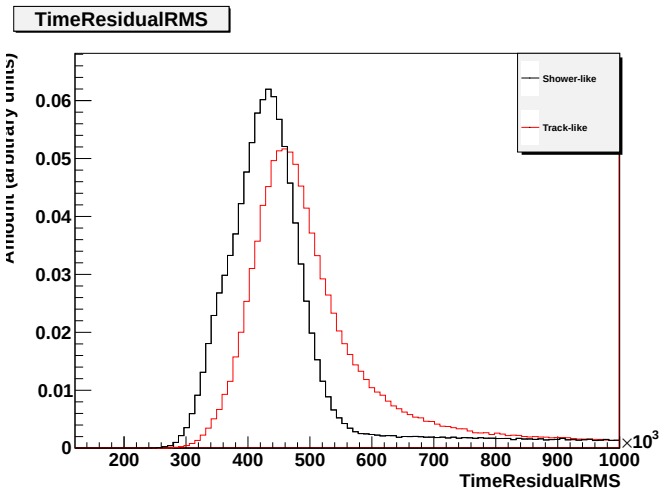
TimeResidualRMS
Amount (arbitrary units)
TimeResidualRMS
Shower-like
Track-like

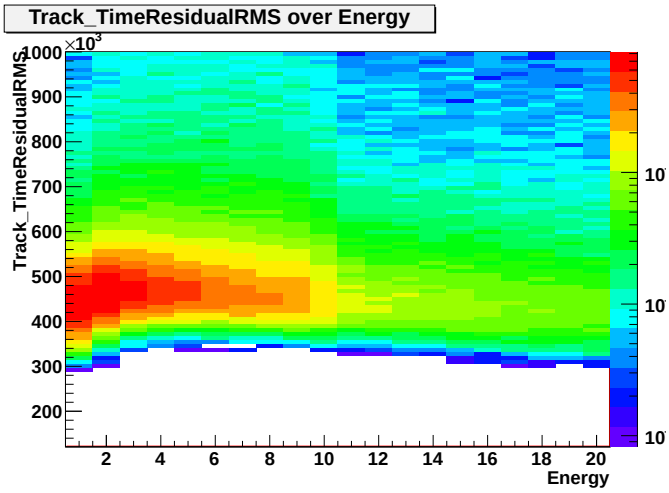
Track_TimeResidualRMS over Energy
Track_TimeResidualRMS
Energy

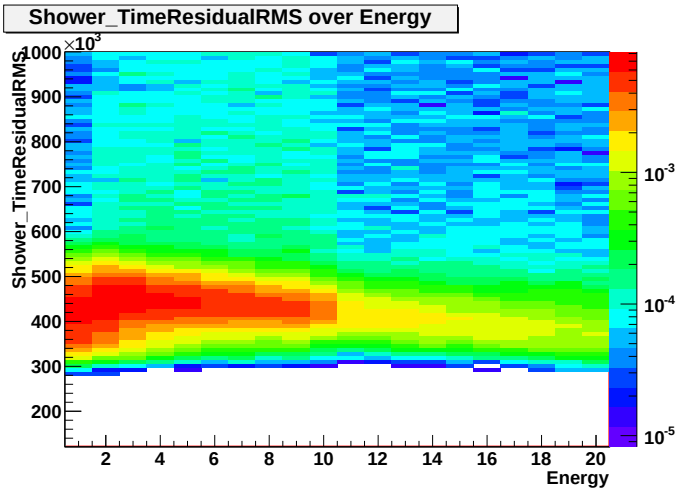
Shower_TimeResidualRMS over Energy
Shower_TimeResidualRMS
Energy

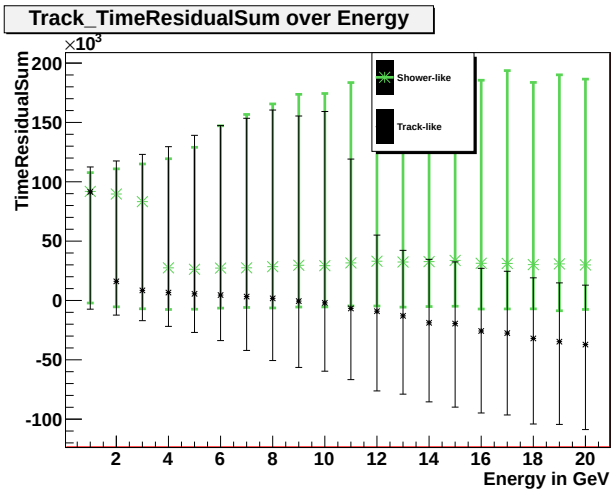
Track_TimeResidualSum over Energy
TimeResidualSum
Shower-like
Track-like
Energy in GeV

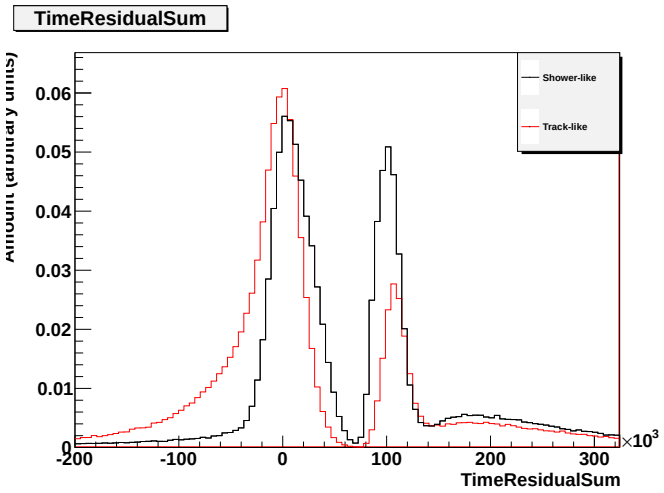
TimeResidualSum
Shower-like
Track-like
TimeResidualSum

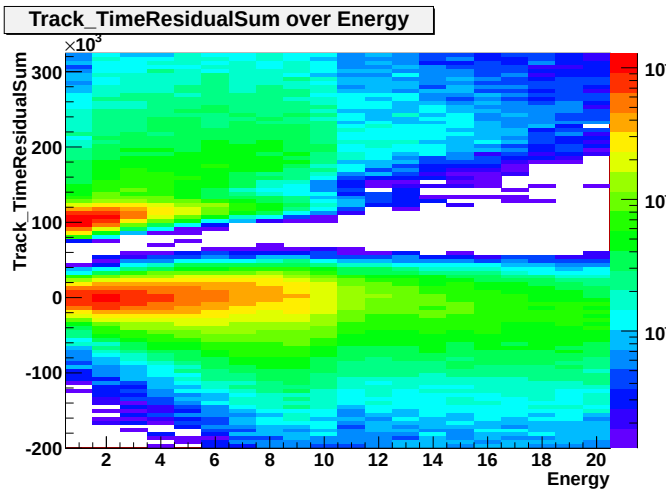
Track_TimeResidualSum over Energy
Track_TimeResidualSum
Energy

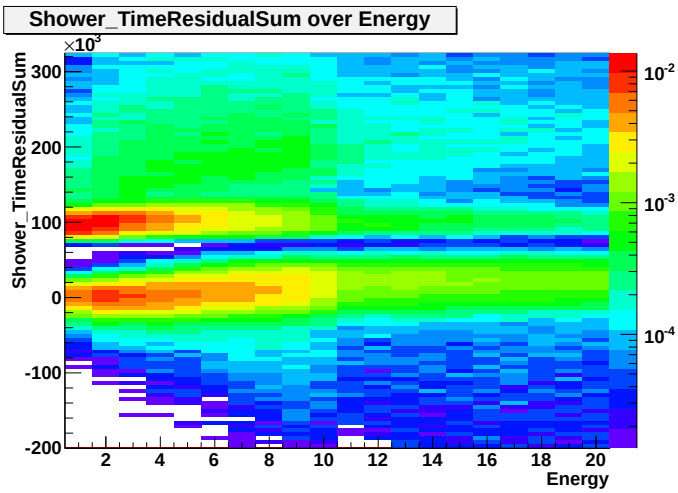
Shower_TimeResidualSum over Energy
Shower_TimeResidualSum
Energy

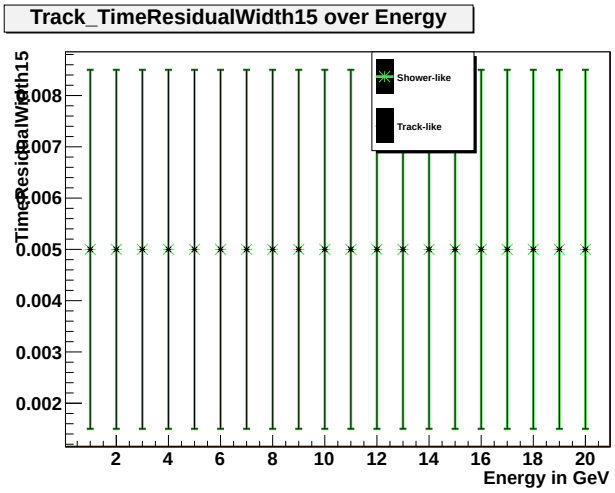
Track_TimeResidualWidth15 over Energy
TimeResidualWidth15
Energy in GeV
Shower-like
Track-like

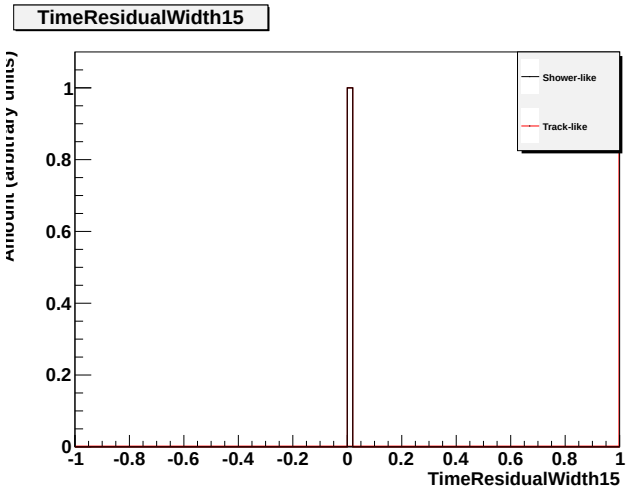
TimeResidualWidth15
Amount (arbitrary units)
TimeResidualWidth15
Shower-like
Track-like

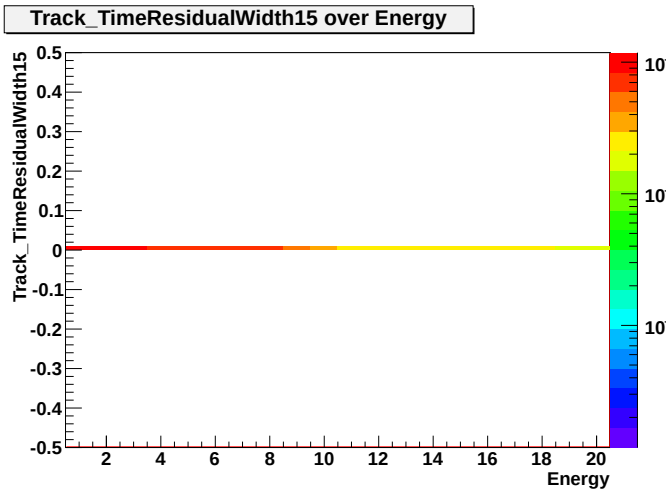
Track_TimeResidualWidth15 over Energy
Track_TimeResidualWidth15
Energy

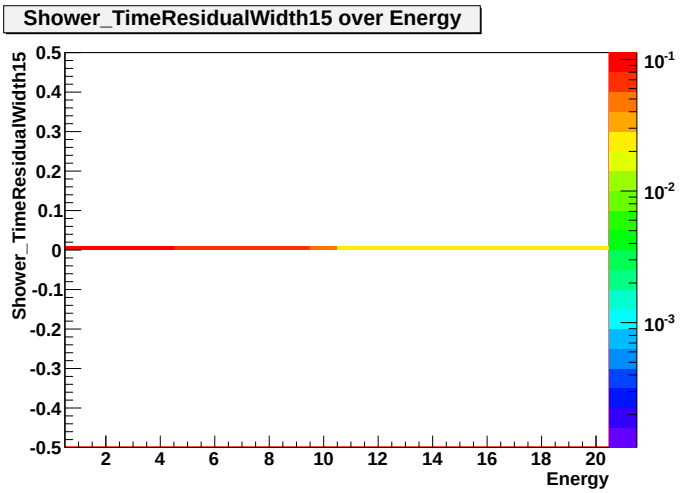
Shower_TimeResidualWidth15 over Energy
Shower_TimeResidualWidth15
Energy

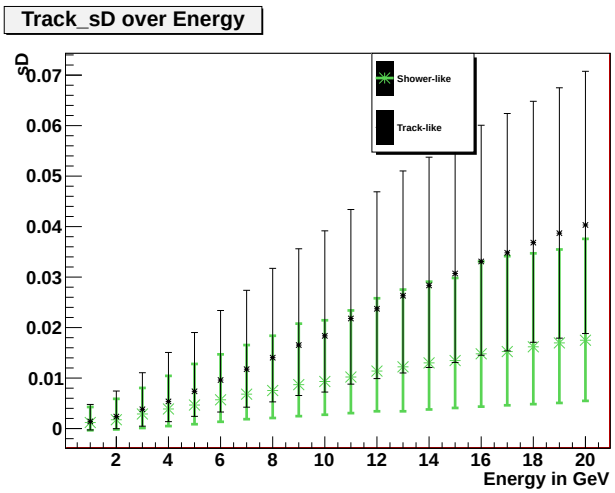
Track_sD over Energy
sD
Energy in GeV
Shower-like
Track-like

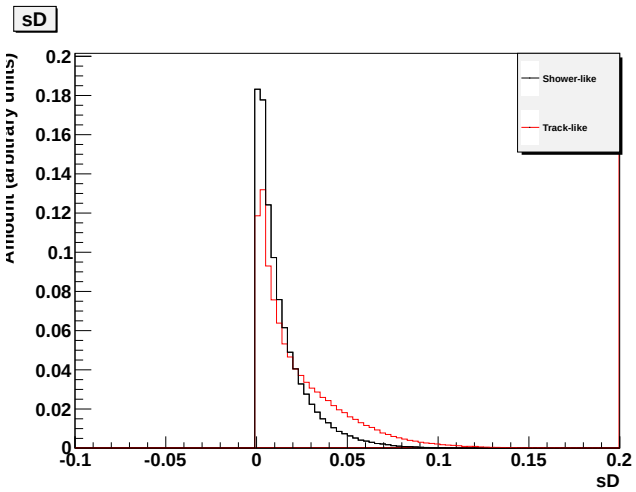
sD
Amount (arbitrary units)
sD
Shower-like
Track-like

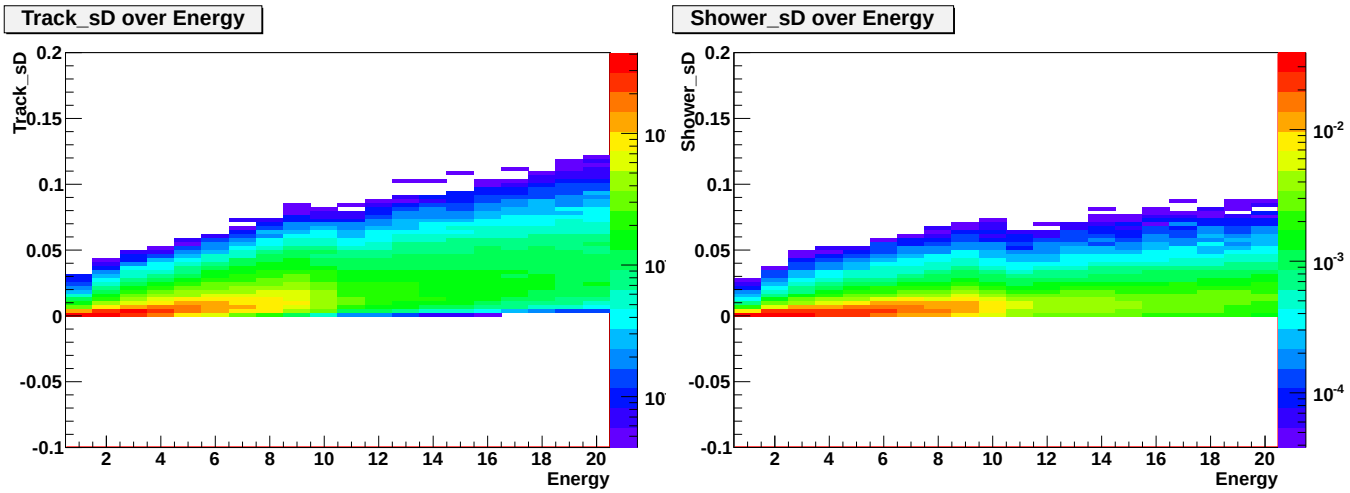
Track_sD over Energy
Track_sD
0.2
0.15
0.1
0.05
0
-0.05
-0.1
2
4
6
8
10
12
14
16
18
20
Energy
Shower_sD over Energy
Shower_sD
10^{-2}
10^{-3}
10^{-4}

Appendix C

Performance Plots

C.1 Physical Events

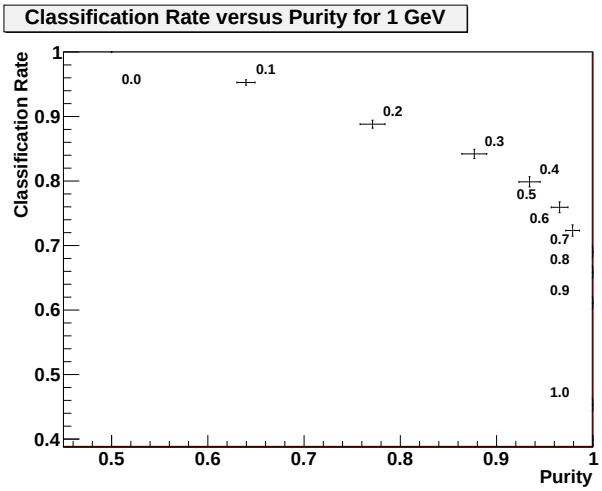

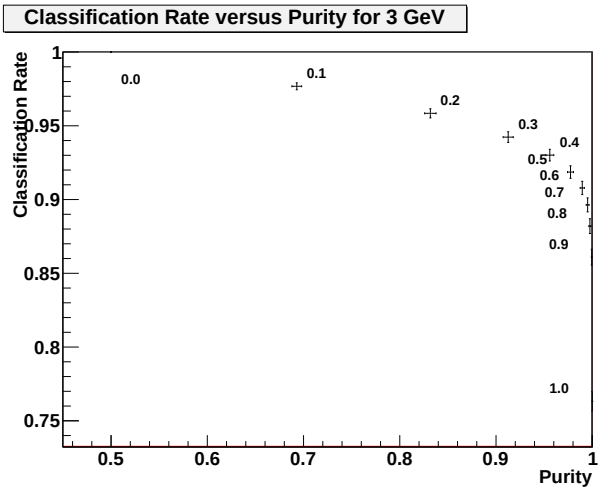

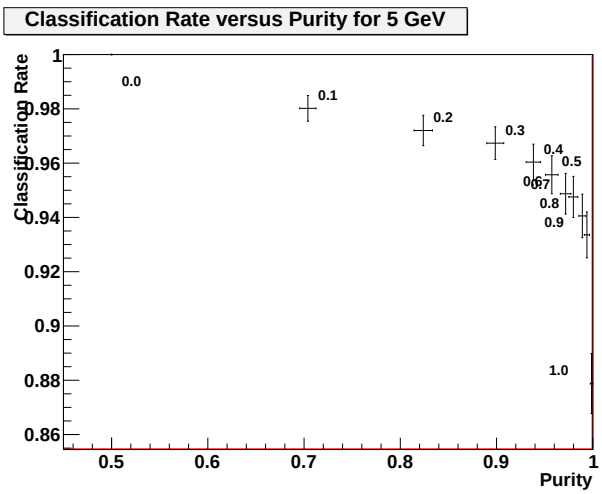

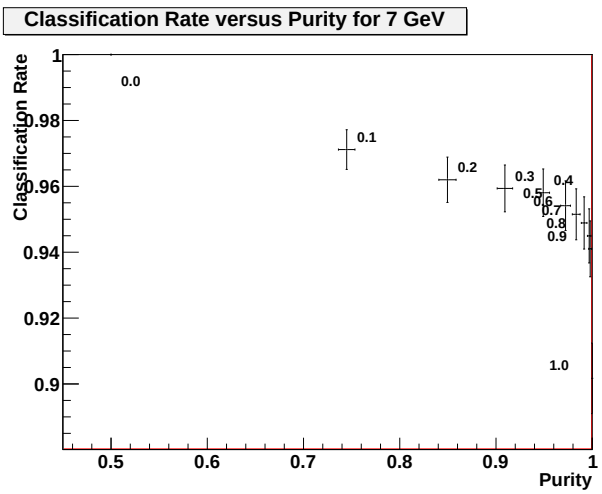

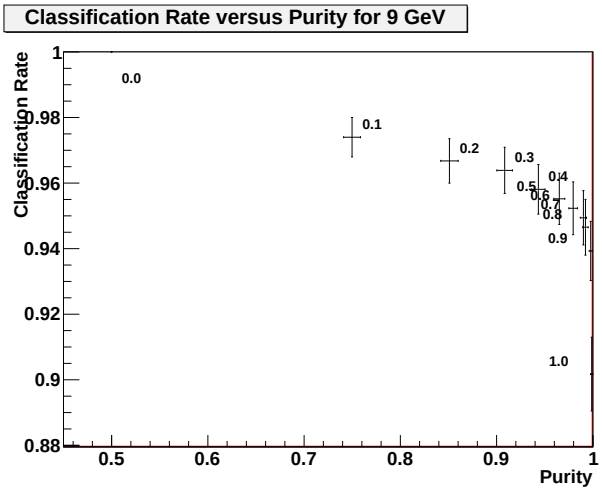
Classification Rate versus Purity for 9 GeV
Classification Rate
Purity

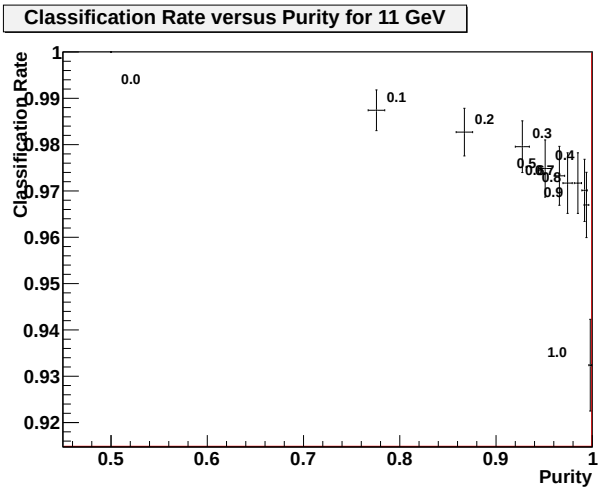
Classification Rate versus Purity for 11 GeV
Classification Rate
Purity

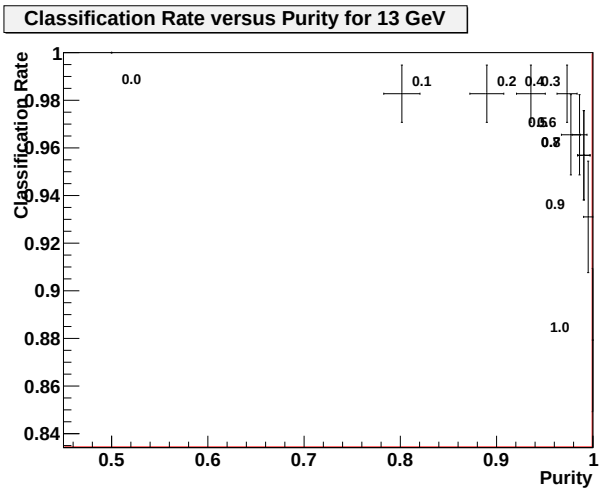
Classification Rate versus Purity for 13 GeV
Classification Rate
Purity

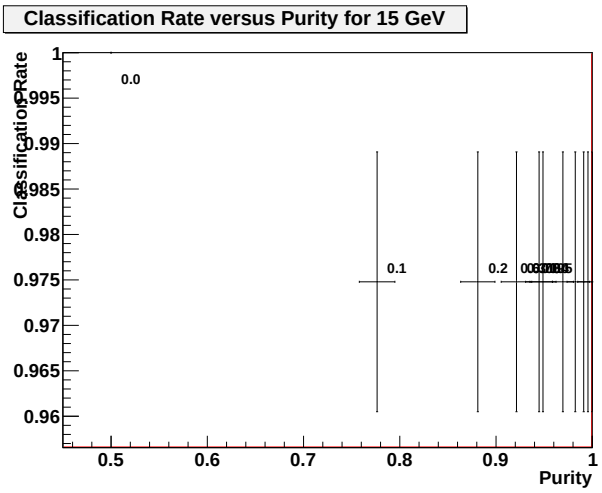
Classification Rate versus Purity for 15 GeV
Classification Rate
Purity

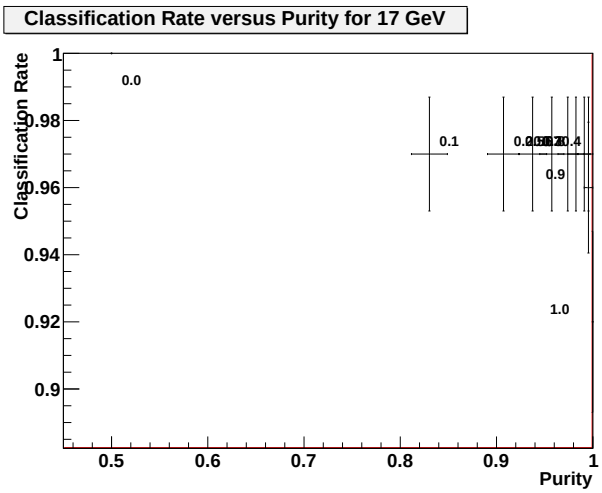
Classification Rate versus Purity for 17 GeV
Classification Rate
Purity

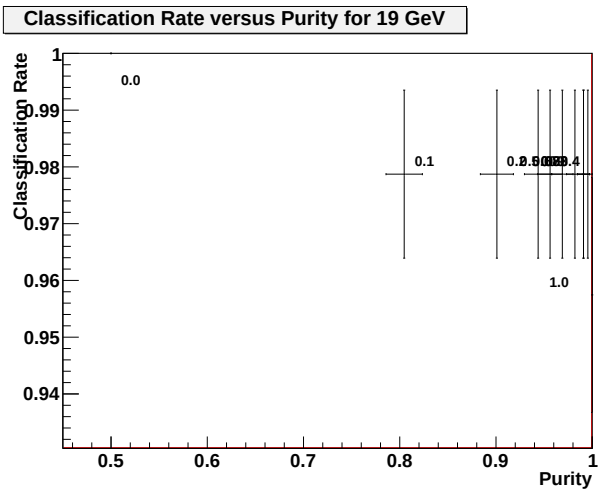
Classification Rate versus Purity for 19 GeV
Classification Rate
Purity

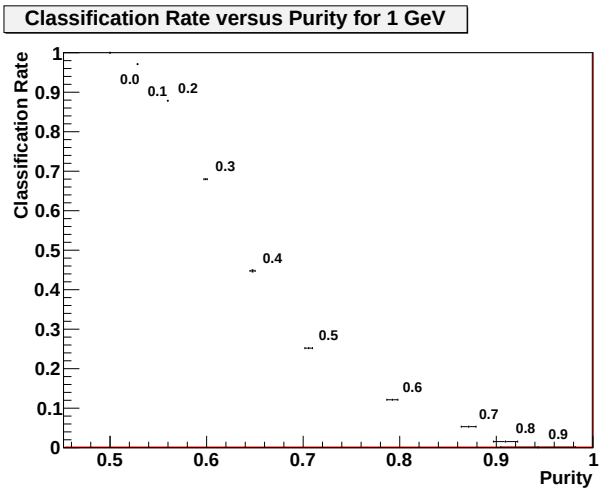

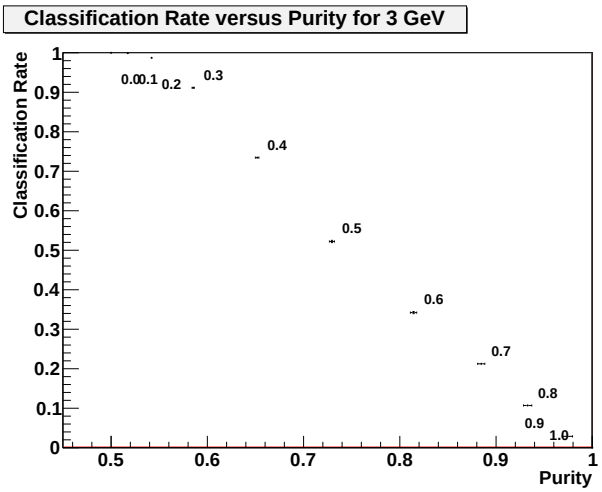

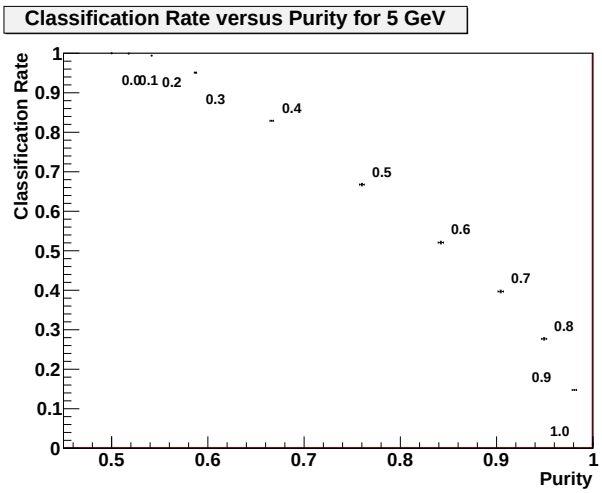

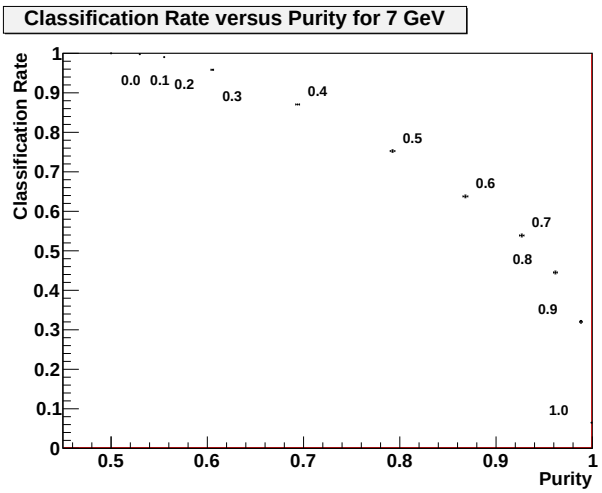

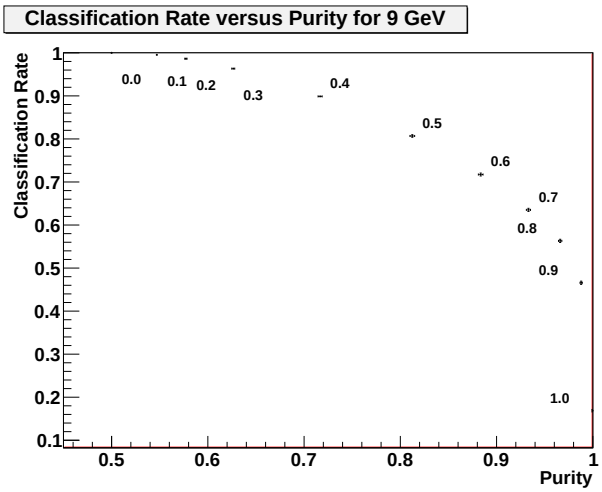

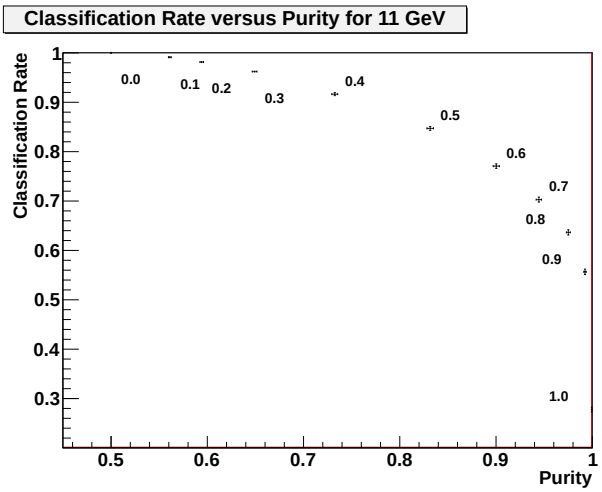

C.2 Premium Events

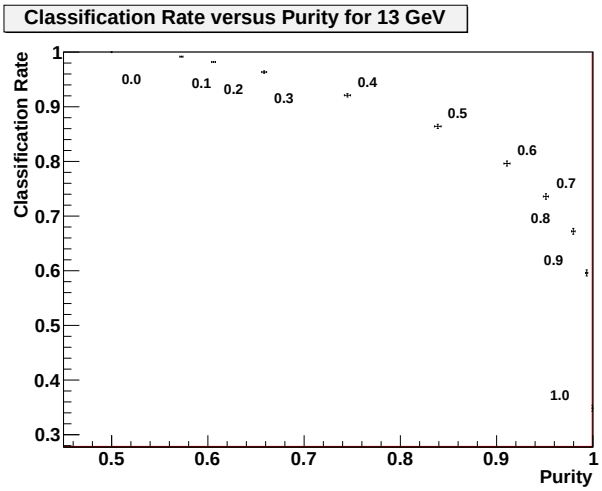
Classification Rate versus Purity for 13 GeV
Classification Rate
Purity
0.0
0.1
0.2
0.3
0.4
0.5
0.6
0.7
0.8
0.9
1.0

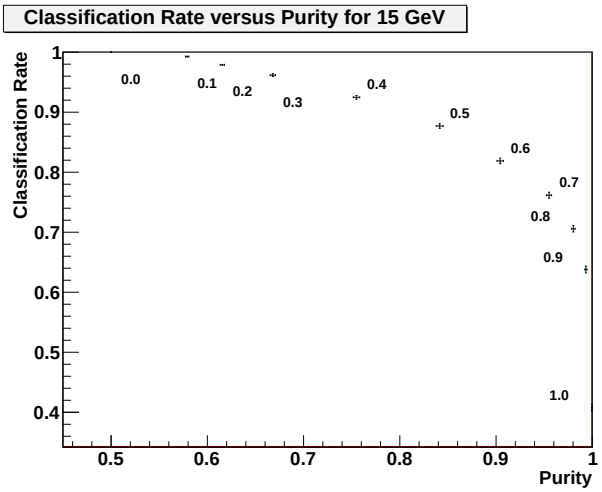
Classification Rate versus Purity for 15 GeV
Classification Rate
Purity
0.0
0.1
0.2
0.3
0.4
0.5
0.6
0.7
0.8
0.9
1.0

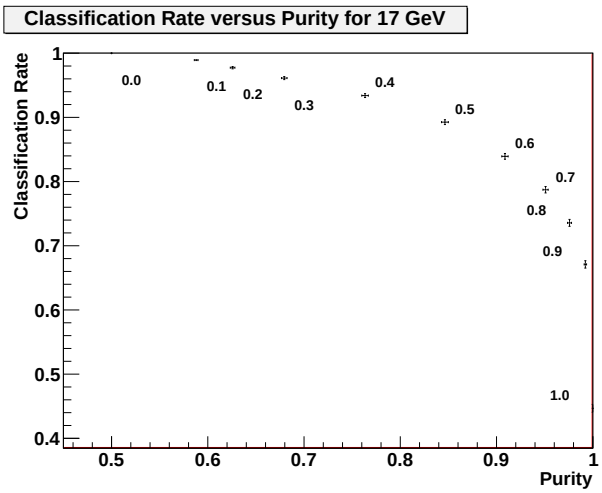
Classification Rate versus Purity for 17 GeV
Classification Rate
Purity
0.0
0.1
0.2
0.3
0.4
0.5
0.6
0.7
0.8
0.9
1.0

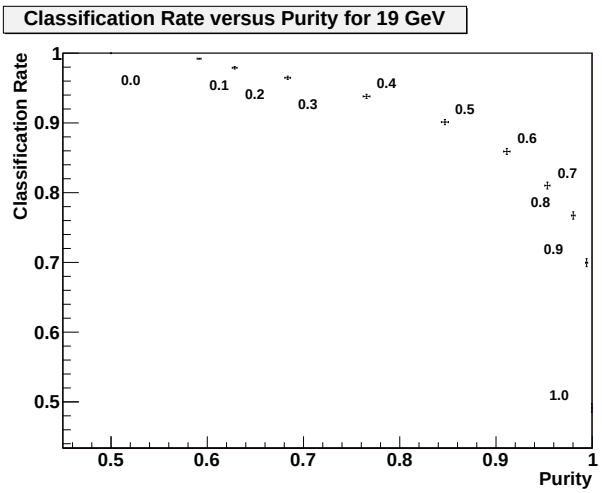
Classification Rate versus Purity for 19 GeV
Classification Rate
Purity
0.0
0.1
0.2
0.3
0.4
0.5
0.6
0.7
0.8
0.9
1.0

C.2.1 Zenith Dependence

Titles are sturctured as ĆutXPurityẅhere X is the cut on the fraction of trees with the result of a track-like event.

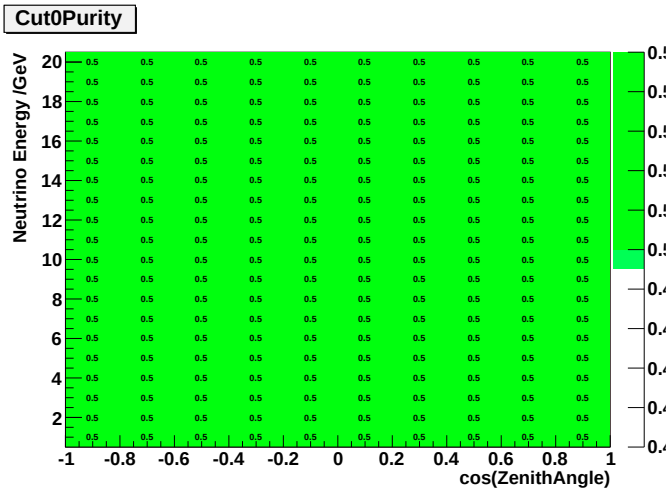

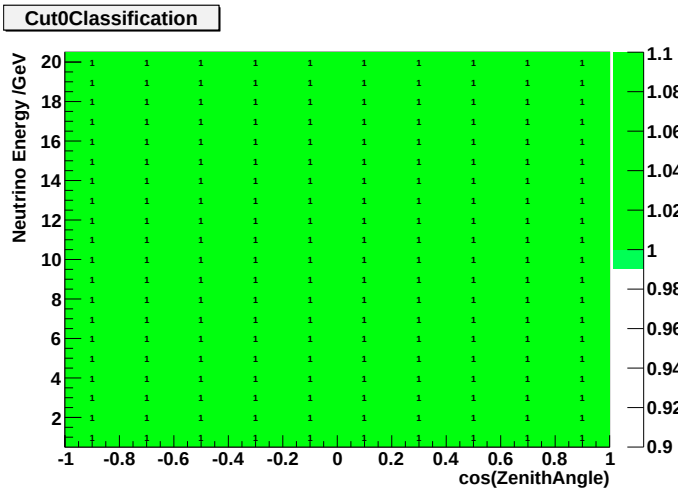

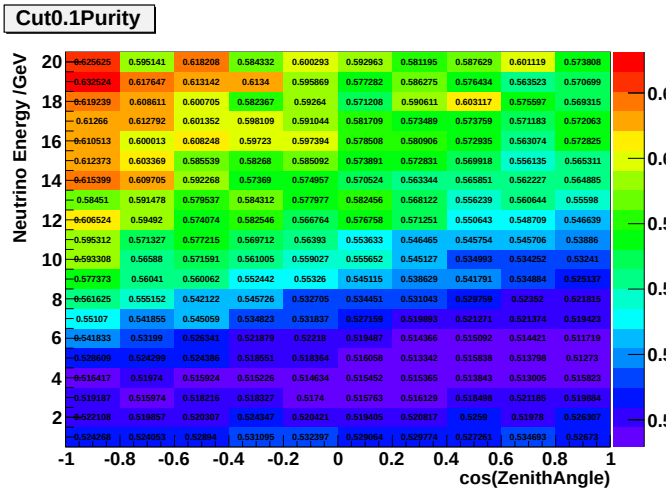

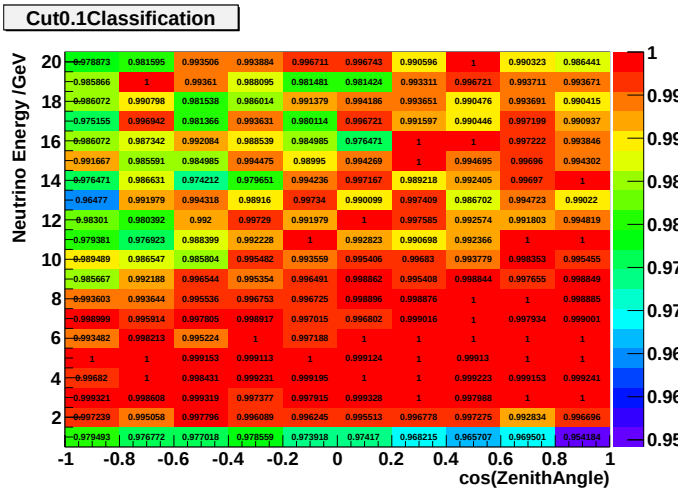

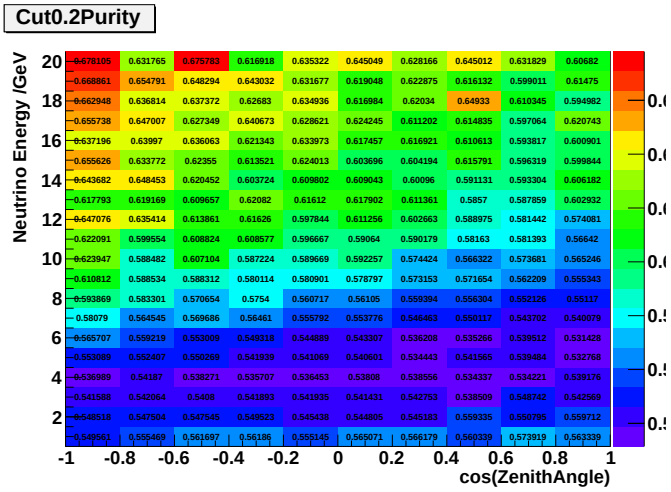

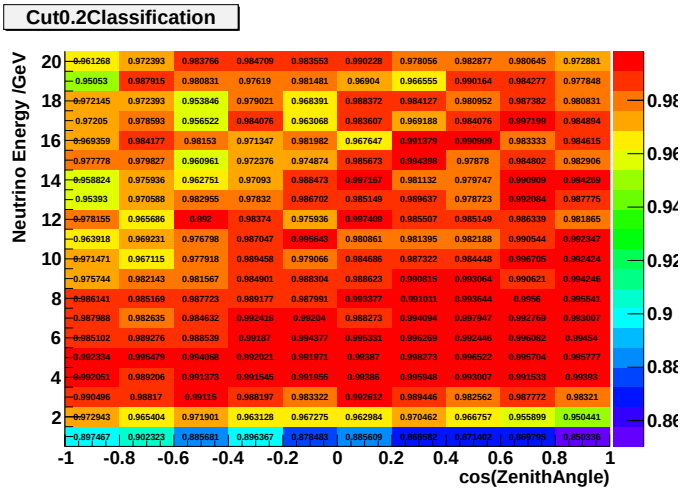

Cut0.3Purity

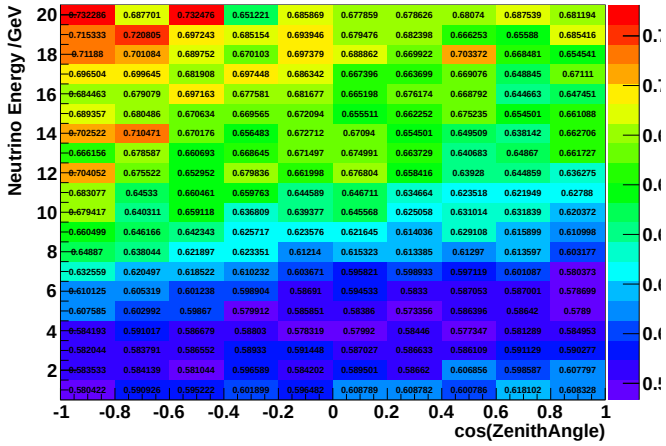

Cut0.3Classification

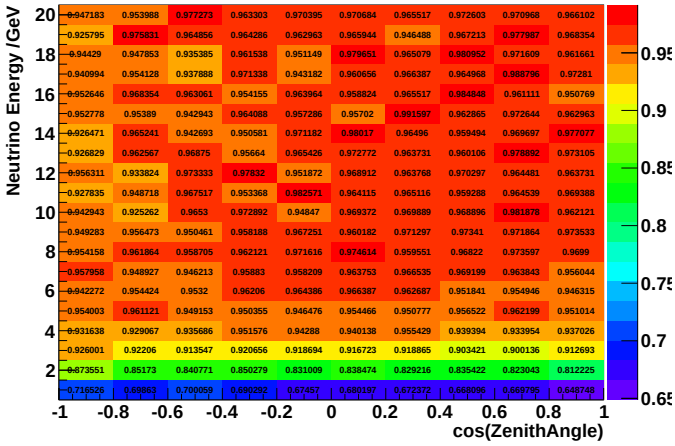

Cut0.4Purity

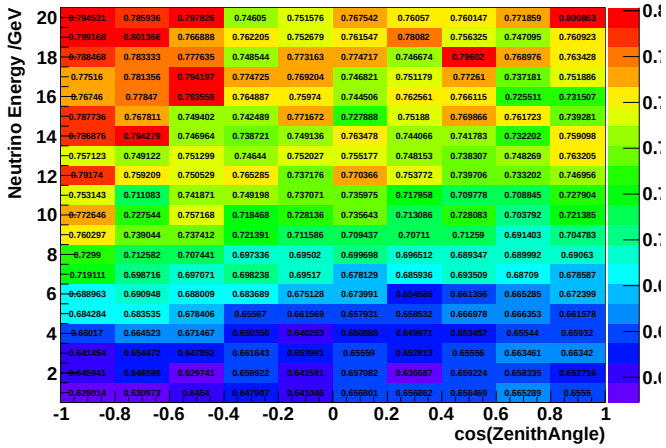

Cut0.4Classification

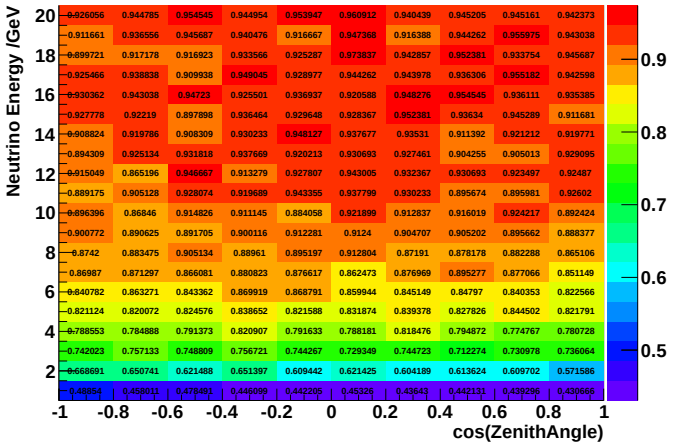

Cut0.5Purity

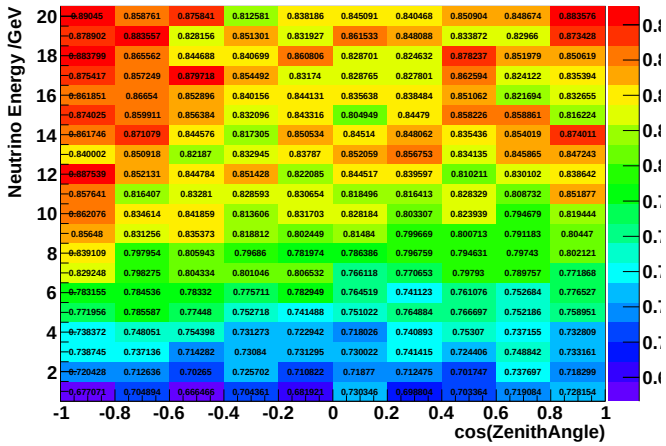

Cut0.5Classification

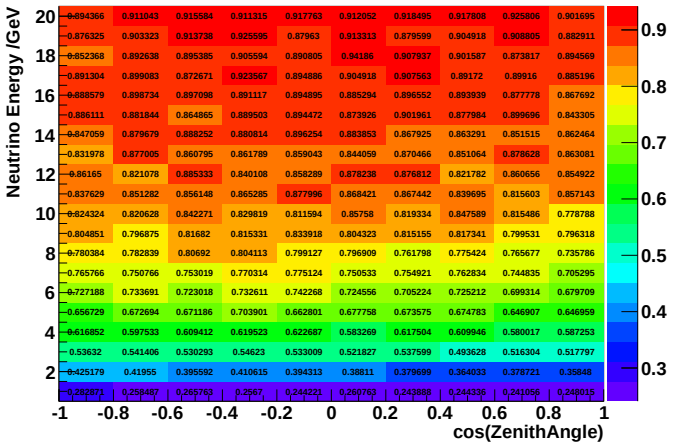

Cut0.6Purity

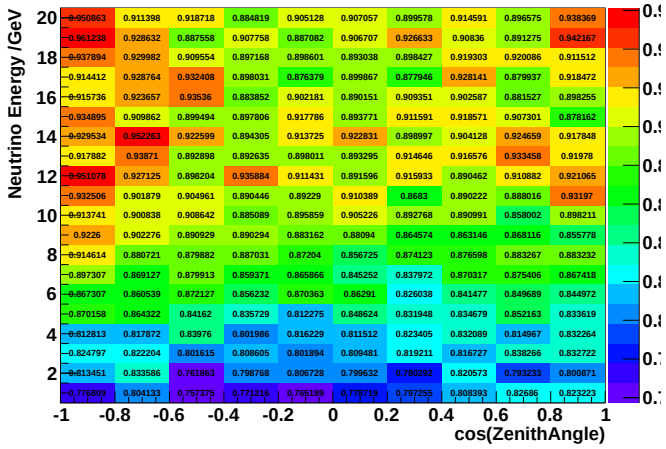

Cut0.6Classification

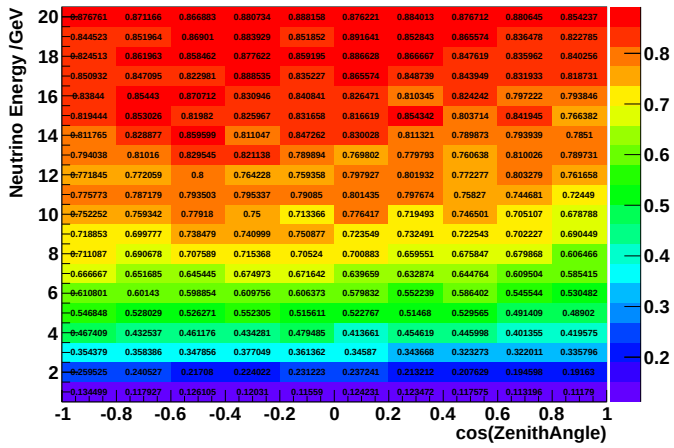

Cut0.7Purity

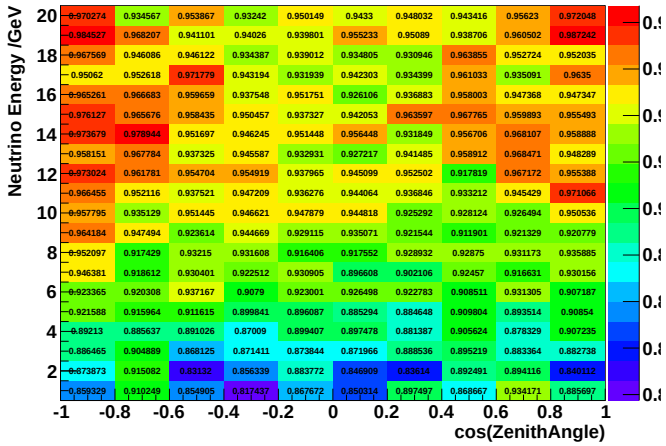

Cut0.7Classification

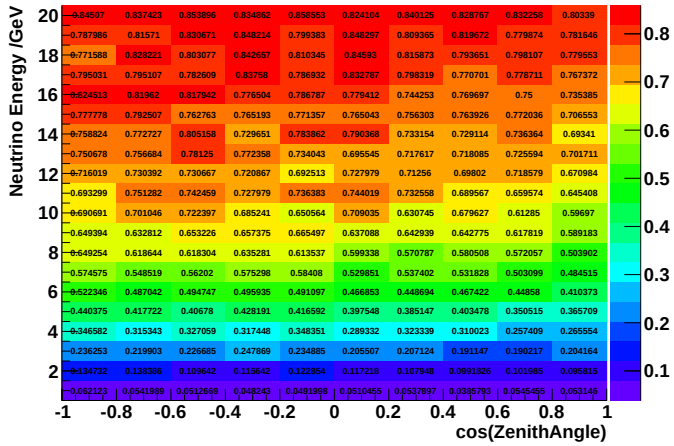

Cut0.8Purity

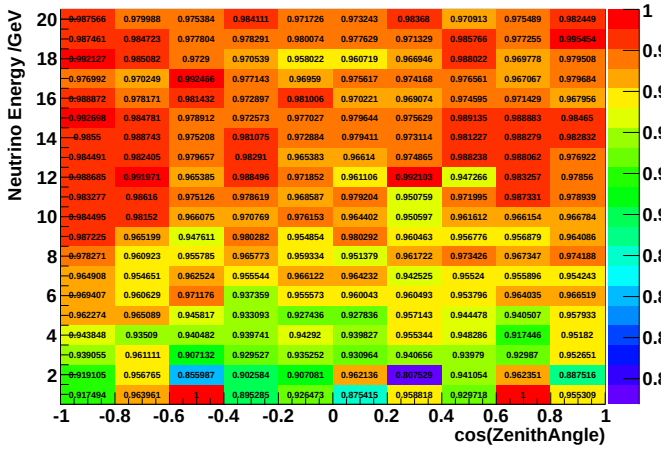

Cut0.8Classification

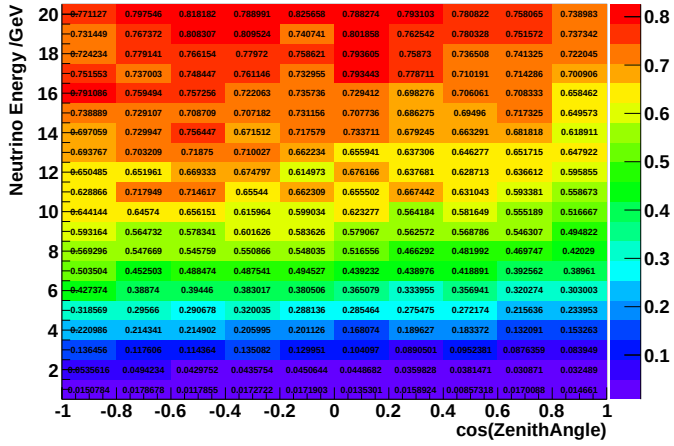

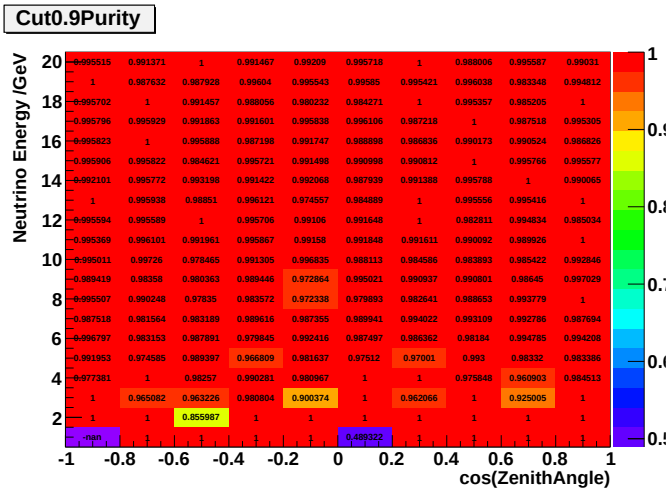
Cut0.9Purity
Neutrino Energy /GeV
cos(ZenithAngle)

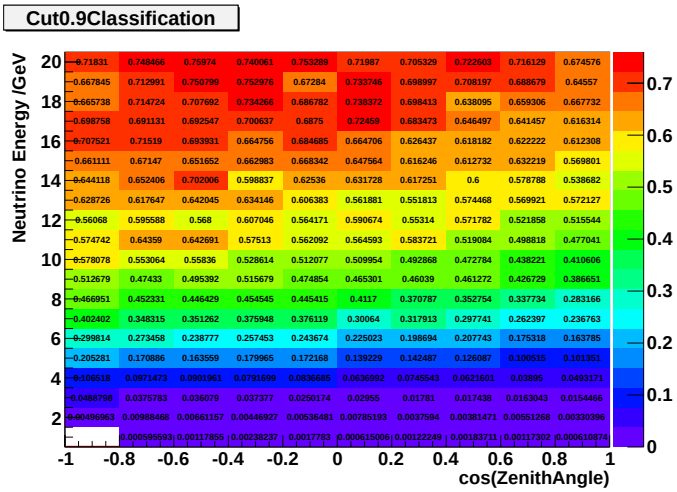
Cut0.9Classification
Neutrino Energy /GeV
cos(ZenithAngle)

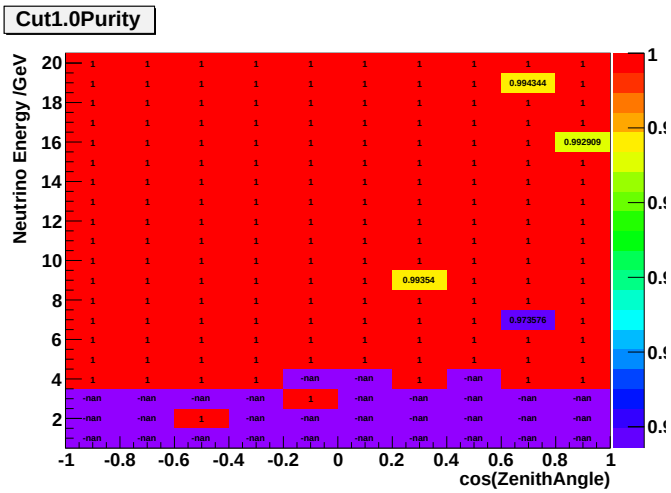
Cut1.0Purity
Neutrino Energy /GeV
cos(ZenithAngle)

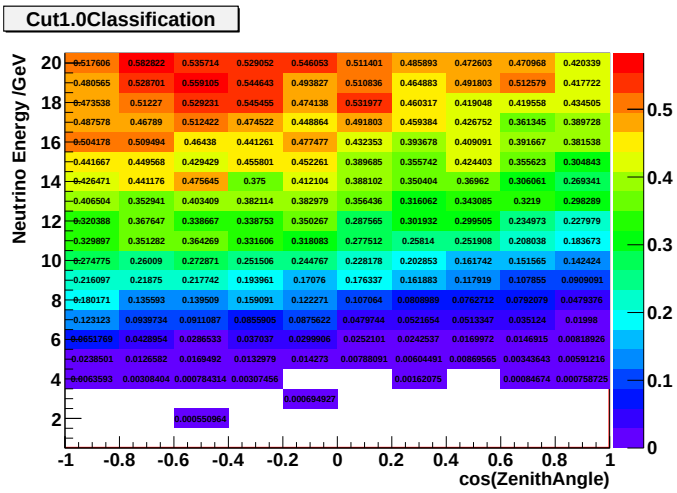
Cut1.0Classification
Neutrino Energy /GeV
cos(ZenithAngle)

C.2.2 Bjorken-y Dependence

Titles are sturctured as ĆutXPurityẅhere X is the cut on the fraction of trees with the result of a track-like event.

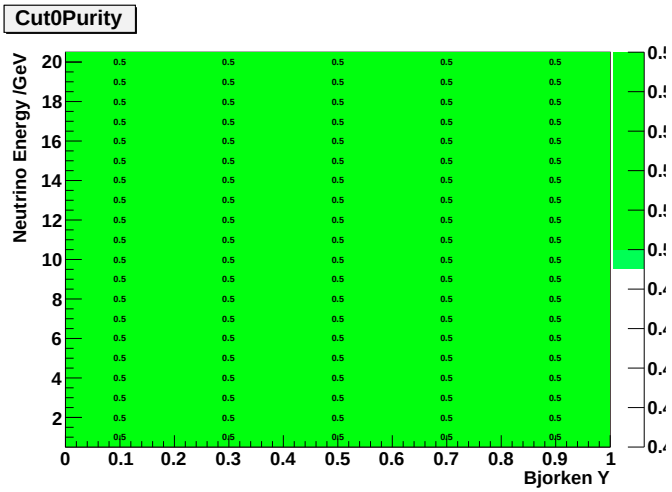

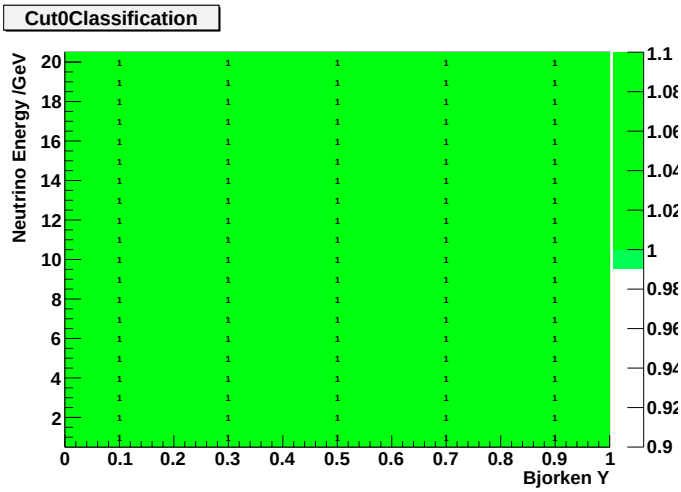

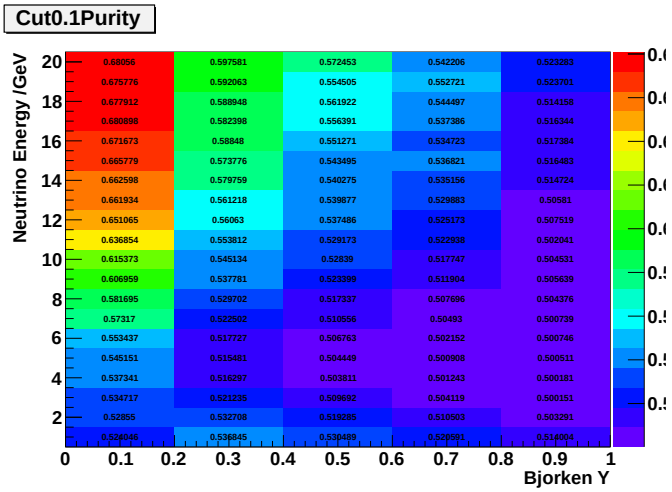

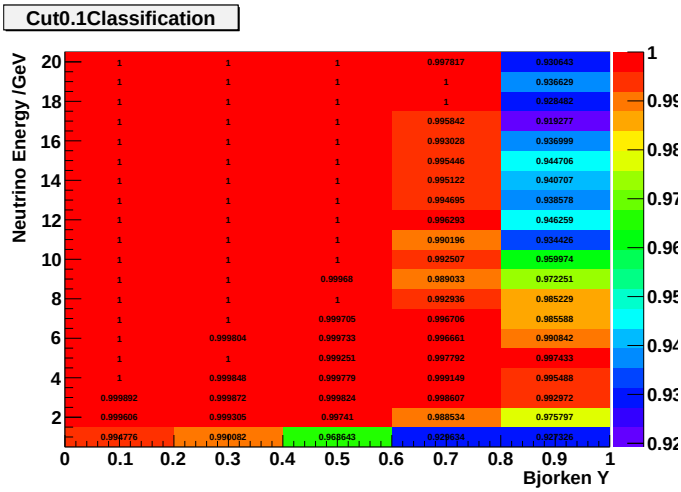

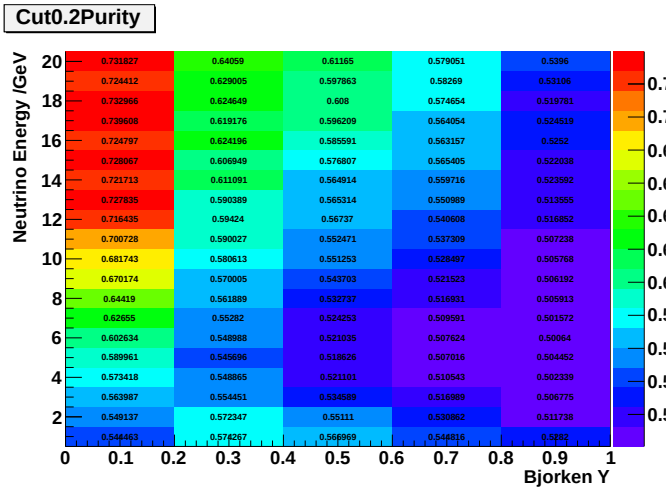

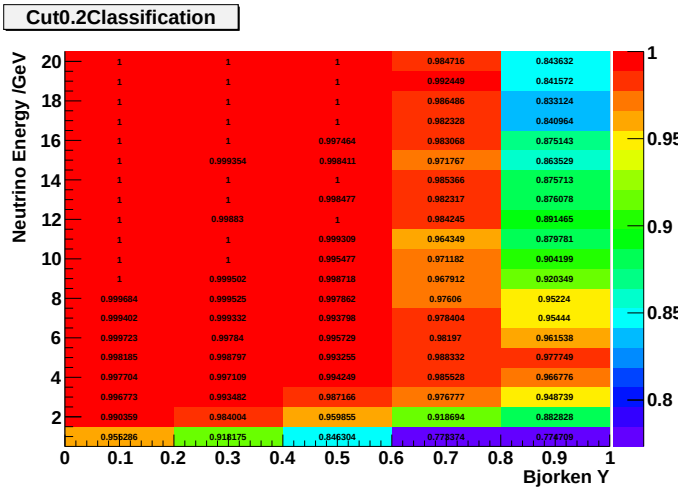

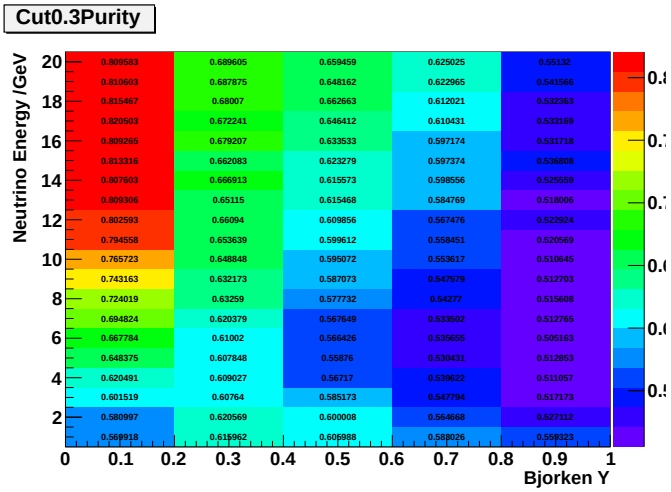
Cut0.3Purity
Neutrino Energy /GeV
Bjorken Y

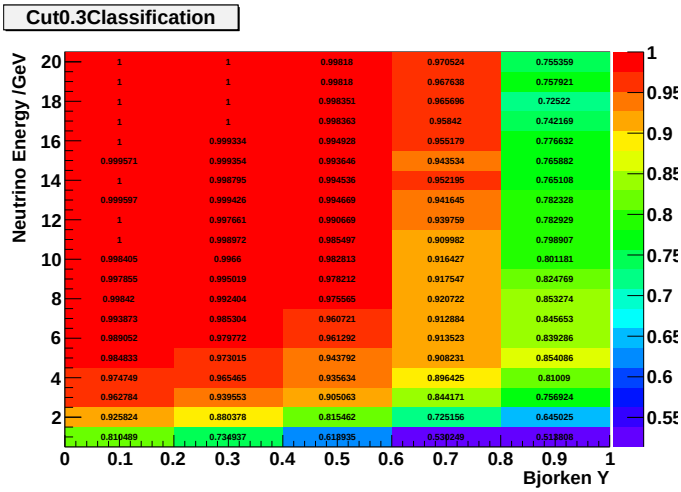
Cut0.3Classification
Neutrino Energy /GeV
Bjorken Y

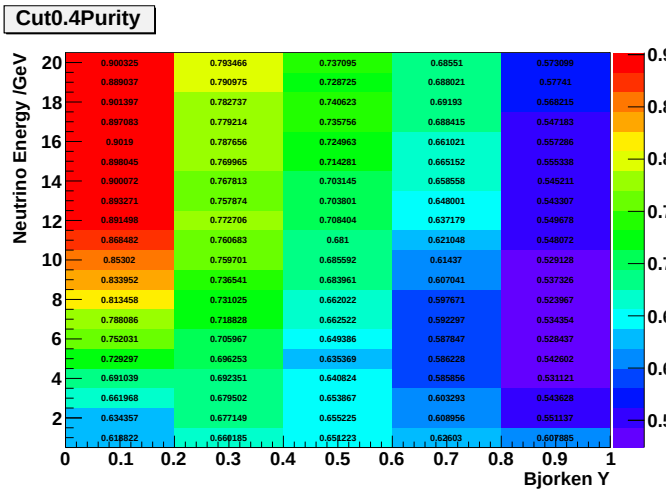
Cut0.4Purity
Neutrino Energy /GeV
Bjorken Y

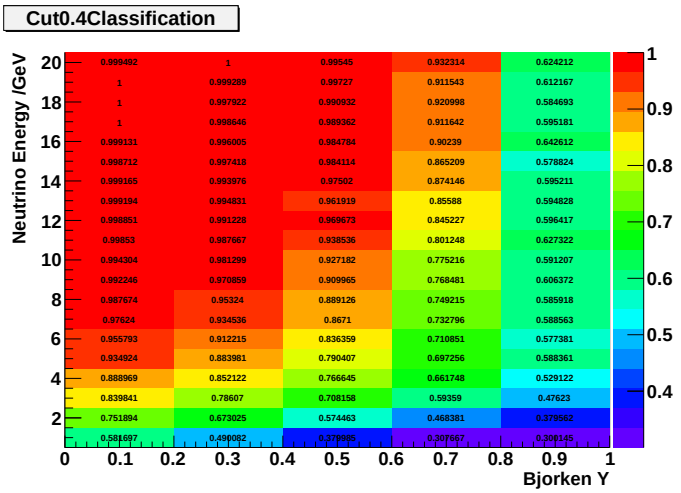
Cut0.4Classification
Neutrino Energy /GeV
Bjorken Y

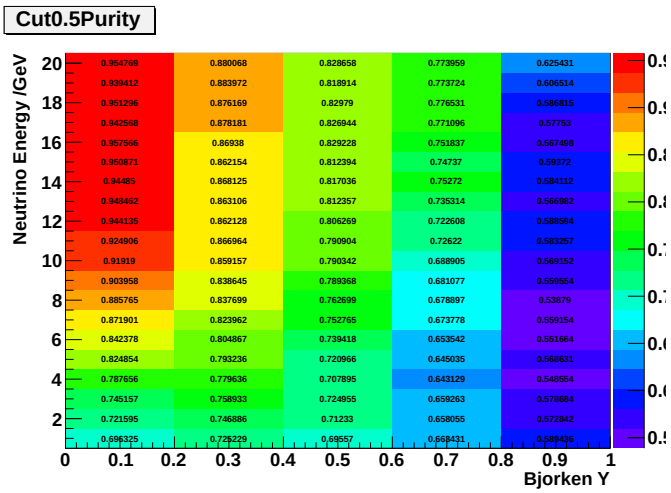
Cut0.5Purity
Neutrino Energy /GeV
Bjorken Y

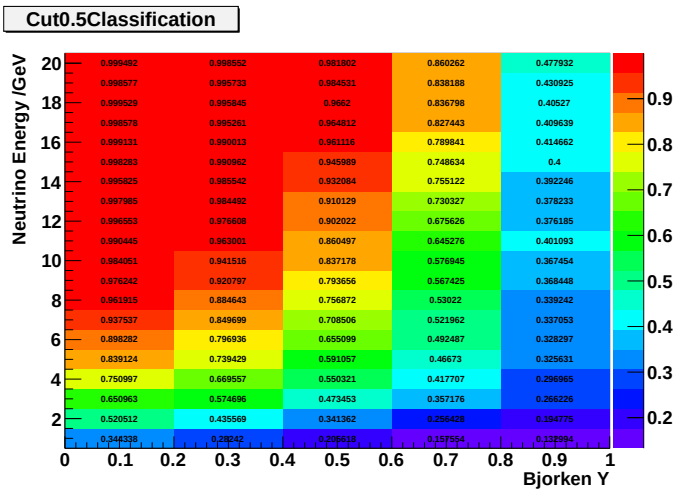
Cut0.5Classification
Neutrino Energy /GeV
Bjorken Y

Cut0.6Purity

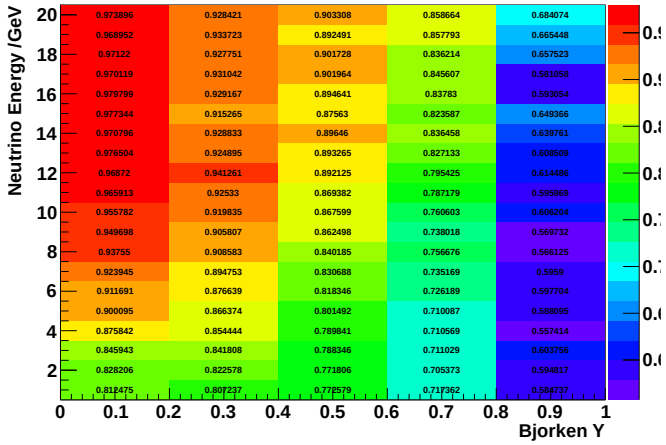

Cut0.6Classification

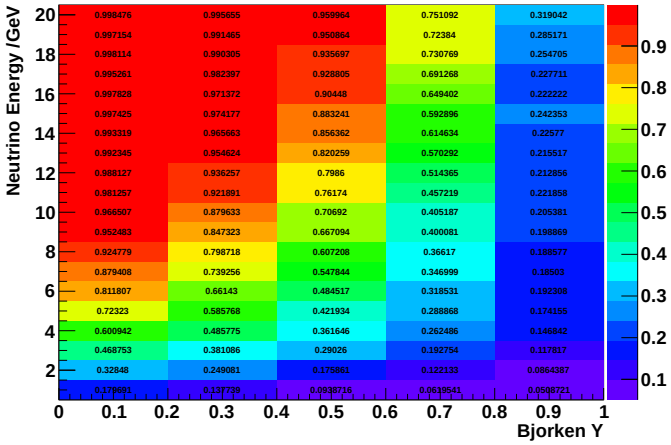

Cut0.7Purity

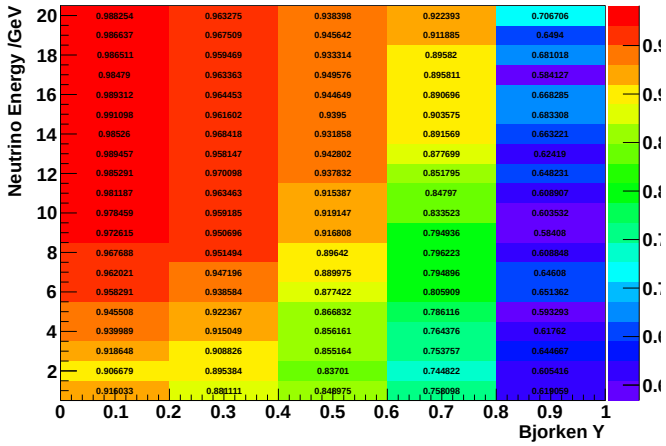

Cut0.7Classification

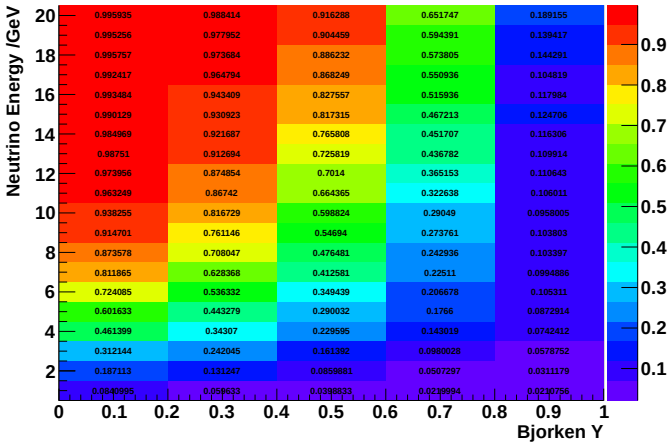

Cut0.8Purity

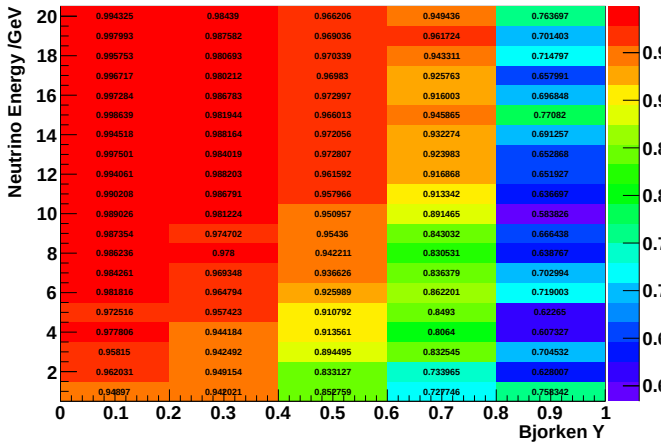

Cut0.8Classification

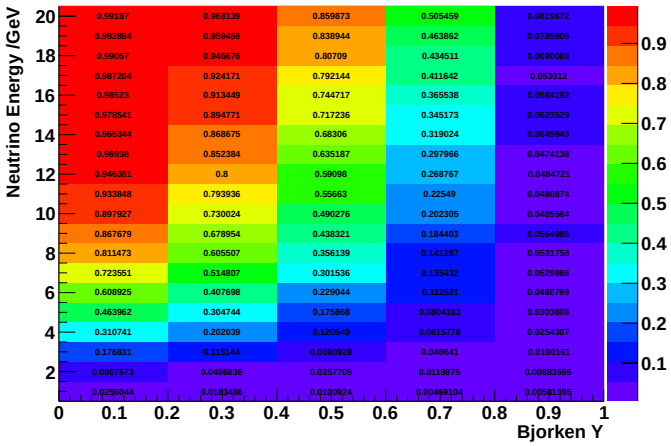

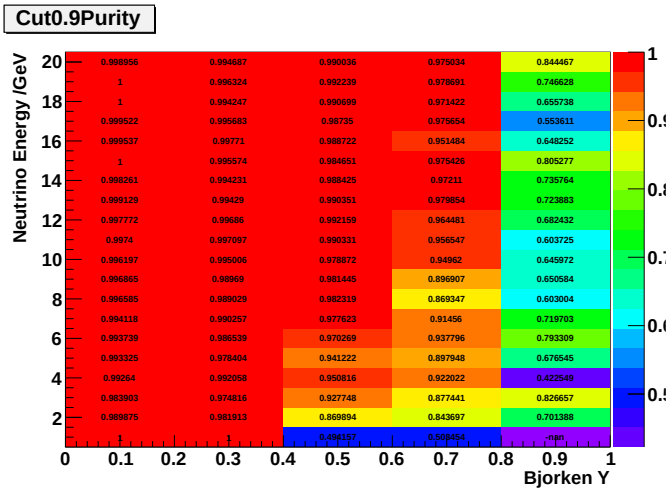
Cut0.9Purity
Neutrino Energy /GeV
Bjorken Y

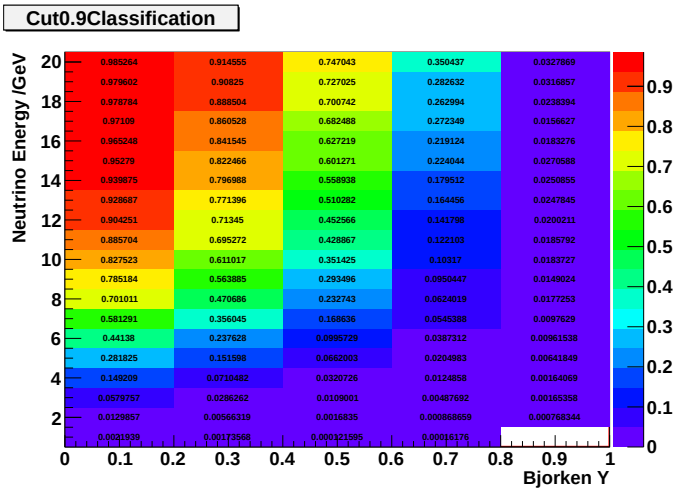
Cut0.9Classification
Neutrino Energy /GeV
Bjorken Y

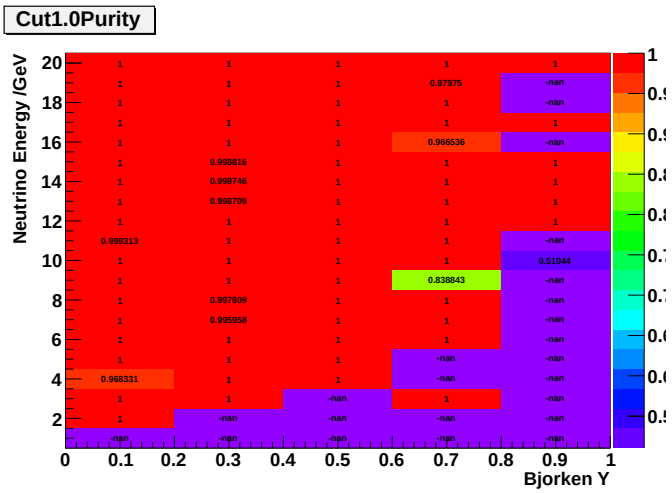
Cut1.0Purity
Neutrino Energy /GeV
Bjorken Y

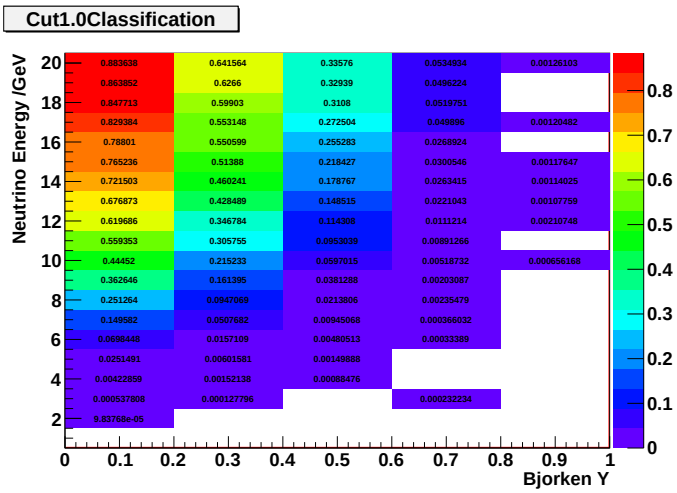
Cut1.0Classification
Neutrino Energy /GeV
Bjorken Y

Danksagung

Am Schluss möchte ich mich noch bei den Menschen bedanken, die diese Arbeit möglich gemacht haben. Bevor hier eine scheinbar endlose Liste entsteht: Eine Liste mit Namen der Mitglieder der Neutrinogruppe in Erlangen kann jeder selbst finden.

Erklärung

Hiermit bestätige ich, dass ich diese Arbeit selbstständig und nur unter Verwendung der angegebenen Hilfsmittel angefertigt habe.

Erlangen,

24.10.2013